FORSCHUNGSZENTRUM
ROSSENDORF e.V.

FZR

FZR 93 - 08
March 1993

HIGH-RESOLUTION SPECTROSCOPY OF FISSION FRAGMENTS, NEUTRONS, AND γ-RAYS

Editors:

H. MÄRTEN and K.D. SCHILLING

Proceedings
of the International Workshop on

HIGH-RESOLUTION SPECTROSCOPY OF FISSION FRAGMENTS, NEUTRONS, AND γ-RAYS

Dresden, Germany, Febr. 1-2, 1993

Editors

HORST MÄRTEN and KLAUS-DIETER SCHILLING

Institut für Kern- und Atomphysik
der Technischen Universität Dresden
Mommsenstraße 13, D-O-8027 Dresden, Germany
and
Forschungszentrum Rossendorf e.V.
Institut für Kern- und Hadronenphysik
Postfach 19, D-O-8051 Dresden, Germany

March 1993

PREFACE

This volume contains most of the contributions presented at the "International Workshop on High-Resolution Spectroscopy of Fission Fragments, Neutrons, and γ-Rays" held at Technische Universität Dresden.

The scientific aim of the workshop was to obtain a presentation of the current knowledge of the methodology of high-resolution fission experiments. The main topics discussed at the workshop were:

- Concepts for high-resolution fission-fragment detectors (systems). Minimization of experimental uncertainties. Detector simulation including all secondary processes.
- Experimental determination of correction coefficients (e.g. pulse height defect, efficiencies).
- Precise data analysis. Correction procedures (e.g. primary-mass determination) and consequences of approximations. Error estimation.
- Special requirements in correlation experiments, e.g. neutron and γ-ray spectroscopy/counting in 4π.

The contributions show, despite the progress achieved in this field, that new experimental methods in fission correlation experiments result in more precise and more reliable data, which are the basis for a developed understanding of fission dynamics.

The co-operation with the colleagues from Institut für Kern- und Hadronenphysik of the Forschungszentrum Rossendorf e.V. in publishing the proceedings is greatfully acknowledged.

I am personally very thankful to Mrs. S. Eckstein for assisting me very efficiently in solving all problems of organization and preparation of the proceedings.

H. Märten

CONTENTS

SPECTROSCOPY OF FISSION FRAGMENTS

F. Gönnenwein
Physikalisches Institut, Auf der Morgenstelle 14, D-72076 Tübingen/Germany

Abstract

The measurement of kinetic energies, velocities, masses and nuclear charges of fission fragments by physical methods is reviewed. The emphasis is put on recent developments aiming at high resolution and precision. The shortcomings of existing techniques are discussed and some improvements in approach are suggested.

1. INTRODUCTION

The present survey of experimental methods for the spectroscopy of fission fragments emphasizes high resolution and precision aspects. Basic principles are merely sketched. Instead of highlighting glamorous achievements, the report dwells on limitations in resolution and precision of existing techniques and points to discrepancies in calibration procedures for detectors which still have to be overcome.

The measurement of the following characteristics of fission fragments are discussed: kinetic energy, velocity, mass and nuclear charge. Only physical methods will be addressed, with notably the well established and widely used radiochemical approach to fragment masses and charges, with and without chemistry, being not covered (see, however [PER 93]). Besides the physical quantities enumerated above there are of course some further fragment properties of interest, like the fragment emission angle relative to a given axis, the fragment spin and most important, the fragment excitation energy. The measurement of these fragment properties will not be described here, but the reader is referred to several contributions to this workshop where advanced detection techniques for neutrons and gammas being emitted from fission fragments are expounded. The fragment excitation energies are deduced from these neutron and gamma data. Furthermore, this report does not aim at giving a survey of the rather complex detector compounds having been proposed and adapted to specific experimental requirements.

In several respects the present review is an updated and complementary version of an account of experimental techniques for fission research having been given some years ago [GON 89].

2. KINETIC ENERGY

2.1 ELECTROMAGNETIC SPECTROMETERS

The challenge to measure with the highest feasible resolution and precision the kinetic energies (and masses) of fission fragments is evidently best met with an electromagnetic spectrometer combining electric and magnetic fields to focus in space unslowed fragments, emerging from a thin target and travelling in high vacuum, according to their energy and mass. The low luminosity of electromagnetic spectrometers necessitates, however, intense sources of fission fragments. This requirement can only be satisfied for fissile targets placed close to the core of a high flux reactor. The use of electromagnetic spectrometers is, therefore, limited to the study of fission reactions induced by thermal neutrons. Two devices of this type have become known: the LOHENGRIN spectrometer installed at the High Flux Reactor of the ILL/Grenoble [MOL 75], and a spectrometer installed at a reactor in Tashkent [ARI 72]. A resolving power δE for the kinetic energy better than $\delta E \approx 100$ keV is routinely achieved on LOHENGRIN. It is not obvious how to match this resolving power with electronic detectors. The calibration of electromagnetic separators is straightforward and may be based, e.g., on the spectroscopy of α-particles from radioactive sources whose energies are reliably known. Although the intrinsic performance of electromagnetic spectrometers is outstanding, it should be pointed out that it is sometimes difficult to maintain a similar level of performance for the physical results, e.g., the kinetic energy distribution for a given fragment mass from a fission reaction. This is due to the fact that, fo the example given, the energy distribution has to be taken

point-by-point for narrow windows in energy and, most cumbersome, for several ionic charges of the fission fragments. The whole procedure is, hence, time consuming and the burnup of the fissile target in the high neutron flux has to be carefully accounted for.

2.2 SEMICONDUCTOR DETECTORS

By far most of fission research has been performed in the last 3 decades by making use of semiconductor detectors. In fact, the workhorse for detecting fission fragments has been and still is the surface barrier detector (SBD), a single crystal silicon wafer with a p-n junction at one of the surfaces and with the wafer being properly contacted at the front and rear side. The SBDs have become very popular since they are easy to put into operation, rugged, versatile as to sizes and shapes, and commercially available in high quality. Basically the working principle of a SBD is similar to an ionization chamber, with electrons and holes created by the incoming radiation being collected at the respective electrodes.

An example for the energy resolution to be achieved with a SBD for heavy ions is shown in fig. 1 [WEI 85]. A commercial SBD (ORTEC F) was placed in the focal plane of the LOHENGRIN spectrometer and irradiated with fission fragments from the light mass group. For a spectrometer setting of mass/ionic charge $A/q = 5$ several "mass lines" with $\Delta A = 5$ come forth in the pulseheight spectrum. The different mass lines correspond to fission fragments with one single ion velocity and, for this reason, they are staggered in kinetic energy by a fixed amount. In the case of fig. 1 the energy shift ΔE from one mass line to a neighboring one is $\Delta E = 4.4$ MeV. With this calibration the energy resolution δE of the SBD is readily obtained. For example: for mass $A = 95$ the energy resolution (FWHM) δE at a kinetic energy of $E = 83.6$ MeV is found to be $\delta E = 1.3$ MeV. More generally, the energy resolution is observed to be $\delta E \gtrsim 1.0$ MeV and $\delta E \gtrsim 2.0$ MeV for fission fragments with typical masses and energies from the light and heavy group, respectively, of asymmetric fission of the lighter actinides.

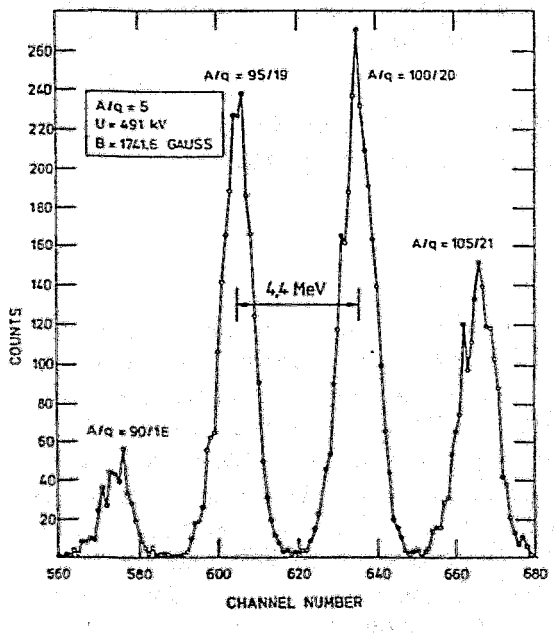

Fig. 1: Pulseheight spectrum of a surface barrier detector for fission fragments with $\Delta A = 5$ and $\Delta E = 4.4$ MeV. Bias at nominal value. From [WEI 85].

The energy spectrum in fig. 1 was taken with the bias voltage on the SBD being set to the nominal value as recommended by the manufacturer. To improve the timing characteristics of SBDs sometimes an overbias is applied. For the same setting of LOHENGRIN as in fig. 1 a pulseheight spectrum of the same diode was registered with an overbias almost twice the nominal voltage. The spectrum obtained is depicted in fig. 2 [WEI 85]. The centres of gravity of the individual mass lines are observed to be shifted to larger pulseheights at the higher bias voltage.

To avoid these shifts in actual experiments, it is common practice to monitor continuously the reverse current and to compensate its increase due to radiation damage so to keep the voltage drop across the diode constant. Of major concern in fig. 2 are, however, the high energy tails showing up in the pulseheight spectrum. The tails are probably due to charge multiplication. Overbias is obviously seen to be liable to impair the energy resolution of SBDs and care should be taken to avoid charge multiplication.

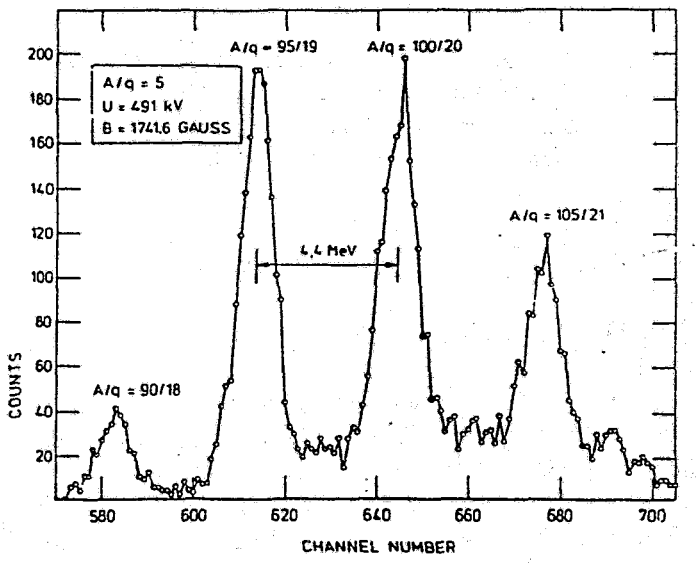

Fig. 2: Same as Fig. 1, but with bias at almost twice the nominal value. From [WEI 85].

The energy resolution of SBDs for incoming heavy ions is somewhat disappointing. By comparison to a gas ionization chamber, the energy required to create an electron-hole pair in a semiconductor like Si is about a factor of ten smaller than the energy needed to form an electron-ion pair in a gas. From this observation an energy resolution improved by a factor of roughly three could have been anticipated for a SBD. This has proved to be not correct. There are three distinct contributions usually invoked to explain the unexpectedly poor energy resolution of SBDs for heavy ions: straggling of the energy loss in the entrance window (dead layer) of the SBD, straggling of the recombination loss in the column of dense plasma along the particle track, and straggling in the total charge produced due to atomic ("nuclear") collisions converting part of the incoming energy into lattice defects and vibrations. The above three effects bring about an even more serious difficulty when calibrating the response of SBDs to heavy ions. It is well known that heavy ions being detected in a SBD suffer a so-called pulseheight defect (PHD) compared to light ions as e.g. protons or α-particles. For a definition of the PHD Δ we refer to fig. 3 [FIN 85]. The figure shows schematically the response function, i.e. incoming energy E versus pulseheight X produced, of a SBD for a light and heavy ion, respectively. As borne out by the schematic, for the same energy E a heavy ion delivers a smaller pulseheight X than a light ion, which justifies the name "pulseheight defect". Slightly misleading, though, the PHD Δ is commonly defined as the difference between the energy E of a heavy ion and the energy of a light ion E_{LI} yielding the same pulseheight X (s. fig. 3). As proposed by H.W. Schmitt et al. [SCH 65] the response function of SBDs for heavy ions may conveniently be parametrized as

$$E = (a + a'M)X + (b + b'M) \tag{1}$$

with M the mass of the heavy ion and a through b' being constants having to be determined for each detector individually. For light ions the respons function is simply

$$E_{LI} = wX \tag{2}$$

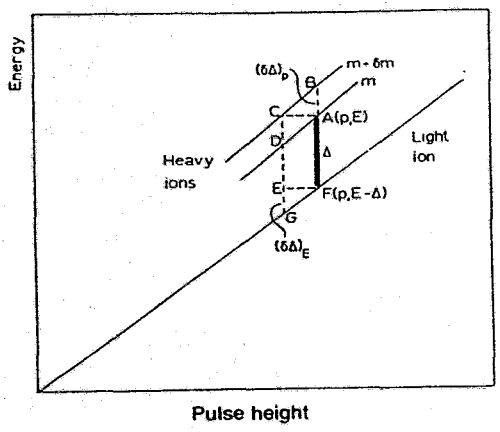

Fig. 3: Schematic presentation of the response function of a surface barrier detector for light and heavy ions. The pulseheight defect Δ is indicated in the figure. From [FIN 85].

with w the energy lost per $e^- - h^+$ pair created. The PHD Δ is then found to be

$$\Delta = E - E_{LI} = (a + a'M)X + (b + b'M) - wX \quad . \tag{3}$$

The PHD has been studied over and again (s., e.g. [FIN 85]). Results from an often quoted more recent systematic investigation of PHDs are presented in fig. 4 [OGI 86]. The PHD is plotted as a function of the incident energy for ^{63}Cu, ^{79}Br and ^{127}I ions. Each panel corresponds to a different detector (ORTEC) with resistivities ranging from $\varrho = 436\Omega$ cm (No.2) to 7700 Ω cm (No.1). The PHD behaves quite similarly for all detectors and increases, both with incident energy and mass of the ion. The authors have derived an empirical analytical function for the PHD which is depicted in fig. 4 as a solid curve for comparison with the experimental data points. The empirical relation is seen to fit closely the experimental results. Also the dependence of the PHD on the electric field strength or bias voltage (not shown in fig. 4) is well described by this relation. Nevertheless, the prescription having been given for the PHD should not be adopted without care for semiconductor diodes from different manufacturers or having been fabricated by different techniques (s. below).

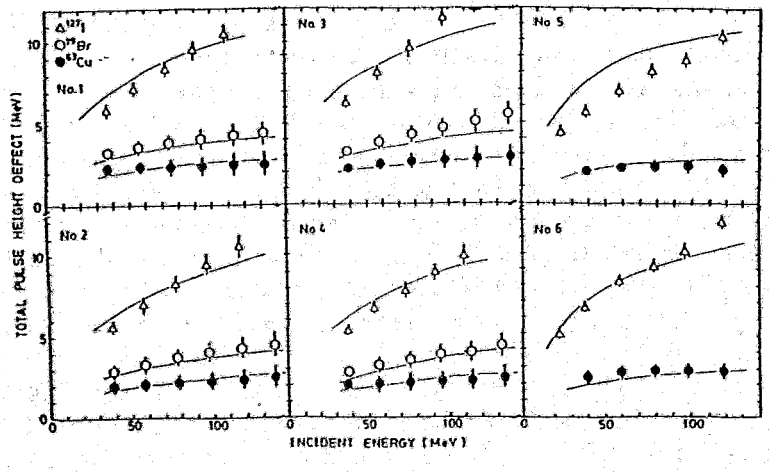

Fig. 4: Total pulseheight defect for several heavy ions and various surface barrier detectors as a function of incoming energy. From [OGI 86].

A new type of semiconductor detector, the PIN diode, has been introduced to fission research in recent years. The PIN diode is made from intrinsic Silicon being doped on the front and rear side of the wafer by ion implantation. Serving usually as a photo diode, its large scale production leads to

attractive prices. Though having been developed with a completely different application in mind, the performance of PIN diodes for detecting fission fragments is remarkable. This is demonstrated in fig. 5 where a pulseheight spectrum similar to fig. 1 obtained again on the LOHENGRIN spectrometer but for $A/q = 4$ is shown [SPI 92]. The energy resolution to be read from the figure

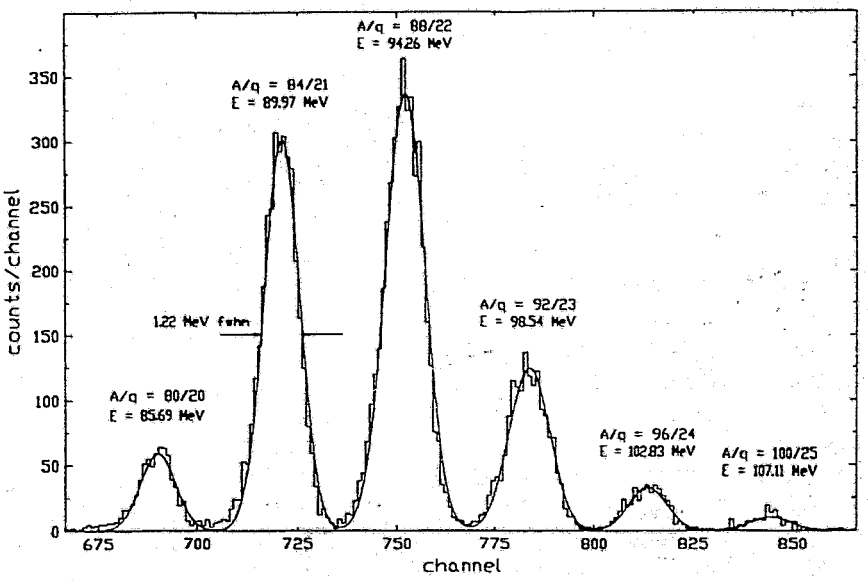

Fig. 5: Pulseheight spectrum of a PIN diode for fission fragments with $\Delta A = 4$ and $\Delta E = 4.29$ MeV. From [SPI 92].

for the mass number $A = 84$ at the incident energy $E \approx 90$ MeV is $\delta E = 1.22$ MeV. For fission fragments from the heavy mass group the energy resolution is typically $\delta E \approx 2$ MeV. These figures compare favorably with those reported for the standard SBD. On the other hand, the PHD for PIN diodes appears to be larger than for dedicated heavy ion SBDs. In fig. 6 the PHD for several PIN diodes from the same brand (SIEMENS) is plotted as a function of the incident ion energy [SPI 92], together with earlier data for an ORTEC heavy ion SBD [FIN 77]. PHD data are shown for three different mass numbers: $A = 84, 101$ and 140 for the PIN diode, and $A = 86, 101$ and 140 for the SBD labelled f. First of all the scatter in the PHD values for given mass and energy catches the eye which for the diodes analyzed amounts to ± 1 MeV. Second, compared to the SBD, the PHD is roughly twice as large for the PIN diode. It should be noted in passing that the PHD for the SBD from the earlier study ([FIN 77] in fig. 6) seems to be systematically lower by about 1 MeV than for the SBDs of more recent production ([OGI 86] in fig. 4), though manufactured by the same company. This underlines the warning given above that it is not advisable to rely on a universal PHD relationship.

An interesting proposal is to exploit the channeling of ions in the single crystal of a semiconductor device. Ions travelling in a channel should suffer no head-on collisions and the longer range, or, equivalently, lower specific ionization should reduce recombination losses. Both effects should help improve the performance of a detector operated in the channeling mode. The response of a channeling detector to fission fragments has been studied in detail at the electromagnetic spectrometer in Tashkent [ALE 92 a]. The pulseheight spectrum for fission fragments with mass number $A = 137$ and kinetic energy $E = 67.3$ MeV is displayed in fig. 7. In the left panel the fission fragment beam entered the detector at an angle of 3° with respect to the $< 110 >$ crystal axis. No channeling is observed. In the right panel the $< 110 >$ crystal axis was oriented parallel to the fragment beam. Two distinct peaks show up in the spectrum. The peak at lower pulseheight corresponds to unchanneled ions (cf. left panel) while the peak shifted to larger pulseheights is due to channeled ions. Evidently, the energy resolution in the channeling mode is markedly improved. Typically, for the

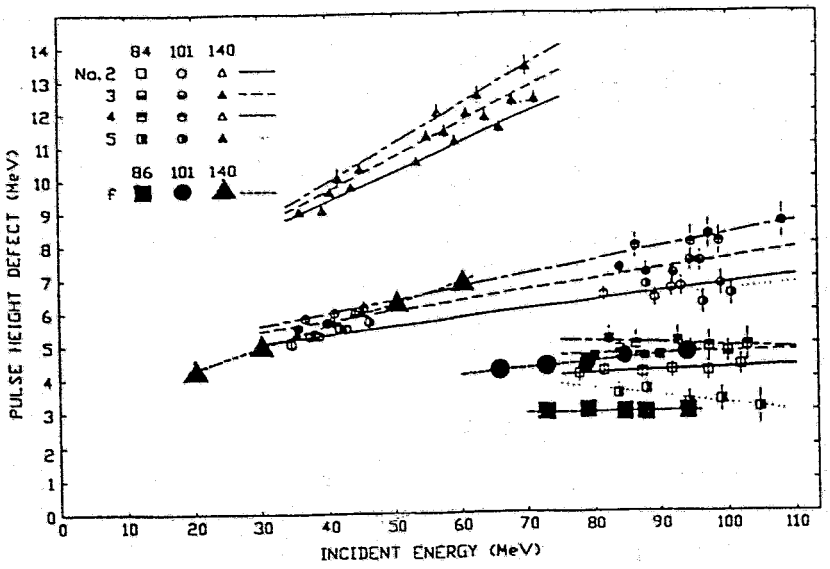

Fig. 6: Pulseheight defect of several PIN diodes (labelled No. 2 through 5) for fission fragments with mass numbers $A = 84, 101$ and 140 as a function of incident energy (small symbols). Same for ORTEC SBD for mass numbers $A = 86, 101$ and 140 (labelled f, large symbols). From [SPI 92].

heavy mass group an energy resolution δE better than $\delta E \approx 1$ MeV is reported and, hence, a gain in resolving power by a factor of 2 is achieved compared to the standard operation of a SBD. It is also found that, the energy loss in the contacting electrode at the surface taken apart, the PHD has dropped to virtually zero in the channeling mode. These are very appealing features. Drawbacks of the channeling technique are the small admissible divergence ($\lesssim 0.5°$) of the ion beam and the fact that, even for perfectly aligned crystals, the fraction of channeled ions does not exceed some 85% [ALE 92 b]. To take full advantage of the technique, the unwanted background due to unchanneled ions has to be suppressed. Possibly, channeled and unchanneled ions could be disentangled by inspecting the timing signal from the diode relative to an independent time-pick-off device in front of the SBD.

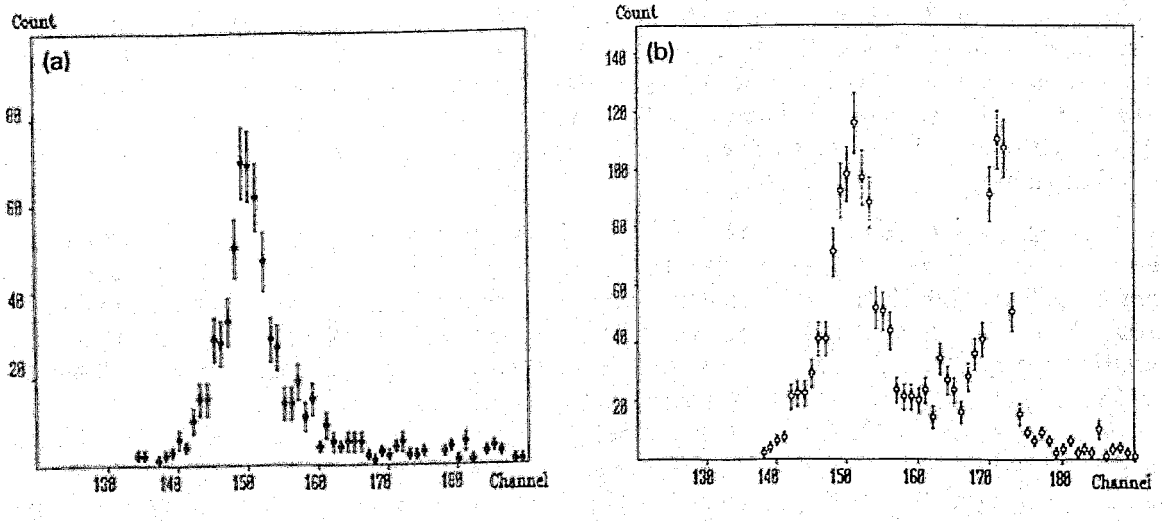

Fig. 7: Pulseheight spectra for fission fragments with mass number $A = 137$ and energy $E = 67.3$ MeV. Left panel (a): angle between FF beam and detector crystal axis $< 110 >$ set to 3°; right panel (b): FF beam parallel to $< 110 >$ crystal axis. From [ALE 92a].

2.3 IONIZATION CHAMBERS

There has been a spectacular comeback of detectors for fission fragments based on the collection of electric charge produced upon the passage of an ionizing particle through gas. The simplest device of this type is the classical ionization chamber (IC) consisting of 2 plane electrodes, a cathode and an anode, placed inside a gas volume. In the operation mode as IC the bias voltage is sufficiently low to avoid charge multiplication, either by electrons in the gas or by ions hitting the cathode. The anode is usually shielded by a Frisch grid and the energy of ions being stopped in the gas is deduced from the electron charges collected on the anode. The ions may enter the sensitive gas volume either perpendicularly to the electric field set up between cathode and anode, or parallel to the field. In the latter case the cathode serves simultaneously as entrance window for ions having been generated outside of the chamber. For reasons to become clearer below, a chamber with this design is called a "Bragg ionization chamber" (BIC).

There are several advantages to be mentioned in favor of ICs compared to SBDs. The specific ionization density in a gas is lower than in a semiconductor material and recombination losses are expected to be reduced accordingly. The harmful influence of atomic (nuclear) collisions may be minimized by employing gases with light constituents like methane, isobutane etc. The thin entrance window separating the sensitive gas volume from the outside (e.g. vacuum) is a delicate part of any IC but, at least, the dead layer due to the window is under better controll of the experimentalist than the dead layer of an SBD. Finally, by continuously exchanging the counting gas any radiation damage to the chamber should be prevented.

Nevertheless, for an IC operated with a light gas, the excellent resolving power for the kinetic energy of fission fragments came as a surprise. An example is provided in fig. 8 [OED 83]. With

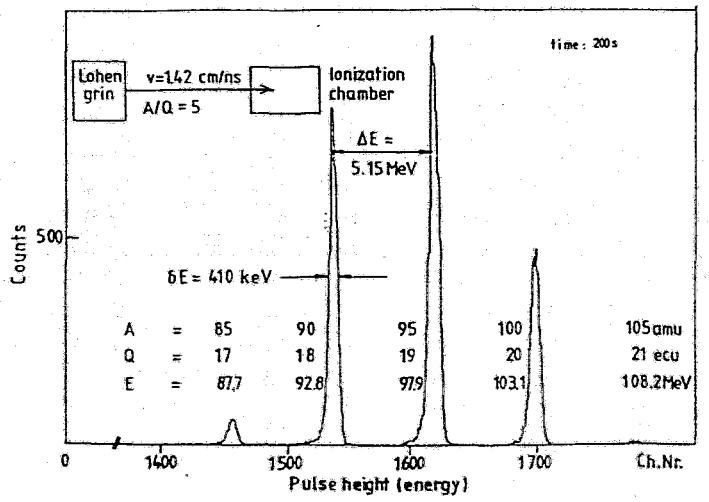

Fig. 8: Pulseheight spectrum of a Bragg ionization chamber for fission fragments with $\Delta A = 5$ and $\Delta E = 5.15$ MeV. From [OED 83].

isobutane (iC_4H_{10}) as gas, the energy resolution was analyzed on the Lohengrin spectrometer and found to vary between $\delta E = 0.4$ MeV and 0.7 MeV for fragments ranging from the light through the heavy mass group. Compared to a SBD (s. fig. 1) this represents a gain in resolution by a factor of 3. It was further observed that the energy resolution depended crucially on the thickness of the polypropylene foil the window was made from. This is due to the energy loss and, hence, energy straggling introduced by the windows (as a rule of thumb, for a thin foil, the energy straggling amounts to 10% of the energy loss). Extrapolating to foil thickness zero, i.e. a windowless chamber, the intrinsic energy resolution of the chamber was estimated to be $\delta E \approx 100$ keV. The findings has been corroborated in an investigation of cold fission [SIM 90]. Since in cold fission, i.e. for the limiting case of large kinetic energy release close to the Q-value, no neutrons are emitted, the masses M_1 and M_2 of two complementary fission fragments are accurately determined

from a measurement of their energies, E_1 and E_2:

$$M_1/M_2 = E_2/E_1 \quad . \tag{4}$$

The experimental setup chosen was a twin Bragg ionization chamber, the two sections of the chamber being mounted back-to-back and sharing a common cathode. The counting gas was pure methane. A thin fissile ^{235}U-target (thickness a few $\mu g/cm^2$) on a thin C-backing (thickness $5\mu g/cm^2$) covering a hole at the center of the cathode was irradiated by thermal neutrons. Complementary fragments were intercepted by the two sections of the chamber. A mass spectrum obtained in the cold fission region is shown in fig. 9. It should be pointed out that the spectacular mass resolving power in fig. 9 is only to be achieved if the intrinsic energy resolving power of the chamber is not impaired by energy straggling in the target and backing. This requirement puts stringent demands on the quality of both target and backing.

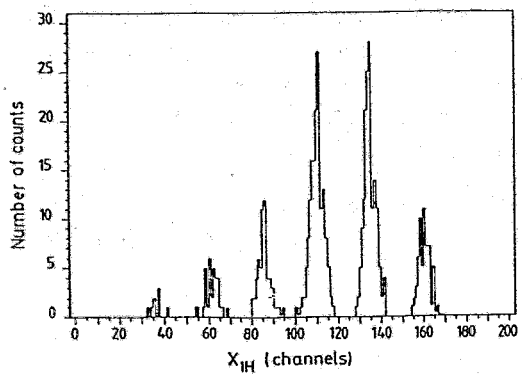

Fig. 9: Fragment mass spectrum measured with a twin ionization chamber in cold fission of ^{236}U*. From [SIM 90].

In strange contrast to the outstanding energy resolution of ICs, the question concerning the pulseheight defect in gas-filled detectors and, hence, the energy calibration is still at issue. All studies conducted so far at least agree that the response of an IC is well described by the ansatz of eq. (1) for the parametrization of the PHD. For an often used gas mixture, viz. (90% Ar + 10% CH_4), there appears to be definitely a non-zero PHD. This is shown in fig. 10 where the PHD Δ is plotted

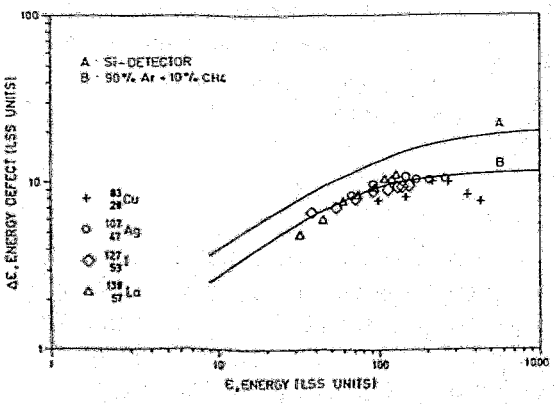

Fig. 10: Pulseheight defect as a function of incident energy for several ions (in LSS units). Curve A: Si-detector. Curve B: ionization chamber with (90% Ar + 10% CH_4) as counting gas. From [BUD 87].

as a function of energy (both in LSS units) for some heavy ions [BUD 87, HAM 93]. Though the PHD for the IC (curve B in fig. 10) is smaller by a factor of 2 compared to a Si-detector (curve A), it is by no means negligible. A similar conclusion was reached for isobutane as the counting gas [WEI 86]. On the other hand, for the windowless twin ionization chamber already mentioned [SIM 90] it has been claimed that the PHD is virtually zero when operating the chamber with methane. The result was inferred from a comparison of the known exact mass in cold fission with the mass

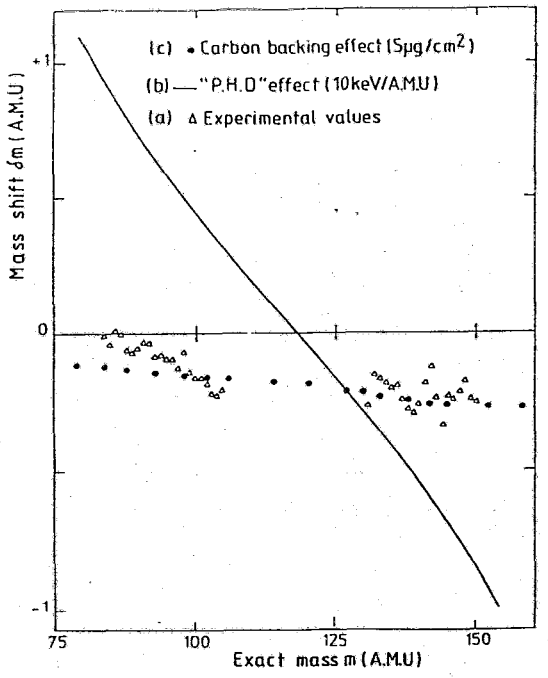

Fig. 11: Mass shift δm between calculated and exact mass for fission events with energy $E = 110$ MeV. Triangles ("experimental values") are calculated with PHD = 0. Full points ("carbon backing effect") take into account energy loss in backing. Curve ("PHD effect") assumes $b' = 10$ keV/amu (s. eq. (1)). From [SIM 90].

calculated from eq. (4) under several assumptions for the PHD. The difference between calculated and exact mass as a function of the latter is mapped in fig. 11 [SIM 90]. The shifts calculated for the PHD set to zero ("experimental values" in fig. 11) are well accounted for by the energy losses in the thin carbon backing, while even a small mass slope of $\partial\Delta/\partial M = 10$ keV/amu for the coefficient b' in eq. (3) is clearly at variance with experiment. It is difficult to conceive that the two gases, methane and isobutane, should behave very differently as to the PHD. For a fair comparison, however, the influence of the entrance window, the ions had to traverse in the isobutane chamber [WEI 86], has to be inspected. The energy loss of fission fragments in polypropylene, a typical window material, is shown in fig. 12 [AIT 90]. The energy loss data were taken on the LOHENGRIN spectrometer and are given for a nominal foil thickness of 100 μg/cm^2, i.e. 2 to 3 times the actual thickness of entrance windows. The energy loss in fig. 12 exhibits a complex pattern as a function of fragment mass and energy. From a detailed analysis of the response of an IC [WEI 86] it is concluded that the contribution to the PHD by the gas is non-zero for isobutane, i.e. at variance with the result quoted for methane. Evidently, the question concerning the PHD in gases employed in ICs still deserves more investigations. It is a pity that the precision in the energy calibration of ICs does not match their energy resolution.

3. VELOCITIES

Velocities of fission fragments are measured by the time-of-flight method. Various working principles have been employed for developing timing detectors. Since no basically new techniques have become known these last years, the reader is referred for details to a recent review [GON 89]. For the sake of completeness the more popular methods are enumerated here.

The timing behaviour of semiconductor detectors has extensively been studied. In principle, timing with resolving powers well below $\delta t = 200$ ps is feasible. A difficulty, however, arises which is linked to the dependence of the pulse shape on the ion's mass, charge and energy. This is demonstrated in fig. 13, where the voltage pulse across a SBD is plotted for α-particles (top panel) and typical fission fragments (bottom panel) [HER 78]. The variation in shape is due to the plasma in the wake of the ion's path which has to decay by diffusion and erosion before an efficient charge collection sets in. The inhibition in the pulse rise time is sensed by the electronics as a "plasma delay".

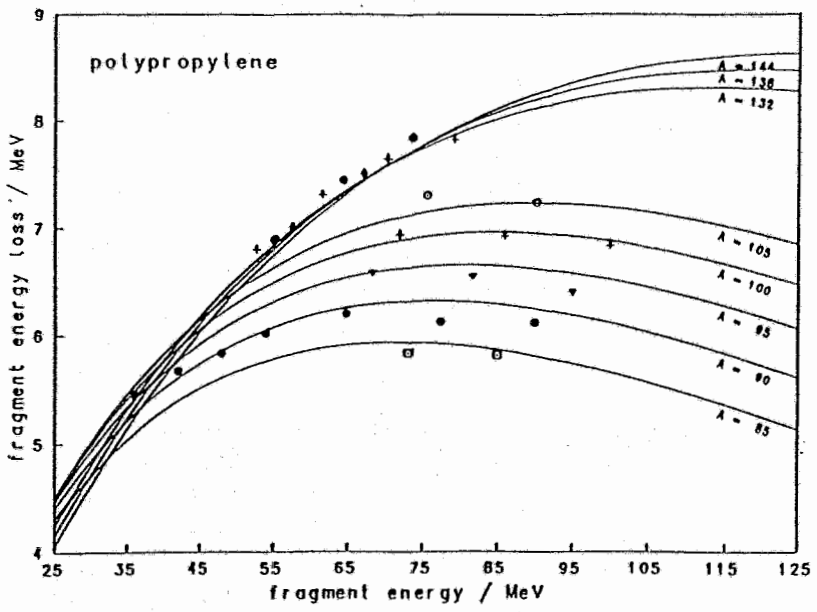

Fig. 12: Energy loss as a function of incident energy for fission fragments with masses ranging from $A = 85$ up to $A = 144$ in polypropylene foil with thickness 100 μg/cm^2. From [AIT 90].

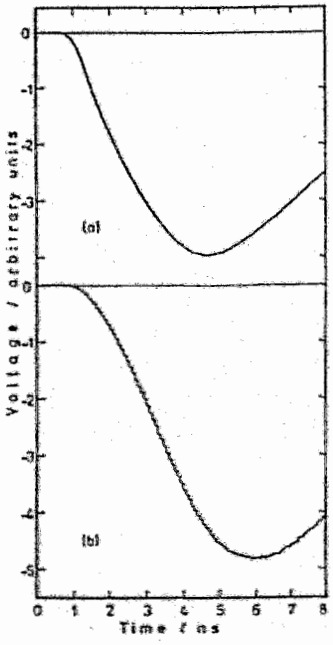

Fig. 13: Voltage pulse in a SBD as a function of time for 6.1 MeV α-particles (panel (a)) and typical light fission fragments from ^{252}Cf(sf) (panel (b)). From [HER 78].

In practical work the plasma delay is delicate to assess and, hence, for demanding applications a semiconductor device is not the appropriate choice.

Gaseous detectors are useful for timing purposes provided fast signals are generated through gas amplification, like in multiwire proportional chambers [CHA 70, BRE 82] or parallel plate avalanche counters [STE 76, BRE 77]. Large area detectors may be built with timing capabilities approaching $\delta t = 100$ ps.

Either semiconductor or gaseous detectors are convenient for providing the stop signal of a time-of-flight setup. Besides good timing, the start detector, on the other hand, ideally has to fulfill

the additional requirement of not altering the ion's velocity to be measured. The condition is best met by detectors sensing the secondary electrons emitted from a thin foil when an ion traverses the foil. The foil can be made very thin, corresponding to energy losses for fission fragments of typically $\Delta E \approx 1$ MeV. The electrons are conventionally registered by multichannel plates delivering a fast timing signal. Various schemes have been proposed for deflecting the electrons without perturbing the ion's path: magnetic deflection [ZEB 77], electrostatic deflection [BUS 80], multichannel plates with a central hole for the free passage of ions [OED 81, NAG 88]. With these devices timing resolutions well below $\delta t = 100$ ps have been achieved. Still further improvements may be expected by carefully so shaping the electron collecting anodes that fluctuations in the transit time of electrons from the foil to the anode and/or in the signal travelling time across the anode to the pickup cable are minimized.

As a side remark we should like to point out that, with the above highly performing timing devices, fission fragment velocities can nowadays be determined quite reliably. It may, therefore, be suggested that time has come to reach an agreement on absolute calibration standards for fission fragment velocities and, in the wake, possibly also kinetic energies. A convenient standard reaction could be spontaneous fission of ^{252}Cf. The reaction has been studied once more in two recent experiments with high precision in mind [HEN 81, KIE 92]. Results for the average velocities, $< V_L >$ and $< V_H >$, and the standard deviations, σ_L and σ_H, of the velocity distributions for the light (L) and heavy (H) group, respectively, are summarized in table 1. As seen from the table, there is assuring agreement in the outcome of the two experiments. The data may, hence, serve with confidence as a base for calibration purposes.

Table 1
Velocity data for fission fragments from ^{252} Cf(sf)

	$< V_L >$ cm/ns	σ_L cm/ns	$< V_H >$ cm/ns	σ_H cm/ns
HEN 81	1.367 ± .006	.067	1.034 ± .005	.081
KIE 92	1.369 ± .009	.064	1.035 ± .007	.078

4. MASSES

For the accurate determination of fission fragment masses electromagnetic separators like LOHENGRIN are unrivalled. Detector based instruments are generally much less performing, the only exception being twin ionization chambers for the special case of cold fission studies (s. fig. 9). The least ambiguous approach to final fragment masses (after prompt neutron emission) is to measure simultaneously the fragment's velocity V and kinetic energy E. But even pushing the resolving powers for V and E close to the limits accessible nowadays, as e.g. in the COSI FAN TUTTE spectrometer of the ILL [OED 84], the mass resolution δM in the light group of fissioning actinides is not better than $\delta M \approx 0.6$ amu, and in the heavy group even worse. The shortcomings is to blame on the energy straggling in the entrance window of the ionization chamber used as energy detector in the spectrometer. If, with a little fancy, this drawback could be overcome to reach the intrinsic resolution of ICs, the mass resolving power could be dramatically improved by a factor of 4.

More conventionally fragment masses are obtained from double-velocity or double-energy measurements on correlated fragments and by relying for the evaluation on mass and momentum conservation. It is well-known that, due to neutron evaporation, even for perfect detectors it is excluded to attain a one-by-one mass resolution with this technique. The methods for correcting for neutron emission from the fragments are well established which does not mean that further

refinements should not be envisaged. So far, in most cases, only average neutron corrections have been considered. With some back-up from theory and/or experiment it should be possible to push the evaluation to also include the dependence of neutron emission numbers on the total kinetic energy release in fission [DUR 93].

5. NUCLEAR CHARGES

The measurement of fragment charges by physical methods is delicate and, as yet, not fully satisfactory. A powerful method is to identify specific nuclides among fission fragments by high-resolution γ-ray spectroscopy [PER 93]. Valuable information on independent yields and global charge distributions has been gained by this tool. It must be said, however, that the method is not applicable to all nuclides and that charges cannot be tagged event-by-event.

Bragg curve spectroscopy for measuring fission fragment charges is superior in this respect but, on the other hand, limited so far to studies in the light fragment group. The idea behind Bragg curve spectroscopy is readily explained by referring to fig. 14. The anode current as a function of time

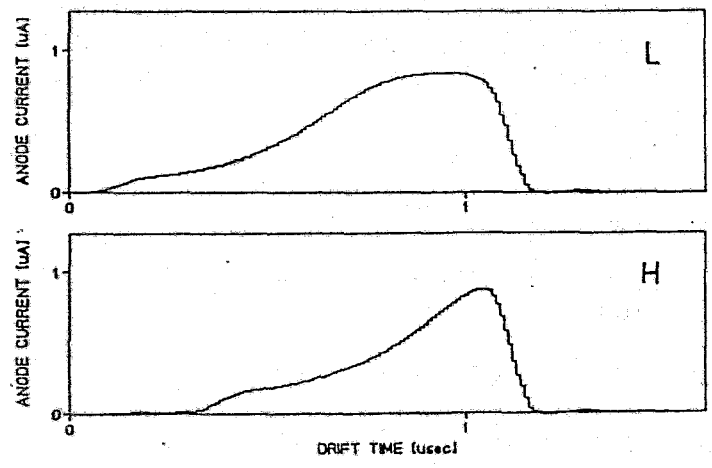

Fig. 14: Anode current in a Bragg ionization chamber as a function of time for typical light (top panel L) and heavy (bottom panel H) fission fragments from ^{235}U(n,f). From [STU 88].

has been registered by a transient recorder in a Bragg ionization chamber (BIC) for typical light and heavy fragments separated by the LOHENGRIN spectrometer [STU 88]. Time zero in fig. 14 corresponds to the time of entrance of the heavy ion through the cathode window into the chamber. This timing signal may be derived from the cathode. In a BIC the anode current as a function of time mirrors the number of electrons having been produced by ionization along the track of an ion as a function of distance from the sensitive grid-anode volume. For a constant drift velocity of electrons in the electric field between cathode and grid, the anode current should fairly reproduce the Bragg curve (specific ionization) of the ion being slowed down in the counting gas. The time integral of the current, i.e. the total electronic charge delivered, is proportional to the total kinetic energy of the ion. The area under the curves and, hence, the energy is seen in fig. 14 to be larger for typical light than for heavy fragments. Relevant for charge separation are, however, the variations in shape of the Bragg curves. The differences in shape for light and heavy fragments are well pronounced in fig. 14 but, unfortunately, in fission the fragments emerge with masses, charges and kinetic energies, where the Bragg curves for neighboring nuclides closely resemble each other. In practice, charge identification of fission fragments has so far only been successful by analyzing the Bragg curves of fragments well separated as to both, masses and energies. The remaining shape variations are in that case uniquely due to the nuclear charge distribution within the sample. It is then sufficient to sense the shape variations by rather gross means. Let us stress once more that only charges smaller than about $Z = 45$ are safely measured with the techniques having been put to work up to now.

In the following some examples of charge separations achieved are given. Best results have been obtained applying the otherwise well-known $\Delta E - E$ method with a passive ΔE energy absorber [QUA 79]. Mass and energy separated fragments from LOHENGRIN passed a thin foil made from Parylene C and the residual energy was determined with a high resolution IC. A charge distribution observed is plotted in fig. 15. In principle a gain in resolution should be expected by measuring

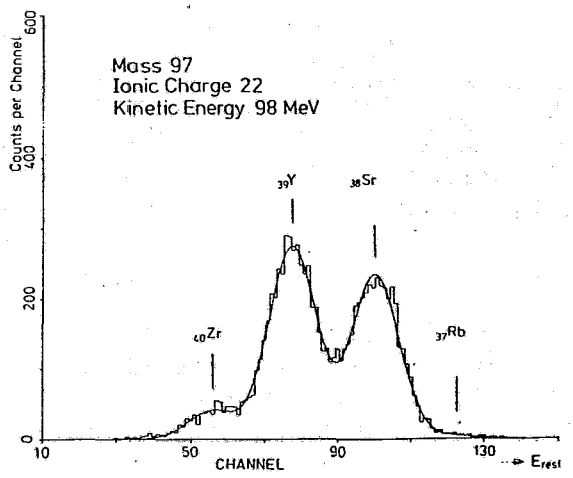

Fig. 15: Pulseheight spectrum of residual energy for fission fragments with mass $A = 97$ and initial energy $E = 98$ MeV having passed through an absorber foil of parylene C. From [QUA 79].

actively the energy loss ΔE on a well-defined part of the track. An obvious approach is to use a standard IC (with field lines perpendicular to the particle's path) and to subdivide the anode into two sections, a ΔE-section for the initial part of the track and a E-section for the residual part [BOC 88]. A charge distribution obtained with a split-anode IC for fragments of mass $A = 78$ and energy $E = 92$ MeV on the LOHENGRIN spectrometer is shown in fig. 16.

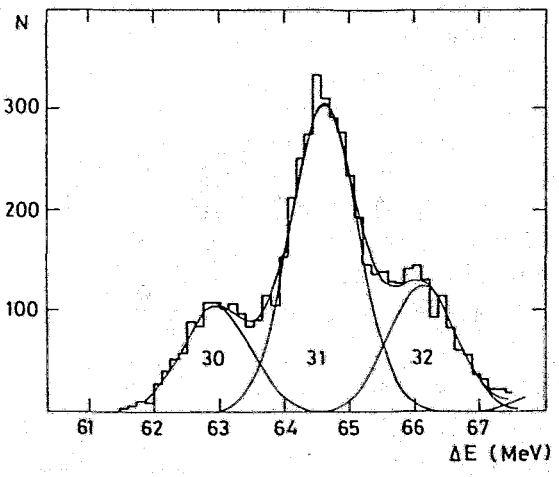

Fig. 16: Spectrum of energy loss ΔE for fission fragments with mass $A = 78$ and energy $E = 92$ MeV in an ionization chamber with split $\Delta E - E$ anodes. Charge numbers 30 to 32 are indicated. From [BOC 88].

Alternatively, but again for mass and energy separated fragments, the ranges of ions in e.g. a gas carry information on their nuclear charges. In a Bragg IC the range is found from the minimum drift time of electrons to the anode (s. fig. 14), since the first electrons to arrive at the anode are those generated at the very end of the track [OED 83]. The method has been tested on LOHENGRIN and a charge distribution for fragments with mass $A = 97$ and energy $E = 96$ MeV is presented in fig. 17. The range method has been applied very successfully in studies of cold fission with a twin BIC [SIM 90]. Charge distributions for the mass ratio 104/132 of fission fragments from $^{236}U^*$ are shown in fig. 18 for different windows in total kinetic energy [SIG 91].

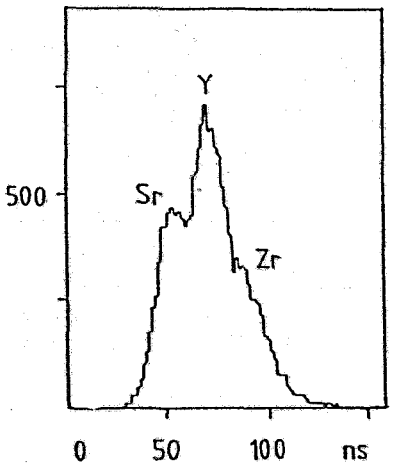

Fig. 17: Charge resolution for fission fragments with mass $A = 97$ and energy $E = 96$ MeV obtained by the range method (minimum electron drift time) in a Bragg ionization chamber. From [OED 83].

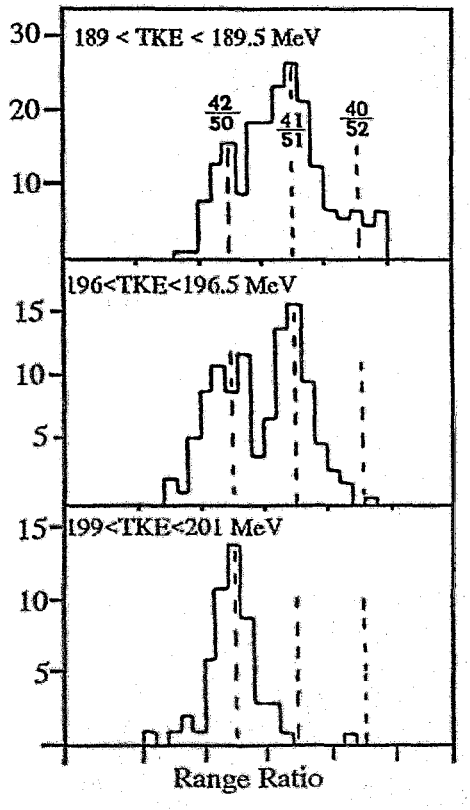

Fig. 18: Charge resolution for fission fragments with mass ration $A_L/A_H = 104/132$ from ^{235}U(n,f) in different total kinetic energy windows obtained by the range method in a twin Bragg ionization chamber. From [SIG 91].

Still another variant of Bragg curve spectroscopy has been proposed for a twin BIC [BUD 87] and put to work for investigating cold fission of ^{252}Cf(sf) [KNI 92]. In this variant signals from all three electrodes of an IC, i.e. cathode, grid and anode, are processed to determine the nuclear charges of fragments from the center of gravity of the charges produced by ionization in the gas.

All methods discussed above have in common to extract for identification of nuclear charges only one single parameter from the Bragg curve, viz. ΔE, or the range, or the center of gravity of ionization charges. It may be wondered whether a more comprehensive analysis of the shape of the Bragg curve could not yield higher resolving powers for nuclear charge. A promising step in this direction has been reported recently for semiconductor detectors [PAU 92]. By analyzing in more detail than heretofore the pulseshape of detector signals, charge numbers up to $Z = 16$ could be resolved for fast fragments. A similar procedure should be applied to the anode signals

from ionization chambers. Especially Bragg ICs appear to be well suited for implementing more advanced techniques of data handling. In fact, the anode current signals shown in fig. 14 represent Bragg curves taken with a BIC and digitized with a transient recorder. These digitized data are directly amenable to a thorough shape analysis of the Bragg curve, encompassing and, hopefully, superseding both, the Δ and the range method. To this purpose the data have to be transferred event-by-event to a small on-line computer and a judiciously chosen function has to be fitted to the data. Guided by theory, the fit parameters should be optimized to yield, besides the fragment energy, the best feasible charge resolution. Note that the analysis should start from mass-separated fragments to yield optimum charge resolution. The technique should on the other hand prove useful to measure the angle between the fragment track and the chamber axis and, most interesting, to identify events having been scattered in targets, backings, entrance windows or by atomic collisions. Of course, the tolerable count rate for the proposed mode of analysis will be limited to some 100 Hz but, for high resolution experiments, the count rate in ICs should anyhow not much exeed this figure.

6. CONCLUSIONS

The present survey of experimental tools for high resolution spectroscopy of fission fragments attempts to point out shortcomings of existing techniques and — in some cases — to suggest improvements. Attention is drawn to the following difficulties and remedies:

1) Energy measurements with either semiconductor or gaseous detectors are hampered by the pulseheight defect. It appears that no general rules, how to correct the response function for the defect, can be given which means that each detector has to be calibrated for heavy ions. Especially our knowledge on the pulseheight defect in different gases used in ionization chambers is scarce. More systematic investigations are definitely needed. The defect in gases might be expected to depend smoothly on gas composition and pressure, electric field strength etc. Once the defect is under control, the response of ionization chambers to heavy ions may be predicted from a calibration with light ions (α-particles) provided the energy loss in entrance windows or, for internal targets, in backings and targets is duly taken into account.
   The intrinsic energy resolution of ionization chambers comes close to the one for electromagnetic separators under actual working conditions. A promising new technique is to operate semiconductor detectors in the channeling mode.

2) Time pick-off detectors for velocity measurements have reached a satisfactory state of development. This is especially true for detectors sensing secondary electrons emitted from thin foils upon passage of an ion with multichannel plates. Some, probably only minor, improvements of these detectors could be foreseen by appropriately shaping the anodes collecting the electrons. The high precision of recent experiments should allow to reach a generally accepted agreement on a still missing standard for the calibration of velocities. A standard with ^{252}Cf(sf) as the reference is proposed.

3) Mass measurements rely on energy and velocity detectors. They will profit from any gain in performance of these detectors. The determination of masses by the popular (2E)- or (2V)-methods is impaired by neutron emission from the fragments. In the evaluation of data the corrections for neutron evaporation could be pushed one step further by taking into account not only the dependence of average neutron number on fragment mass but also the dependence of neutron number on kinetic energy release.

4) The measurement of nuclear charges of fission fragments is still in a not too satisfactory state. The technique of γ-ray spectroscopy is limited to a few selected nuclides, while Bragg curve spectroscopy has so far not met the challenge to identify charges in the heavy fragment group. A more powerful shape analysis of Bragg curves, as e.g. those observed in Bragg ionization chambers, may lead to significant progress in charge resolving power.

It is a pleasure to acknowledge help in the preparation of this report by M. Ait Salem, U. Graf, M. Khalil and A. Möller. The work was supported by the BMFT/Bonn under contract number 06 TÜ 243.

References

[AIT 90] M. Ait Salem, et al., Verhandl. DPG (VI) 25 (1990) 1483, and to be published
[ALE 92a] A.A. Alexandrov, et al., Nucl. Instr. Meth. **A312** (1992) 542
[ALE 92b] A. A. Alexandrov, et al., Rad. Effects 124 (1992) 191
[ARI 72] U.A. Arifov, et al., Sov. Phys. Doklady 17 (1972) 485
[BOC 88] J.P. Bocquet, et al., Nucl. Instr. Meth. **A267** (1988) 466
[BRE 77] A. Breskin, et al., Nucl. Instr. Meth. **A146** (1977) 461
[BRE 82] A. Breskin, Nucl. Instr. Meth. **A196** (1982) 11
[BUD 87] C. Budtz-Jørgensen, et al., Nucl. Instr. Meth. **A258** (1987) 209
[BUS 80] F. Busch, et al., Nucl. Instr. Meth. **171** (1980) 71
[CHA 70] G. Charpak, Ann. Rev. Nucl. Sci. **20** (1970) 195
[DUR 93] I. Düring, et al., these proceedings
[FIN 77] E.C. Finch, et al., Nucl. Instr. Meth. **142** (1977) 539
[FIN 85] E.C. Finch, et al., Nucl. Instr. Meth. **A228** (1985) 402
[GON 89] F. Gönnenwein, Nucl. Phys. **A502** (1989) 159 c
[HAM 93] F.-J. Hambsch, these proceedings
[HEN 81] H. Henschel, et al., Nucl. Instr. Meth. **190** (1981) 125
[HER 78] B. Hering, et al., Nucl. Instr. Meth. **153** (1978) 235
[KIE 92] J. Kieseweter, et al., Nucl. Instr. Meth. **A314** (1992) 125
[KNI 92] H.-H. Knitter, et al., Nucl. Phys. **A536** (1992) 221
[MOL 75] E. Moll, et al., Nucl. Instr. Meth. **123** (1975) 615
[NAK 88] T. Nakagawa, et al., Nucl. Instr. Meth. **A271** (1988) 523
[OED 81] A. Oed, et al., Nucl. Instr. Meth. **179** (1981) 265
[OED 83] A. Oed, et al., Nucl. Instr. Meth. **205** (1983) 451 and 455
[OED 84] A. Oed, et al., Nucl. Instr. Meth. **219** (1984) 569
[OGI 86] M. Ogihara, et al., Nucl. Instr. Meth. **A251** (1986) 313
[PAU 92] G. Pausch, et al., Nucl. Instr. Meth. **A322** (1992) 43
[PER 93] K. Persyn, et al., these proceedings
[QUA 79] U. Quade, et al., Nucl. Instr. Meth. **164** (1979) 435
[SCH 65] H.W. Schmitt, et al., Phys. Rev. **B137** (1965) 837
[SIG 91] C. Signarbieux, Proc. "Dynamical Aspects of Nuclear Fission", Smolenice, CS 1991, p 19
[SIM 90] G. Simon, et al., Nucl. Instr. Meth. **A286** (1990) 220
[SPI 92] A. Spieler, diploma thesis, TH Darmstadt 1992
[STE 76] H. Stelzer, Nucl. Instr. Meth. **133** (1976) 409
[STU 88] B. Stütz, PHD thesis, Univ. Tübingen, 1988
[WEI 85] E. Weissenberger, PHD thesis, Univ. Tübingen, 1985
[WEI 86] E. Weissenberger, et al., Rad. Effects 96 (1986) 47
[ZEB 77] A.M. Zebelman, et al., Nucl. Instr. Meth. 141 (1977) 439

Experimental determination of corrections for fission fragment investigations using a Frisch gridded ionization chamber

F.-J. Hambsch
JRC-CBNM, Steenweg naar Retie, B-2440 Geel, Belgium

Abstract

Although the invention of the ionization chamber dates back nearly 50 years the last decade has seen a remarkable revival of this device for charged particle detection. It has become apparent that such a detector has distinct advantages. Not only does the ionization chamber allow measurements of total particle energy with energy resolution far superior to that of surface barrier detectors but also simultaneously the particles' specific ionization density distribution (the socalled Bragg-curve) can be determined. Therefore, besides the particle kinetic energy, mass and angular distribution, also information about the atomic number of the detected ion can be obtained using a double Frisch gridded ionization chamber. This type of detector is in use at CBNM since almost 10 years. It has been substantially improved during this period. The special electronic treatment of the chamber pulses will be described. The necessary corrections to the raw chamber signals will be demonstrated step by step giving typical key-figures and the way they are implemented. An error estimation will be given too.

1 Introduction

Ionization chambers with Frisch grids were used as early as in the 40's for charged particle detection. Already in 1949 Bunemann et al. [1] discussed in detail signal generation and corrections to be applied due to grid inefficiency and electron losses due to diffusion. However, with the advent of commercially available solid state surface barrier detectors of high quality some 30 years ago the interest in ionization chambers was strongly reduced. The last decade in contrast has seen a remarkable revival of the ionization chamber due to the fact that it became apparent that this detector has distinct advantages. At CBNM several ionization chambers have been developed over the past 10 years and successfully applied to charged particle counting ranging from protons, alphas, fission fragments to low energetic heavy ions [3]-[6]. Although a paper about the chamber and signal generation and treatment has been published [7] not all the details and implementations of the corrections had been given. Furthermore the ionization chamber originally developed at our institute has been copied at several places. So this paper is intended to clarify the different steps of the analysis.

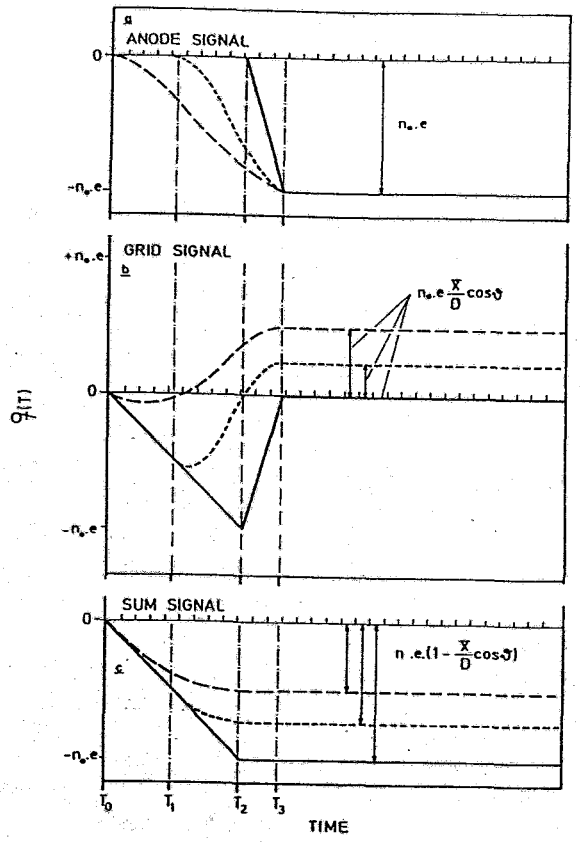

Figure 1: Time dependence of the ionization chamber signals. The curves are given for $cos\theta$=0 (full line), $cos\theta$=0.5 (dotted line) and $cos\theta$=1 (dashed line).

2 Signal generation and treatment

The chamber construction and signal generation has been treated in different papers [3]-[6] and in even more detail in PhD thesis works [8, 9]. Nevertheless, as at other places copies of our design are in operation and sometimes questions concerning signal treatment arise, it was found necessary to repeat part of it with special emphasis on the corrections which have to be applied to the raw signals. The most crucial point is the grid signal, due to its complicated time dependence as seen in Fig. 1. As long as the electrons move towards the grid, negative charges are induced. But positive charges are induced as the electrons move away from the grid to the anode. The total charge induced therefore is

$$Q_g = -ne(1 - \overline{X}/D\ cos\theta) + ne \qquad (1)$$

where n is the number of ion pairs created and $\overline{X}$(E,A,Z) is the distance of the centre of gravity of the ionization density distribution from the origin of the track and is in general a function of fragment energy E, mass A, and charge Z. The grid signal is a bipolar signal (see Fig. 1b) and therefore difficult to treat with conventional electronics. A much simpler signal, however, is obtained when the sum of the anode and grid signal is formed electronically, since the electrons moving between grid and anode induce the same charge on the grid and the anode but of opposite sign. The sum signal is given by

$$Q_s = -ne(1 - \overline{X}/D\ cos\theta). \qquad (2)$$

This summation is actually done using wide band amplifiers and splitting of the anode signal

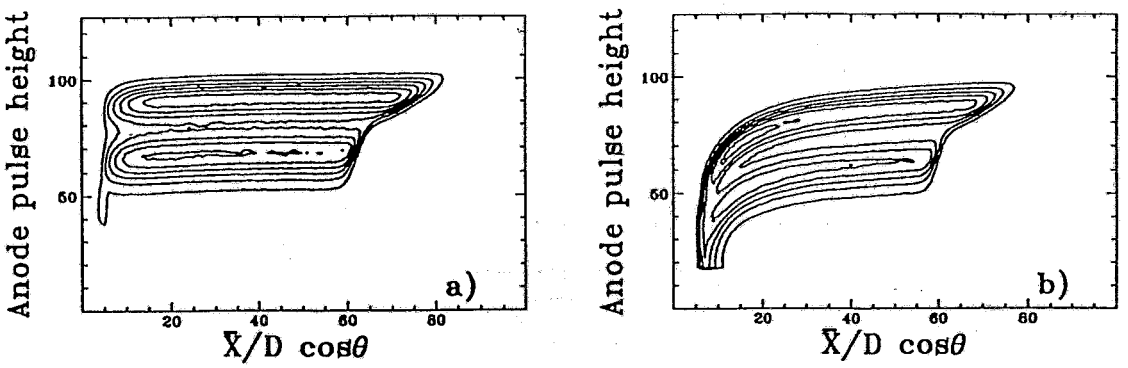

Figure 2: $\overline{X}$/D $cos\theta$ versus energy distributions for both chamber sides in case of ^{252}Cf(sf). a) Only active sample is traversed. b) Active sample and backing are traversed.

to maintain the original information, see e.g. refs. [8, 9]. For fission fragment investigations usually a double Frisch gridded ionization chamber is used. The two anode and sum signals are acquired by a multi parameter acquisition system and stored on disk or tape.

3 Determination of the corrections

The offline analysis starts with a check of the stability of the experiment by monitoring the position of a precision pulse generator peak, continuously connected during the experiment. Electronic drifts are corrected by stabilizing to the pulse generator peak position at the begin of the acquisition period, where a calibration was made. Also the positions of the means of the distributions are checked to assure that not only the pulser peak has drifted.
The next step is to read off the $\overline{X}$/D-values from the experimental distributions needed for the calculation of the angular distribution. For this purpose, the dependence of the grid signal (eq. (1)) on $\overline{X}$/D is used. From the raw anode signal Q_a the sum signal Q_s (eq. (2)) is subtracted giving

$$Q_a - Q_s = ne\overline{X}/D\ cos\theta. \tag{3}$$

Due to electron losses at the Frisch grid, the socalled Frisch grid inefficiency σ (see ref. [1] for details), a correction must be applied to the anode signal, because the $\overline{X}$/D-values should be known as function of the energy of the fragment leaving the target

$$Q_a = Q_a^{unc} + \sigma(Q_a^{unc} - Q_s). \tag{4}$$

Than eq. (3) is divided by the corrected anode signal resulting in an distribution ranging from 0 ($cos\theta = 0$) to $\overline{X}$/D ($cos\theta = 1$) and shown in Fig. 2 for both sides of the fissioning target. It is obvious that there is much more deterioration of the spectral distribution for the part where the fission fragments have to pass in addition to the active material also the backing (Fig. 2b). The $\overline{X}$/D-values are then taken as the length at half height of the spectral shape at each anode pulse height. Doing so the dependence of $\overline{X}$ on fragment energy is taken into account.
One additional remark must be made here concerning the grid inefficiency σ and the voltages applied to the different plates of the ionization chamber. Both are dependent on the chamber dimensions. The grid inefficiency σ can be minimized choosing appropriate radii and distances

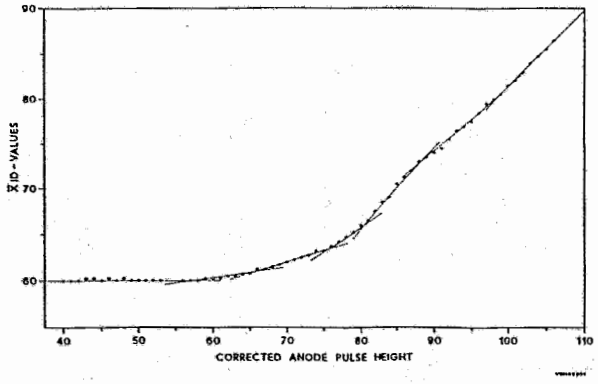

Figure 3: $\overline{X}/D$ values versus energy as read off from Fig. 2

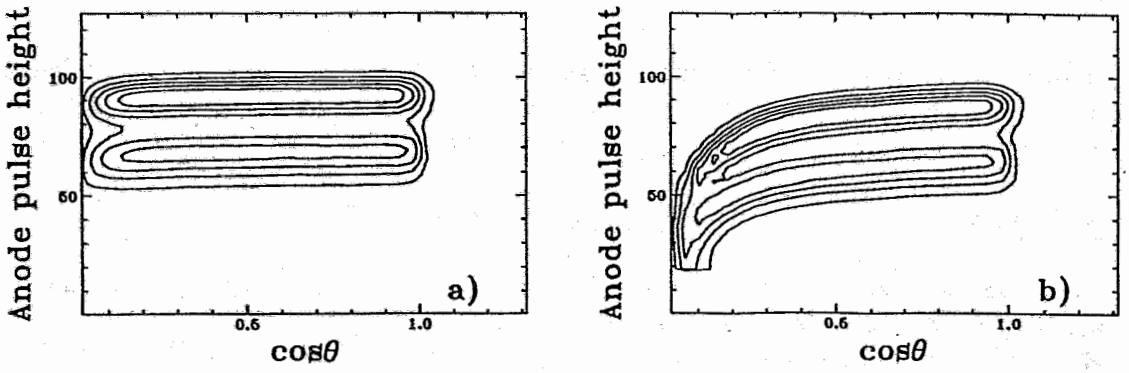

Figure 4: $cos\theta$ versus energy distributions for both chamber sides

of the grid wires. In our applications the values for σ lie typically between 0.015 to 0.030, so the correction applied to the anode is in the order of maximum 3% of eq. (3). The voltages of the cathode V_c, grid V_g and anode V_a have to be chosen to fulfil the following equation

$$\frac{V_a - V_g}{V_g - V_c} \geq \frac{p + p\rho + 2l\rho}{a - a\rho - 2l\rho}, \tag{5}$$

where p, a, l and ρ can be deduced from the chamber dimensions (see ref. [1]). Also the gas mixture used as counting gas has to be considered and chosen according to the experimental needs. Due to differences in the electron drift velocities of different gas mixtures also the voltages applied to the electrodes have to be adapted. If possible a voltage in the plateau region of the drift velocity should be chosen, so that voltage changes do not affect the pulse heights. Figures of drift velocities of different gas mixtures can be found, e. g. in ref. [10]. The $\overline{X}/D$ values read off from the experimental distributions are then plotted in Fig. 3 versus the corrected anode pulse height (eq. (4)). Straight line interpolations are used to reduce the amount of data as seen in Fig. 3. Taking now these interpolated $\overline{X}/D$ values and eq. (3) the distribution as function of $cos\theta$ can be calculated

$$cos\theta = \frac{Q_a - Q_s}{Q_a * \overline{X}/D}. \tag{6}$$

With the knowledge of $cos\theta$ the angle dependent energy loss in the sample and backing can be experimentally determined if the anode pulse height is plotted versus $1/cos\theta$. This is done

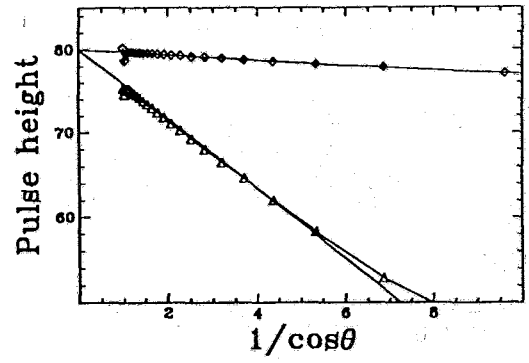

Figure 5: Anode pulse height versus $1/cos\theta$.

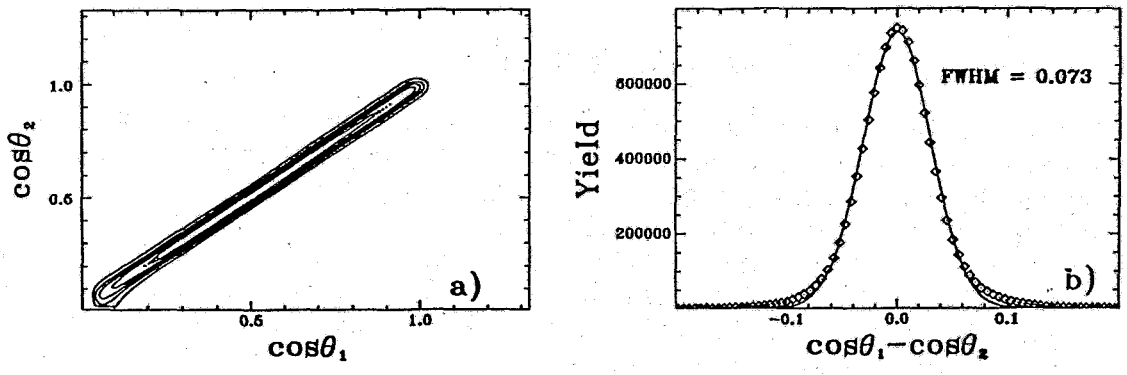

Figure 6: Resolution in angle. a) Two dimensional distribution $cos\theta_1$ versus $cos\theta_2$. b) Difference $cos\theta_1$-$cos\theta_2$ for all fragments and $cos\theta > 0.5$.

because the length of the track within the sample increases with $1/cos\theta$. Fig. 4 shows as example the $cos\theta$ versus anode pulse height distributions for both chamber sides. Calculating the mean of the anode pulse height distribution and plotting it versus $1/cos\theta$ gives the energy loss values to be incorporated into the analysis (Fig. 5).

At this point a crucial calibration check is possible, because the straight line interpolation through the points of both lines must intersect in the same point with the ordinate. If the two chamber sides are, however, not well calibrated the two lines will not coincide at the same intersection. Even calibration differences of less than 1% are visible. The intersection point is a measure of the energy the fragments would have if no energy is lost. The energy loss correction is found by taking the difference to the true energy given by the intersection point and the lines in Fig. 5 and is added in the next analysis step to the anode signal. Again intermediate values are interpolated. Of course due to the finite thickness of the active sample only the mean energy loss can be accounted for. The origin of the fission event within the target is not known. The error due to this fact is dependent on the target thickness. For very thin targets, e.g. ^{252}Cf, shown in Fig. 5, this is certainly below 0.1 MeV and can be neglected. For thicker targets (e.g. 50 $\mu g/cm^2$ $^{235}UF_4$) however, this amounts to about $\pm$ 0.25 MeV. The quality of the angle determination can be demonstrated when the difference $cos\theta_1$-$cos\theta_2$ is plotted (Fig. 6b). This figure shows the achieved angular resolution of FWHM = 0.073 for all fragments and $cos\theta > 0.5$. The subscripts 1,2 refer to the two chamber sides. In Fig. 6a a two dimensional contour plot of $cos\theta_1$ versus $cos\theta_2$ is given, demonstrating the quality of the angle determination.

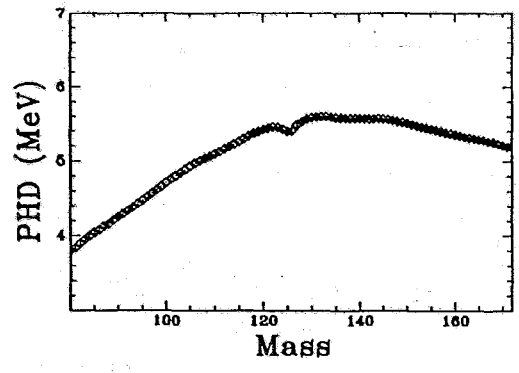

Figure 7: PHD correction as function of mass for ^{252}Cf(sf).

4 Energy and mass calculations

Now the anode signal is corrected in a way that the mass and kinetic energy of the fission fragment can be calculated, as well as the angular distribution. As the energy loss is increasing with increasing angle to the normal on the cathode, the energy determination becomes dubious for large θ. For the mass calculation therefore only fragments in a forward cone ($cos\theta > 0.5$) are taken into account. Yet another quantity, the pulse height defect (PHD) has to be considered. This effect is mainly due to nonionizing collisions between the fragments and the gas. Unfortunately the ionization chamber does not allow to determine the PHD experimentally at the same time with all the other corrections already mentioned. Also the PHD correction is different for surface barrier detectors and ionization chambers. Therefore the PHD was determined at the Physics Institute, University of Åarhus, Denmark [11]. A detailed description of the results is already given in [7]-[9]. Here only the results of the actual PHD correction in the case of ^{252}Cf(sf) with CH_4 as counting gas is given in Fig. 7. However, it is also planned to check the quality of our PHD corrections by calculations performed for given mass and energy of the fission fragments with the TRIM program based on the energy loss tables of Ziegler et al. [12]. Up to now only socalled provisional quantities can be calculated due to the fact that only the energies of the fission fragments are measured. For preneutron quantity calculations the neutron evaporation as function of fission fragment mass and energy must be taken into account. Already with the provisional mass calculations and plotting the resulting mass versus $cos\theta$ (Fig. 8) it is seen that the mass dependence of $\overline{X}$ is not considered yet. An improvement of the $cos\theta$ resolution is possible if this dependence is taken into account [7]. However, the resolution is still limited because the ionization chamber does not allow a complete seperation of individual charges, so the charge dependence of $\overline{X}$ cannot be implemented.

5 Conclusions

This paper is intended to describe in detail the different steps of the analysis of the raw ionization chamber signals. Especially those which have not been mentioned in [7] nor published elsewhere. The critical steps and possibilities for cross checks have been emphazised. The quality of the fission fragment properties determination has been demonstrated in different publications, e.g. [6, 13].

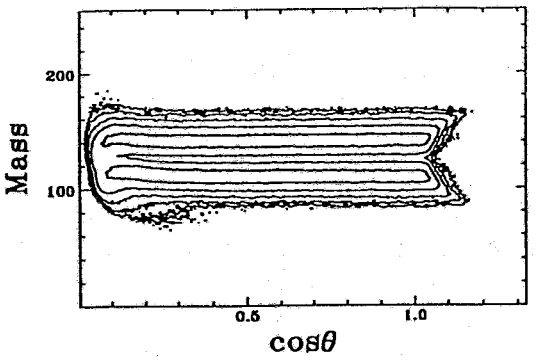

Figure 8: $cos\theta$ versus provisional mass for ^{252}Cf(sf).

References

[1] O. Bunemann, T.E. Cranshaw and J. A. Harvey
Can. J. Res. A27 (1949) 191

[2] C. Budtz-Jørgensen and H.-H. Knitter
Nucl. Instr. Meth. 154 (1978) 121

[3] C. Budtz-Jørgensen and H.-H. Knitter
Nucl. Instr. Meth. 223 (1984) 295

[4] C. Budtz-Jørgensen, H.-H. Knitter and G. Bortels
Nucl. Instr. Meth. A236 (1985) 630

[5] Ch. Stræde, C. Budtz-Jørgensen and H.-H. Knitter
Nucl. Phys. A462 (1987) 85

[6] F.-J. Hambsch, H.-H. Knitter and C. Budtz-Jørgensen
Nucl. Phys. A491 (1989) 56

[7] C. Budtz-Jørgensen, H.-H. Knitter, Ch. Stræde, F.-J. Hambsch and R. Vogt
Nucl. Instr. Meth. A258 (1987) 209

[8] Ch. Stræde
Ph.D thesis, CBNM, Geel, Belgium, 1985

[9] F.-J. Hambsch
Ph.D thesis, TH. Darmstadt, Darmstadt, Germany, 1987

[10] F. Sauli
Internal Report CERN 77-09 (1977)

[11] P.T. Nielsen and N. Rud
University of Åarhus, private communication (1983)

[12] J.F. Ziegler, J.P. Biersack and U. Littmark
The stopping and range of ions in solids,
Pergamon Press, New York (1985)

[13] H.-H. Knitter, F.-J. Hambsch and C. Budtz-Jørgensen
Nucl. Phys. A536 (1992) 221

Cold Fission Studies using a Double-Ionization Chamber*

A. Möller[1], F.Gönnenwein[1], J.Kaufmann[1], G.Petrov[2], I.Düring[3], H.Märten[3], A.Ruben[3], P.Geltenbort[4], and A.Oed[4]
[1] Physikalisches Institut, Universität Tübingen, W7400 Tübingen, Germany
[2] St.Petersburg Nuclear Physics Institut, Gatchina, Russia
[3] Institut für Kern- und Teilchenphysik, O8027 Dresden, Germany
[4] Institut Laue Langevin, 38042 Grenoble, France

Abstract

An investigation on spontaneous fission of ^{252}Cf is described. Both fission fragments are detected coincidentally with a double ionization chamber as a 4 π detector. Special techniques are demonstrated which allow the determination of nuclear masses and charges for cold fission fragments. Detector properties such as systematic errors and their correction are studied with the help of α particles.

Introduction

By definition cold compact fission fragments do not loose neutrons through evaporation. Thus the initial nuclear mass is conserved for both fragment masses A_1 and A_2. Due to momentum conservation the ratio of kinetic energies E_1/E_2 is proportional to the ratio A_2/A_1. In this case, corresponding to the highest total kinetic energies, the exact masses can be determined by the coincident registration of the fragment energies in a double ionization chamber.
This resolution is not obtained in the region of average kinetic energies, where intrinsic excitation energy is distributed stochastically on the fragments and the multiplicity of evaporated neutrons is unknown.
In the case of cold deformed fission /1/, similar to cold compact fission, the initial intrinsic excitations are low. Each of the fragments has a well defined deformation energy at the scission point. The deformation energy is converted into intrinsic excitation energy in well defined amounts for each fragment. For these configurations the number of emitted neutrons is expected to be a constant. Thus there could be a chance to observe fine structure because the sum of A_1 and A_2 will also be a constant.
If the fragment masses are perfectly resolvable, the fragment nuclear charges can be determined by a measurement of the ionization track length in the chamber. Consequently it will be possible to determine the yield for fragment configurations in nuclear mass and charge as a function of total kinetic energy.
Further investigations are planned in the field of far asymmetric fission.

* This work has been funded by German Federal Minister for Research and Technology (BMFT) under the contract number 06TU243.

Principle of the gridded double ionization chamber

Figure 1 shows a cross section of the chamber used in the experiment. All electrodes are axially symmetrical. The cathode at the centre is common to both chambers. The ^{252}Cf source is supported by a 4.4 $\mu g/cm^2$ carbon foil and stretched over the centre hole. The Frisch grids are facing the cathode at a distance l=38 mm. They shield the anodes which are spaced 5.3 mm from the grids. Appropriate electric voltages are applied to the electrodes. The chamber is filled with pure methane (CH_4) at a pressure of 1 bar.
As shown for an arbitrary fission event, the fragments are stopped in the area between cathode and grid. Gas molecules are ionizied along their tracks. All of the produced free electrons drift towards the anodes and penetrate the grids within 300 ns. The anode signal, amplified with a charge sensitive preamplifier, is proportional to the amount of produced ion-electron pairs, which to a first approximation is proportional to the fragment kinetic energy disposited in the gas. Since the anodes are shielded, the pulse rising does not occur before the first electrons penetrate the grid.
The ions remain much longer in the gas because their drift velocity is approximately one thousand times slower. They influence electric charge to the cathode immediately when the electrons drift away. Once the electrons have disappeared, the induced charge on the cathode, originated by a fission decay, will be proportional to the total kinetic energy of both fission fragments and also a function of the emission angle θ with respect to the chamber axis. The normalised cathode pulse-height, i.e. the cathode pulse height divided by the sum of the anode pulse heights, is a monotone function of $\cos\theta$.
Apart from the measurement of pulse heights and emission angle, it is easy to evaluate the distance d between the end of the ionization track and the grid by measuring the time delay from cathode to anode pulse, which is the drift time t of the first electrons penetrating the grid. The relation between track length r, emission angle θ, electron drift

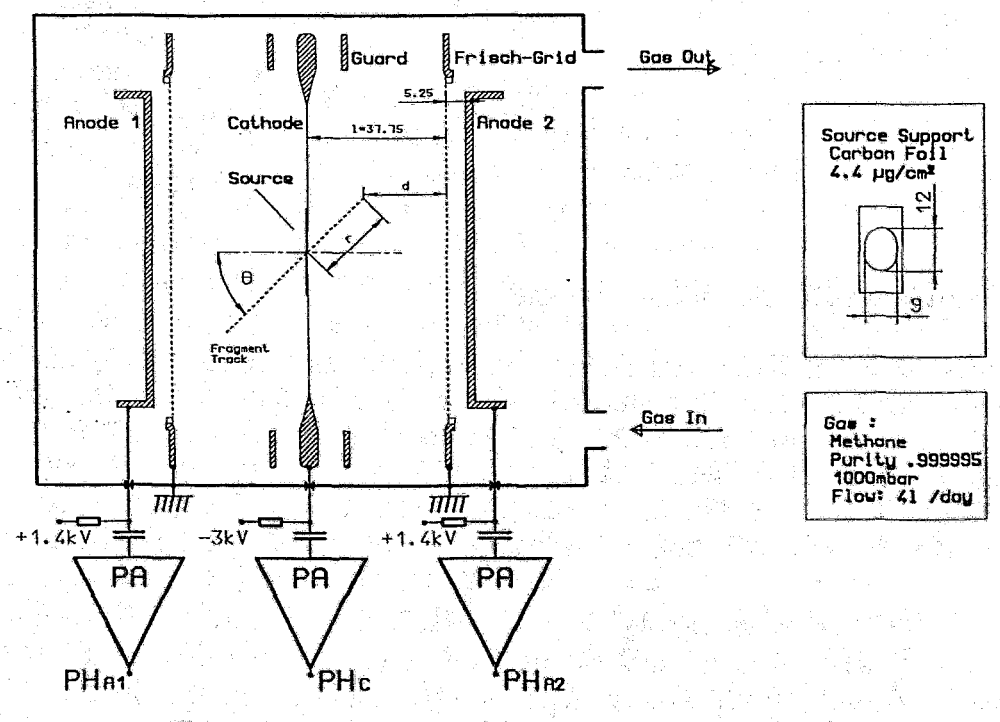

Figure 1: Cross section of the double ionization chamber.

velocity and chamber length l is given by (see Fig. 1):

$$t_{drift} = \frac{l - r \cdot \cos\theta}{v_{drift}} .$$

With the measured drift time and emission angle, the fragments' track length can be calculated. Fragments with the same nuclear mass and the same kinetic energy but of different nuclear charge have different track lengths. Therefore, when the mass resolution is perfect - as it is in the case of cold fission events (Fig. 2) -, it is possible to distinguish fragments with respect to the nuclear charge.

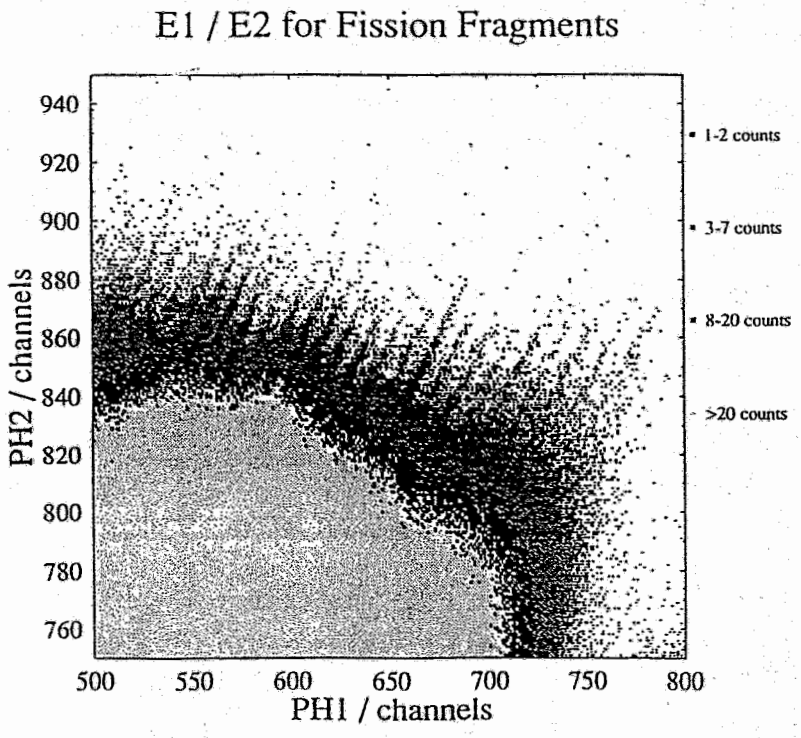

Figure 2: Scatter plot, E_1 E_2 in the region of cold compact fission of ^{252}Cf. Discrete mass lines are visible. Result without any correction or angle collimation.

Electronic treatment of the chamber signals

Figure 3 shows the scheme of the electronic set-up. Three preamplifier signals are shaped in spectroscopy main amplifiers. A high resolution, highly linear CAMAC ADC. converts the charge pulse amplitude to digital numbers (13 bit).

The drift time information is derived from the preamplifier outputs by means of timing filter amplifiers (TFA) and leading edge discriminators (LE). As the cathode signal comes first, it is converted to a START and the anode signals to STOPs for the CAMAC TDC.

A special pile-up rejector detects signal pile-up due to the more probable α decay of the ^{252}Cf source. For such events the data acquisition is blocked. The remaining time window where the rejector does not discern a pile-up has a width of approximately 1 µs. With an α activity of 5000/s the pile-up probability is in the order of 0.5%.

One fission event generates five parameters: Three pulse heights and two drift time signals. These are initially stored in list mode on a personal computer and later transferred to a magnetic tape recorder. A special program /2/ controls the data flow and generates one- or two-dimensional spectra which can be monitored on-line.

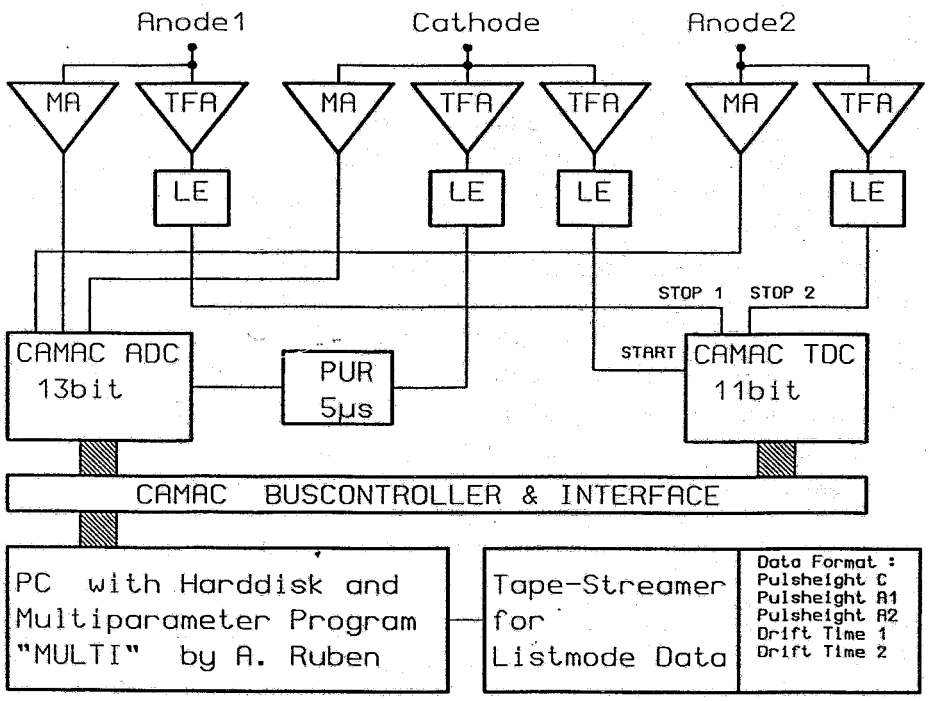

Figure 3: Electronic set-up of the experiment.

Resolution

The intrinsic energy resolution of the ionization chamber is known to be 100 keV (FWHM) for heavy ions with a kinetic energy of 100 MeV, i.e. 0.1% /3/. The electronic noise of 15 keV for the electronic set-up was measured with a precision pulse generator. The average energy straggling of the fragment penetrating the backing foil is estimated to be 25 keV for emission angle $\theta=0$ and 50 keV for emission angle $\theta=60°$.

Another error occurs if the grid transparency for the produced electrons is less than 1. Figure 4 shows the pulse amplitudes from α events measured as a function of electric field strengths ratio on both sides of the grid. Since α decays have a very sharp main line in the kinetic energy distribution, the particles are very useful for testing purposes. The ratio of field strengths on the grid have an influence on the amount of electrons collected by the grid. This amount decreases and approaches zero for higher field strengths on the rear side of the grid. With the used geometry the ratio of 3 is necessary to avoid losses in pulse amplitude and also in energy resolution because the amount of collected electrons on the grid varies with the track orientation with respect to the grid wires.

The resolution in drift time is limited by the electronic noise of the preamplifiers and was measured to be 1 ns. This value does not include the intrinsic error due to range straggling. The statistical variation in fragment range is expected to be small compared to the spread caused by the electronic noise.

Correction of systematic errors

As the pulse height may not be perfectly proportional to kinetic energy, it is mandatory to calibrate the chamber empirically by the so called Schmitt calibration procedure /5/. This calibration assumes the pulse height p to be a function of particle mass m and kinetic energy E. The relationship is assumed to be of the form:

$$E = (a + a'm)p + (b + b'm).$$

The free parameters might be found by the use of at least 4 calibration-points. Three points are already known in literature: 1. the α line of ^{252}Cf, 2. and 3. the energies of the most probable light and heavy fragments. These energies were basically deduced from precise time of flight measurements. As a fourth calibration point the zero point might be used, which is measured with the aid of a precision pulse generator.

Another important systematic error is due to the shielding inefficiency of the Frisch grid. As the grid's shielding is not perfect, the positive ions remaining in the gas affect the anode signal. The signal decreases when the centre of gravity of charge comes closer to the grid. Thus, track length, charge density distribution along the track (so called Bragg curve) and emission angle θ are crucial factors to signal amplitude. Figure 5 shows a scatter plot of drift-time versus pulse height for α particles, demonstrating this effect.

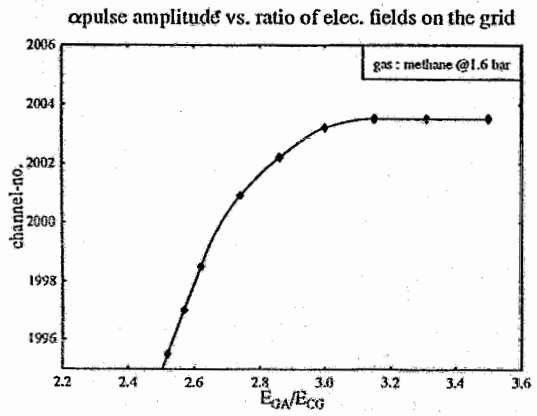

Fig. 4: Effect of grid transparency

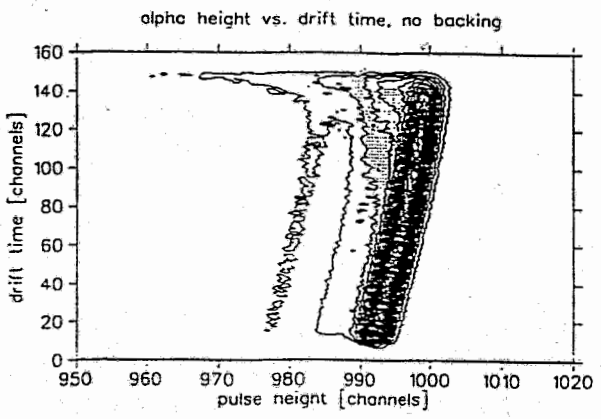

Fig. 5: Grid shielding inefficiency

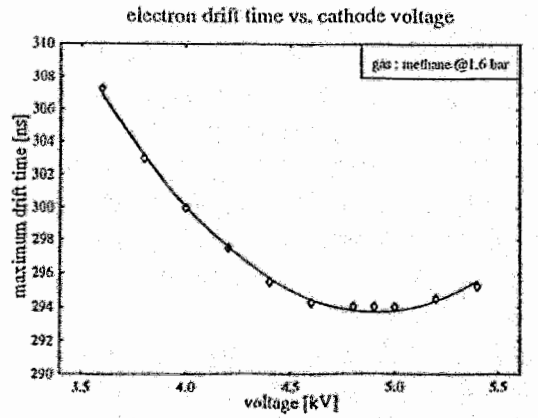

Fig. 6: Maximum drift time

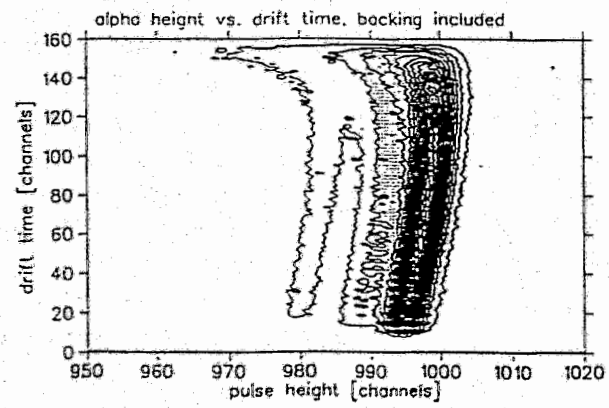

Fig. 7: Energy loss in the backing

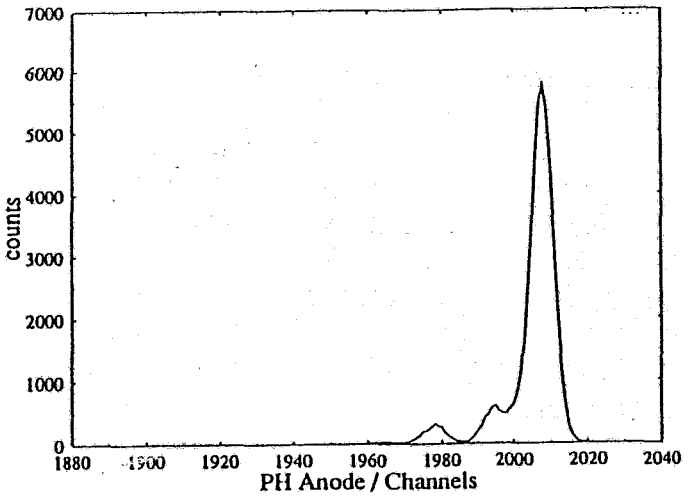

Figure 8: Energy spectrum of α particles, measured in the chamber with no backing loss, after correcting for the effect of grid shielding inefficiency. The resolution is 20.5 keV (FWHM). The tree lines are (from left to right): α_0 (6.031 MeV) from ^{250}Cf, α_{43} (6.076 MeV) and α_0 (6.118 MeV) from ^{252}Cf

The shift in pulse height from the shortest (θ=0) to the longest (θ=90°) drift times is about 0.7%. However, this result has to be adapted to fragment pulses as α particles and fragments have different Bragg curves. Figure 8 illustrates the high energy resolution for α particles after correcting for the shielding inefficiency effect.
Finally, one has to correct for the energy loss of the fragment which penetrates the backing. Figures 5 and Figure 7 present the results of the same experiment, with the latter including the energy loss caused by the backing foil. Comparing the two diagrams a pulse decrease is revealed on the backing side for long drift times (corresponding to large emission angles). The correction has to be done taking into account the measured emission angle and the average value of specific energy loss for fragments in carbon /4/.
Drift time measurements might suffer of electric field inhomogeneities in the chamber. Fortunately, the electron drift velocity as a function of field strength has a maximum in methane. Figure 6 shows the maximum drift time as a function of applied cathode voltage measured in the chamber. Operating the chamber with the appropriate voltage, electron velocity will not vary much for slight variation of field strength.

Angle collimation

The determination of nuclear charge, using the drift time information becomes critical for higher emission angles. In order to improve the charge resolution, the emission angle has to be collimated by filtering the list mode data. The normalised cathode pulse height is an appropriate parameter to determine the emission angle. Since this parameter varies slightly with the fragments' masses and charges, the use of a fixed value for cut-off introduces errors in the calculation of yields. Therefore it is necessary to generate a spectrum of emission angles for each of the combinations of mass and charge. Then a fixed fraction of the distribution in angles corresponds to a fixed solid angle of emission which should be unbiased.

Conclusions

Double ionization chambers are very suitable instruments for fission experiments. The energy resolution is the best being attainable with ionization detectors. The possibility to detect coincident fission products in a solid angle of almost 4 π makes this instrument favourable for investigations on fragment configurations with low probabilities. Response and systematic errors of the detector are suitably studied with the aid of a α particle source.

In the present investigation on cold fission of ^{252}Cf the experimental situation is very advantageous. The mass resolution is perfect and the determination of nuclear charges becomes possible. Total yields as a function of kinetic energy will be measured for each fragment configuration of mass and nuclear charge.

References

/1/ J.Kaufmann, W.Mollenkopf, F.Gönnenwein, P.Geltenbort, A.Oed, Zeitschrift für Physik A 341,319-326 (1992)

/2/ A.Ruben, MULTI: computer base multi-parameter data acquisition system, private communication

/3/ A.Oed,Nucl. Instr. and Meth. 205 (1983) 455-459

/4/ M.Ait Salem, et al., Verhandl. DPG (VI) 25 (1990) 1483, and to be published

/5/ H.W.Schmitt, W.E.Kiker and C.W. Williams, Phys. Rev. 137 (1965) B837

NEW IONIZATION CHAMBER FOR THE MASS SPECTROMETER LOHENGRIN (ILL GRENOBLE)

M.Hesse (Universität Tübingen)

H.R.Faust, G.Fioni (ILL Grenoble)

M.Gross (TU Braunschweig)

F.Gönnenwein (Universität Tübingen)

January 30, 1993

Abstract

We descripe a new ionization chamber for the upgraded mass separator LOHENGRIN at the ILL in Grenoble. With a new additional dipole magnet in the focal plane the counting rate can be increased up to a factor of 7 and the background generated by scattering of fission fragments in the beam line and by charge exchange collisions will be reduced. The measured beam optics of the focusing magnet is in a good agreement with the calculations. A strong divergence of incoming fragments in the ionization chamber with respect to the chamber axis calls for the measurement of the fragment entrance angle. The ionization chamber works in the ΔE-E mode. With the anode partitioned into two parts we have generated an angle proportional signal which is the electron drift time difference between the anode signals. The measured angle resolution was 3°.

1 Introduction

Ionization chambers are a powerful detector system in nuclear physics. The main advantage is the simple design and the free choice for shapes and sizes of electrodes, and for the distances between anode, Frisch grid and cathode. During the last years ionization chambers were developed with an outstanding energy resolution (some 100 keV's for fission fragments). For the LOHENGRIN spectrometer ionization chambers were used for the detection of fission fragments and the determination of the nuclear charge. Measurements have shown that it is possible to detect fission fragments with a very low yield down to 10^{-9} [BOC88].

2 RED magnet and the beam optic

To increase the counting rate of fission fragments on the LOHENGRIN exit slit the installation of a focusing dipole magnet (reverse energy dispersion - RED) was proposed and realized [FIO91]. In future the investigation of regions in the mass distribution of fissile systems with a low yield will become possible with a higher efficiency. These regions are tripartition, symmetric fission and far asymmetric fission. Another aspect is the investigation of rare isotopes with very small quantities [FAU91].

The advantage of a dipole magnet compared to a quadrupole magnet is the very small influence of this focusing system in the mass direction in the focal plane. The dipole magnet can suppress background events which originate in scattering processes of fragments in the beam tube and charge exchange collisions during the flight of charged fission fragments in the spectrometer tube.

The pole pieces were specially shaped to optimize the focusing properties for the deflected particles. In the following figure 1 a calculation of the horizontal beam optics is shown. The dimension of the focal point is calculated to be 6 mm, provided the trajectories of incoming fagments are parallel to each other.

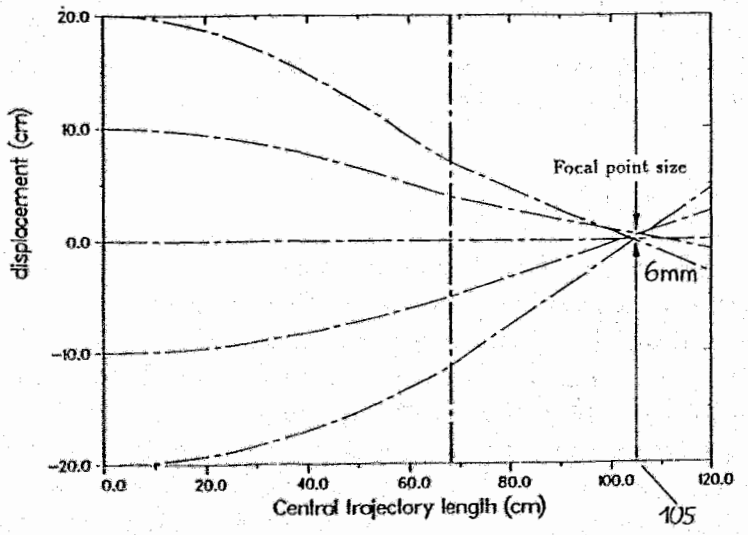

Figure 1 : Deflection properties in the pole piece plane

With an α particle source ^{241}Am the beam optics of the dipole magnet was investigated. The source was placed successively in three different positions on the entrance side of the magnet. The configurations used were the central position and two off-center positions which correspond to a spatial dispersion of $\pm$ 20 cm on the separator parabola. The energy dispersion for LOHENGRIN along the exit slit was simulated by varying the $B\rho$ values with respect to the source position.

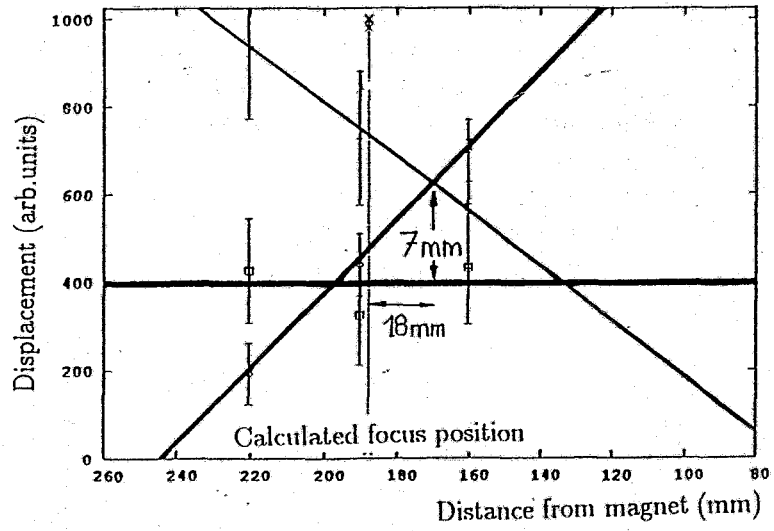

Figure 2 : The measured beam optics inside the focusing magnet

The measurement is in a good agreement with the calculation. The experimentally determined size of the focal point was 7 mm. Taking into account the angular spread in the deflecting plane of the incoming α particles, which corresponds roughly to the actual spread in angle for the fission fragments from LOHENGRIN, the size of the focus increased to about 20 mm.

3 The ionization chamber

We have made use of a standard construction with a Frisch grid and a rectangular electrode shape (see figure 3). The grid cancels the dependence of the pulse height on the entrance position of fragments into the chamber. The length of the electrodes is about 260 mm and the distance beetwen the cathode and the grid is 70 mm. With isobutane as chamber gas it is possible to work with a typical pressure of 40 mbar. This has the advantage to reduce the difference between the pressure (vacuum) in the separator and the pressure in the chamber. In consequence leak rates and deformations of the entrance window are diminished. In front of the ionization chamber an adapter piece allowing turbo pumps to be used for the magnet vacuum chamber was constructed.

Generally the chamber is of cylindrical form and has standard flanges on the front and rear. The chamber works in the ΔE-E-mode for the determination of the nuclear charge number. In this mode the anode is divided in two sections.

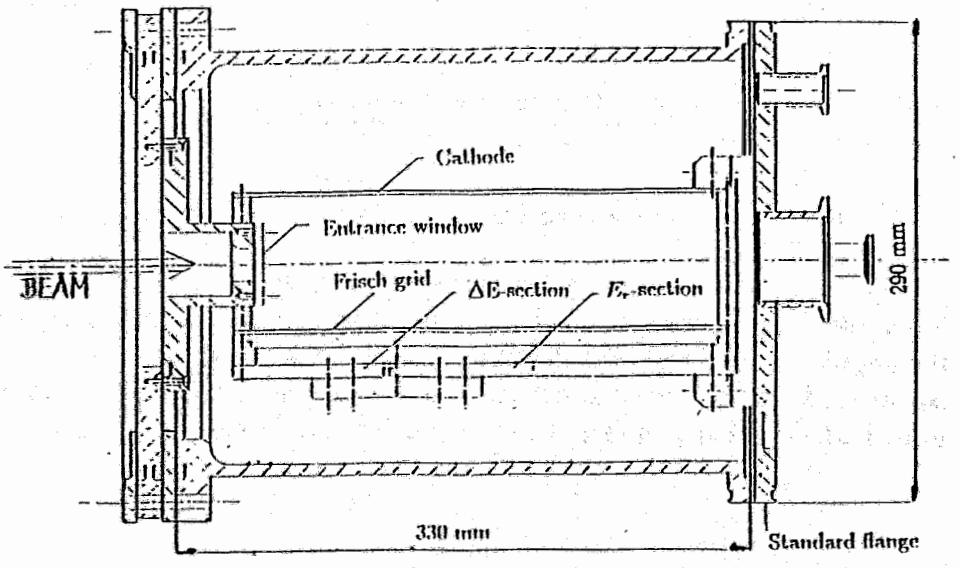

Figure 3 : Cross section of the ionization chamber

The first part (called ΔE-part) generates a signal which is linked to the energy loss in this section. The sum of both signals is proportional to the

fragment energy. From ΔE-E plots we determine the fragment characteristics. The fragment angle is found through the measurement of the electron drift time since the direction of the chamber electric field is in the deflection plane of the fission fragments.

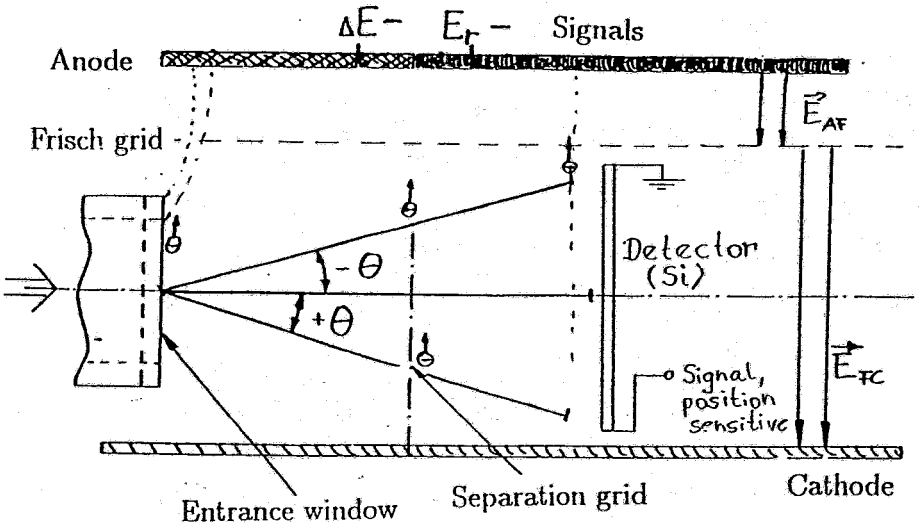

Figure 4 : Exp. setup for the investigation of the dependence Θ=f(ΔT)

The measurement of the drift time for both anode parts creates a time difference ΔT which is approximately proportional to the entrance angle for the slowed down particles. A schematic setup of this angle measurement is shown in figure 4. For the experimental test of the angular dependence from the drift time difference ΔT a solid state detector was used. The position resolution of this device was better than 0.7 mm. This value corresponds to an angle inaccuracy of $\delta\Theta \approx 1°$. The α particle source was collimated with a foil with a hole of 1.5 mm in diameter.

In the following figure 5 the experimentally measured dependence of the entrance angle Θ on the electron drift time difference ΔT is presented. Projecting in figure 5 events corresponding to a fixed time difference ΔT=0 onto the angle axis, the distribution in angle depicted in figure 6 is obtained. The FWHM amounts to 3°. The measurement was carried through with a reduced electric field strength between cathode and Frisch grid of 0.68 $Vcm^{-1}mbar-1$ (p=97.6mbar).

Note that this value does not correspond to the maximum drift velocity of electrons in the gas.

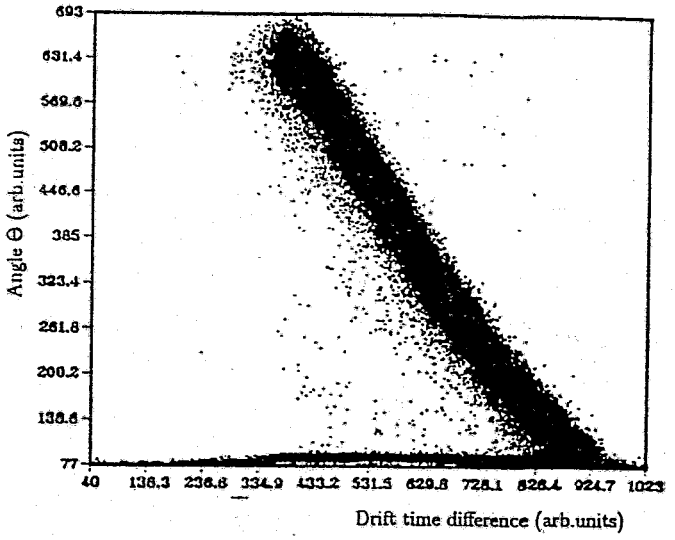

Figure 5 : The measured dependence between Θ and ΔT

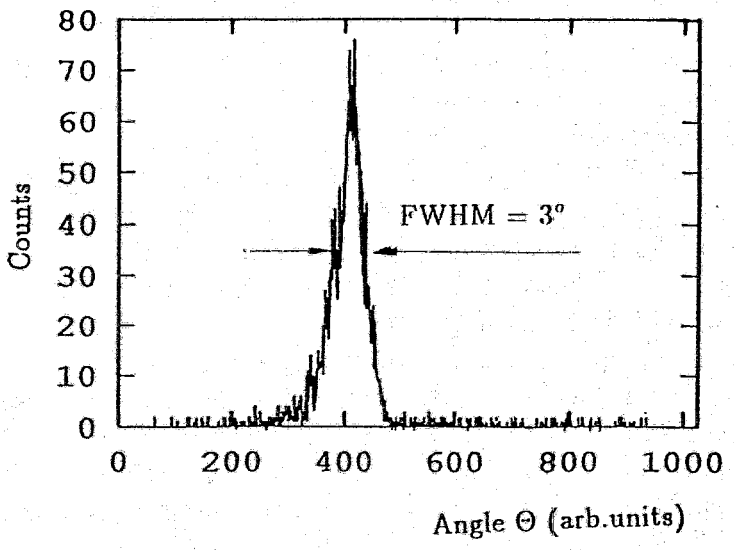

Figure 6 : The angle projection for $\Delta T = 0$

4 Conclusions

The descriped ionization chamber in connection with the fission fragment separator LOHENGRIN can be used for the detection of fission fragments. In the ΔE-E mode the determination of the nuclear charge distribution is feasible.

While the fragment directions exhibit a strong divergence (opening angle about 25°) the measurement of the electron drift time difference between the two anode parts allows the determination of the entrance angle and the correction for the effective ΔE length.

The time resolution as the main condition for a precise angle determination can be further optimized. The reduction of the entrance window size may permit to produce more homogeneous and thinner entrance windows.

The main advantage of the device presented is the simple operation of the chamber, data acquisition and analysis system.

We thank the BMFT Bonn for financial support under contract number 06TU243.

References

[BOC88] J.P.Bocquet et al., Nucl.Instr. and Methods A267 (1988) 466

[FIO91] G.Fioni, H.R.Faust, M.Gross, ILL-Report 91FI25T (1991)

[FAU91] H.R.Faust, ILL-Report 91FA24T (1991)

Multi-Parameter Spectroscopy of Fission Fragments and Related Emission Products

A. Ruben[1], M. Adler[1], I. Düring[1], and H. Märten[1]
B. Cramer[2], and U. Jahnke[2]

[1]Technische Universität Dresden
Institut für Kern- und Atomphysik
Mommsenstrasse 13, D-O-8027 Dresden, Germany

[2]Hahn-Meitner-Institut Berlin
Glienicker Str. 100, D-W-1000 Berlin 39

Abstract

An exclusive measurement of the $^{252}Cf(sf)$ fragment distribution in mass and energy in coincidence with the related emission products by combining a twin ionization chamber with a 4π-neutron tank, a n-γ-detector, and a solid-state detector telescope is presented. The experimental set-up, data handling and aquisiton is described followed by a discussion of the raw data evaluation.

1 Introduction

The gridded ionization chamber is a standard tool for the spectroscopy of charged particles [1,2]. Its application in nuclear fission experiments became rather attractive due to its high resolution, e.g. in the case of cold fission phenomena [3,4], and due to the possibility to measure the polar fragment angle with reference to sample plane normal. Combining two gridded ionization chambers back-to-back with a fission sample on the central cathode and operating it with light gases the fragment energies, masses and in some cases the charges could be deduced with high precision. This gridded twin-ionization chamber TIC is predestinated for studying cold fission where the mass resolution is not disturbed by neutron emission and the several fragment charges can be obtained.

In order to measure fission fragment energies (total kinetic energy TKE as a measure of scission point elongation) and masses A (mass asymmetry A_1/A_2) in coincidence with the related emission products we have combined the TIC with a 4π-neutron tank, a n-γ-detector, and a solid-state detector telescope in an exclusive measurement. The correlations of the fragment distribution in A and TKE with integral observables (neutron multiplicity ν, total γ-ray energy $\overline{E_{\gamma,tot}}$) and differential data (energy and angular

distribution of all emission products with reference to light-fragment direction) can be analyzed.

From the integral data the (asymptotic) excitation energies of the complementary fragments can be deduced. In particular, the neutron multiplicities are a measure of fragment deformation at scission. To some extent, this method allows to study rare fission modes with extreme shape asymmetry.

The combination of neutron multiplicity measurement with neutron spectroscopy (for given A and TKE) makes it possible to analyze emission processes from highly excited fragments to be specified.

The angular distribution of γ-rays bear information on fragment angular momentum and, hence, the degree of collective excitations at scission (bending modes).

In the present work, we focus on a discription of the experimental set-up, the multi-parameter data acquisition, and TIC data analysis.

2 Experimental Set-up

The gridded TIC constructed according to Butz-Jørgenson et al. [5] is schematically shown in Fig. 1. It consists of a back-to-back ionization chamber with an inner diameter of 180 mm and a total height of 137 mm. The ^{252}Cf source is placed on the upper side in the centre of the cathode, which has a central hole of 15 mm diameter. The source with a fission rate of 330 fissions per second is deposed on a 111 μg / cm^2 Ni-backing. At both sides of the cathode there is a Frisch-grid and an anode plate at distances of 23 mm and 30 mm, respectively. The one dimensional grids consist of 30 μm thick copper wires equally spaced with 0.3 mm distance.

Pure Methane (CH_4) at constant pressure of 10^5 Pa is used as counter gas. The chamber is operated in a gas flow regime (0.7 l/h). The electric potentials for cathode and anode have been adjusted according to Buneman [1]: cathode: – 1.8 KV; grids: 0 V; anodes: + 1.5 KV.

At the bottom side of the TIC at 80 mm distance to the source, a solid-state ΔE-E-telescope is mounted to detect the light charged particles accompanying fission. To allow these particles to pass the bottom anode a central hole of 16 mm diameter covered by a 9.26 μm thick Al-foil was set.

The twin ionization chamber is placed in the inner reaction chamber of the Berlin 4π-neutron counter [6] in the most symmetric way, i.e. the cathode plane corresponds to the plane between the two hemispheres of the spherical neutron tank. The counter sphere has an outer diameter of 1400 mm and an inner diameter of the reaction chamber of 400 mm. It is filled with 1500 l liquid scintillator NE 343 containing 0.3 ... 0.5% natural Gadolinium. Both hemispheres are equiped with 12 fast photo-multipliers XP 2041. To suppress the diffusion of thermal neutrons between the hemispheres, a 0.5 mm thick Cd-plate is placed in the interspace. The neutron capture by Cd nuclei leads to a multiple emission of γ-rays registered in both hemispheres. These cross talk events appear within the 25 ns coincidence window and are marked by the data acquisition system.

In addition to neutron counting a NE 213 n-γ detector allows for the spectroscopy of neutrons and to some extent γ-rays. The 4" thick detector with a 2" diameter is placed within the upper counter hemisphere at 50 cm flight path in sample plane normal direction. Hence, the angle between neutron (and γ-ray) direction and fragment direction (measured by TIC) can be obtained. The spectroscopy of neutrons is done by time-of-flight technique. In the case of γ-rays, one gets light output distributions, where the emission probability of γ-rays with given energy is folded by the response function (mostly due to Compton effect). This is considered in data analysis.

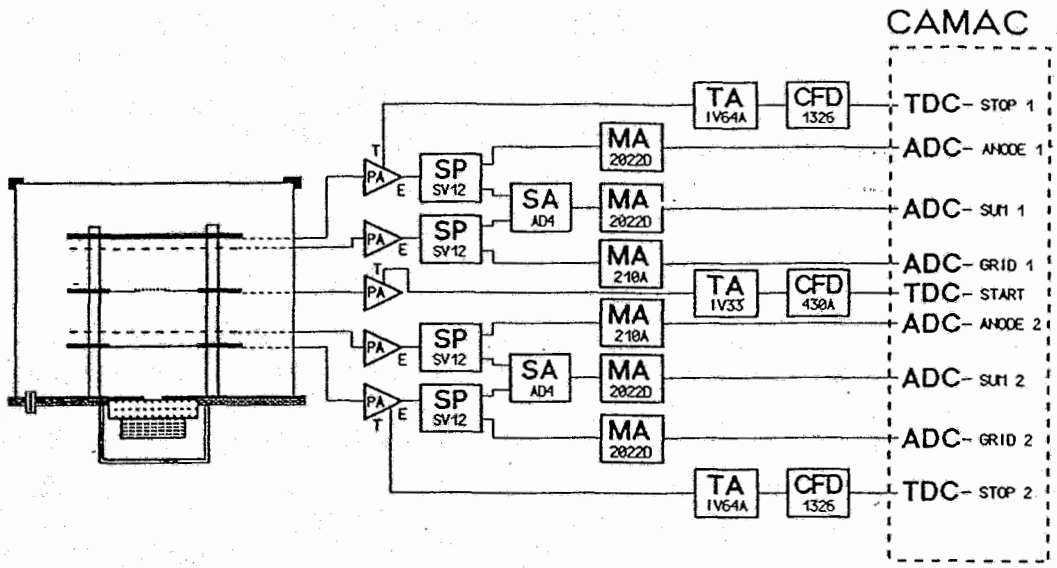

Figure 1: Scheme of the gridded twin ionization chamber and the electronic signal processing (see text)

3 Data Handling and Acquisition

Each fission event is characterized by a cathode, two grid, and two anode signals. Due to the shielding effect of the grid, the anode signals P_A correspond to the number of electron-ion pairs of the ionization track in the space between cathode and grid, and, consequently, to the kinetic energy E_k of the fission fragments,

$$P_A = -n_0 e \sim E_k. \tag{1}$$

Opposite to this behaviour, the bipolar grid signals P_G consisting of two components, i.e. a negative charge caused by the electron drift in grid direction and a positive charge influenced after passing the grid, bear information about the emission angle Θ with reference to the sample plane normal,

$$P_G = P_G^+ + P_G^- = n_0 e \frac{\overline{X}}{D} \cos\Theta \tag{2}$$

where $\frac{\overline{X}}{D}$ is the center of the ionization track over the grid to cathode distance D. In order to process the signals it is useful to replace the bipolare grid signals by unipolare sum signals P_Σ which contain the angular information as well,

$$P_\Sigma = P_A + P_G = -n_0 e(1 - \frac{\overline{X}}{D}\cos\Theta). \tag{3}$$

Measuring the drift times T, i.e. the times the electrons need to move from the ionization track to the anode, a further method to deduce the emission angle Θ is given,

$$T = \frac{D - R\cos\Theta}{v_e}, \tag{4}$$

where R corresponds to the ionization track length. v_e is the electron drift velocity.

Fig. 1 shows a scheme of the electronic signal processing. After pre-amplifying **(PA)** with Silena charge-and-time sensitive pre-amplifiers (CATSA), the anode and grid pulses are splitted **(SP)** and added **(SA)** to get the sum signals. The time signals (start - cathode pulse, stop - anode pulse) are derived from the fast time outputs of the pre-amplifiers using constant fraction discriminators **(CFD)** .

Neutron multiplicities are registered by the $2x2\pi$ neutron counter. Fission neutrons are thermalized by elastic scattering in the liquid scintillator and then captured within an effective time of up to 35 μs due to the Gd(n,γ) reaction. Each neutron capture yields in the average to three γ - quanta with a total energy of 8.5 and 7.9 MeV for ^{155}Gd and ^{157}Gd, respectively [6]. Thus, neutrons can be counted by detecting the γ-flashes within a time interval of about 40 μs. In order to suppress the background, a coincidence of at least two γ registrations is required. However, one has to consider a prompt, fast scintillator signal caused by the prompt fission γ-rays and the recoil protons. Therefore, the neutron counting starts at about 1 μs after the fission reaction. In addition to the scaling of the neutron multiplicities of the complementary fragments ν_1 and ν_2 as well as the sum ν_{tot}, one gets the total energy of the γ-rays emitted in the fission process by analyzing the prompt peak.

All cross talk events, i.e. simultaneous registrations in both hemispheres, appearing within a 25 ns coincidence window are marked.

For pile-up reduction, the number of fission events during the counting time is also scaled. Further, the neutron-counter background is simultaneously measured within the time gaps between fission events.

From the n-γ detector the time of flight t_{TOF} of the detected neutrons and γ-rays as well as the pulse height E (scintillation light output) is measured. The n-γ-discrimination is done by the help of the "QDC-method". Some organic scintillators are characterized by a significant difference in the slow component of the detector signals due to different charged particles (here, recoil protons and Compton electrons). Therefore, the integral light output in the slow component ΔE is also measured by a QDC for an appropriate time window. The E-ΔE-scatterplot (Fig. 2) represents the two different loci for neutrons and γ-rays.

For data acquisition, an IBM-PC-CAMAC system based on the CAMAC controller DSP 6002 and a 386/33MHz-AT computer is used. The conversion of the analogue

signals (amplitudes and charges) as well as the times into the digital data is done by fast octal Silena converters 4418 V/Q/T with word lengths of 12 bit, i.e. 3840 channels. The neutron counter events, cross-talks, pile-up events, and background events are scaled by a 32-channel LeCroy scaler 4434 within a time gate of 40 μs. The end of this gate triggers for data read out.

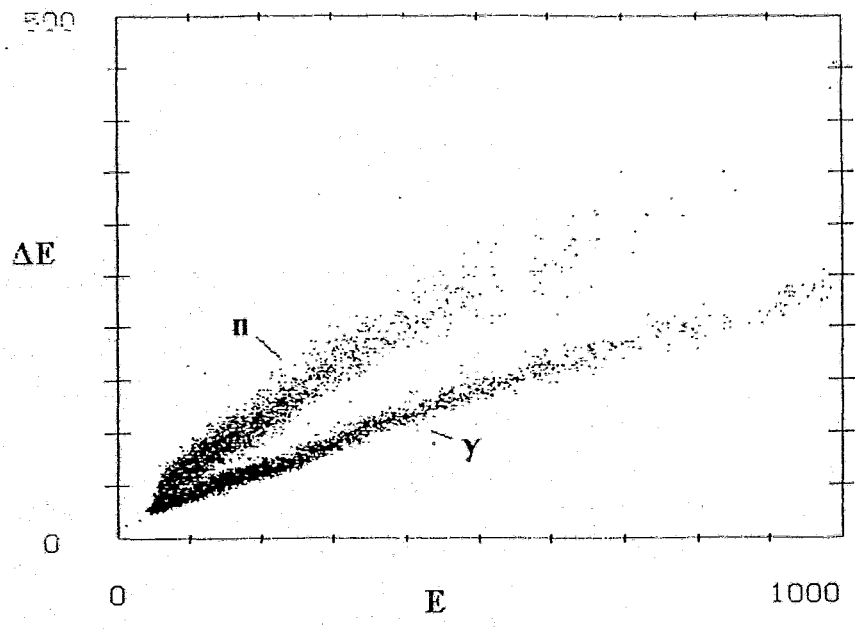

Figure 2: Scatter plot of n-γ-discrimination by the "QDC-method": The slow component of the scintillator signal is plotted vs. total light output

For data collection and CAMAC control of the multi-parameter experiment, the computer code *TIC* was developed [7]. In addition to the programming, control and fast data acquisition of up to four CAMAC moduls with up to 32 parameters several monitoring procedures as well as a first evaluation of the measured data is possible. Via Ethernet connection, all measured data can be transmitted to VAX station and stored on Exabyte video tapes. Whereas the full data analsis is performed at a VAX station (OLYMP), a first evaluation of measured data is also possible at PC by reading the list-mode data from file and analyzing them by setting various gates and by applying routines for data transformation including calibration parameters.

4 Raw Data Evaluation

Operating the twin ionization chamber at higher gas pressure first of all the 6.1 MeV α-rays from the ^{252}Cf source have been measured with a resolution of 120 keV (FWHM). Fig. 3 presents an example of the measured fission fragment raw data. The colours in the scatter plots (here, represented as gray scale) correspond to the counts per channel.

As described above, the pulse height of the anode signals is proportional to the kinetic energy of the fragment. The proportional factor α is given by the energy calibration

performed with the 6.1 MeV α-rays of the californium source. However, one has to consider corrections due to

1. grid inefficiency σ
2. pulse height defect PHD
3. energy loss in the fission sample and backing $\Delta E_{loss}/\cos\Theta$

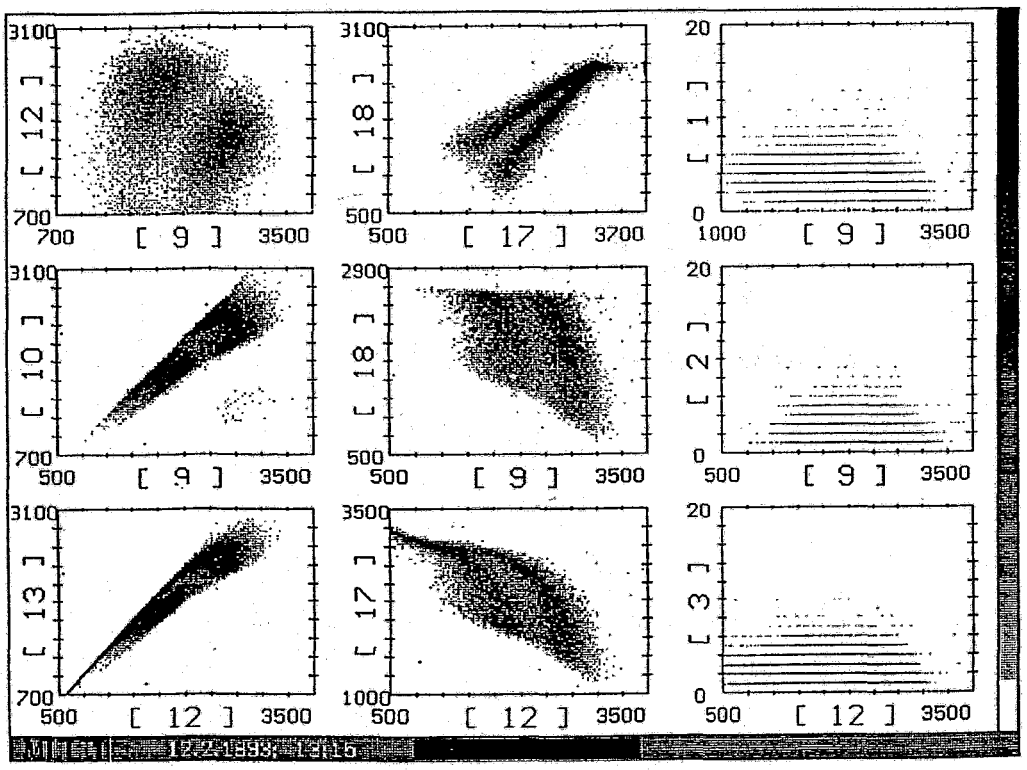

Figure 3: Scatter plot of fragment raw data (the parameter numbers correspond to : 9 – P_A^1, 13 – P_A^2, 17 – T^1, 18 – T^2, 1 – ν_{tot} , 2 – ν_1, 3 – ν_2, 10 – P_Σ^1, 12 – P_Σ^2)

Thus, the anode pulse heights have to be calibrated and corrected according to

$$E_k = \alpha P_A + PHD(E_k, A, Z) + \frac{\Delta E_{loss}}{\cos\Theta} + \sigma(P_A - P_S). \tag{5}$$

In contrast to a perfect grid with ideal shielding, in reality charges moving between cathode and grid have influence on the anode signal, too. According to Buneman [1] this grid inefficiency can be corrected using eq. 5, whereby σ is determined by the geometrical relations (0.03 mm grid wire diameter and 0.3 mm distance, 7 mm grid to anode distance). For our grid and chamber geometry a value of 0.01 was deduced. The average energy loss of the fragments in the fission sample or in the sample and backing depends on the length of the path through these materials. In a first order approximation it can be assumed to be reciprocally proportional to $\cos\Theta$.

The corresponding factors ΔE^0_{loss} for both sides of the source can be easily deduced from the measured anode pulse heights as function of $1/\cos\Theta$.

In the case of the rather thick Ni backing used in this work it was not possible to estimate the quantity of the pulse hight defect PHD. Supposed values range between zero according to Signarbieux et al. [7] up to 6 MeV according to Budtz-Jørgenson et al. [5]. We neglected the PHD in the analysis of the present data.

As discussed above, different methods to deduce the fragment emission angle Θ are available. However, the resolution differs for the three methods.

signal	$\Delta\cos\Theta$ (fwhm)
P_G	0.41
P_Σ	0.10
T	0.14

The best resolution shown in Fig. 4 was obtained by analyzing the sum signals, where $\cos\Theta$ is given by

$$\cos\Theta = \frac{P_A - P_S}{P_A \frac{\overline{X}}{D}}. \tag{6}$$

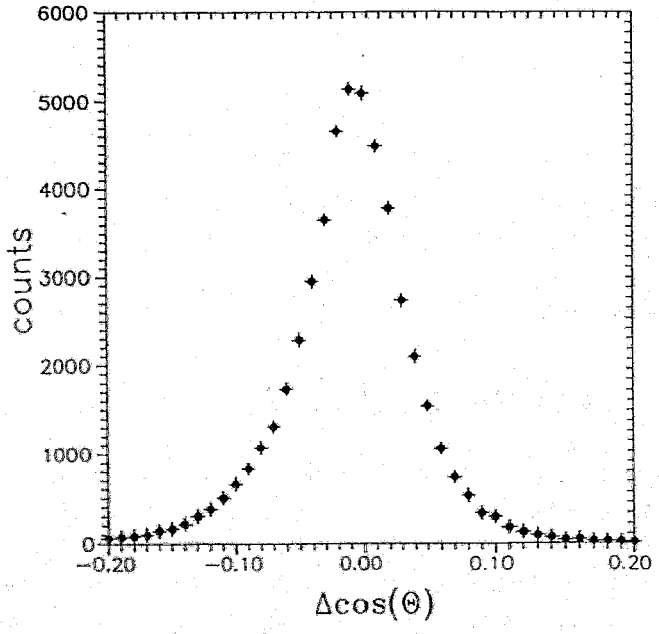

Figure 4: Resolution of the $\cos\Theta$ determination ($\Delta\cos\Theta = \cos\Theta^1 - \cos\Theta^2$)

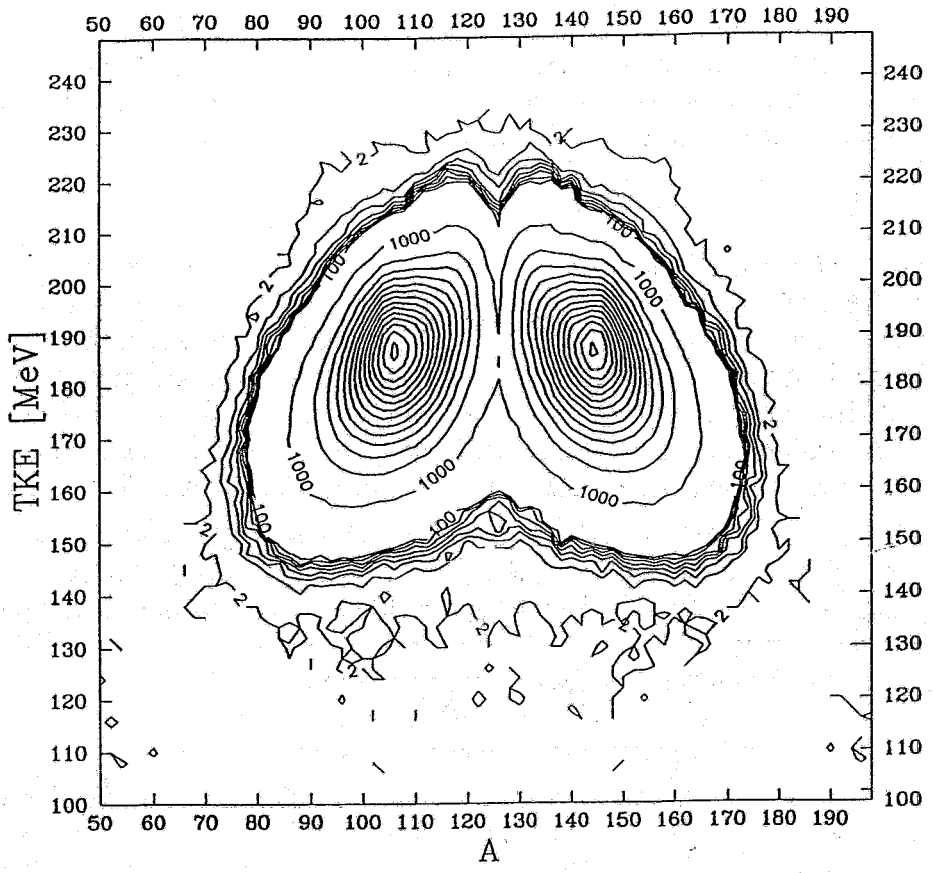

Figure 5: Contour plot [events $A^{-1}MeV^{-1}$] of the ^{252}Cf(sf) yield as function of A and TKE. The rare-event region is plotted in a 2(14)100 scale, whereas the "normal"-region scale is 1000(2000)27000.

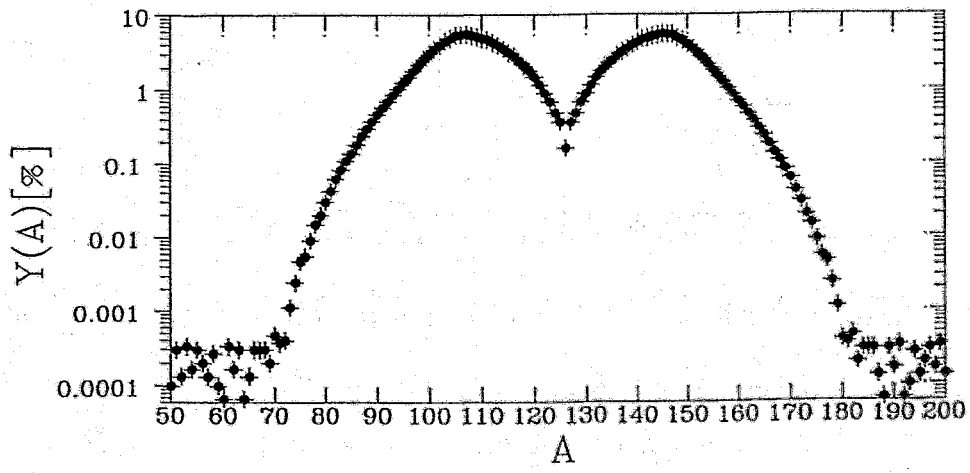

Figure 6: Mass yield Y(A) (corrected data) of ^{252}Cf(sf) fragments

According to kinematic relations, the masses of the measured fragments are given by the ratio of the kinetic energies, $E_k^1/E_k^2 = A_1^*/A_2^*$. However, due to the neutron emission after fission these masses A^* are reduced by the neutron multiplicity ν. To get the primary pre-neutron emission masses one has to add ν,

$$A_1 = A_1^* + \nu(A_1) \qquad A_2 = A_2^* + \nu(A_2). \tag{7}$$

In a first evaluation of the measured data performed within the data acquisition program TIC, this transformation was done based on $\overline{\nu}(A, \overline{TKE})$ values calculated within the scission point model TSM [9]. This method yields reliable data for the most probable mass end energy regions. It is less verified in the case of rare fission events. A contour plot of the fragment distribution in A and TKE is represented in Fig. 5. The projection on mass scale, i.e. the fragment mass curve, is shown in Fig. 6. The super-asymmetric fission mode appears at $A_1 \leq 72$ corresponding to $A_2 \geq 180$.

Fig. 7 shows the neutron multiplicty yield curves detected by the 4π-neutron counter. Compared with the standard value of $\overline{\nu}_{tot} = 3.766$ for ^{252}Cf(sf), this corresponds to an efficiency of 85 %. In principle, a higher efficiency can be obtained by reducing the detector thresholds. This yields, however, a higher background. The present compromise corresponds to an average background 0.25.

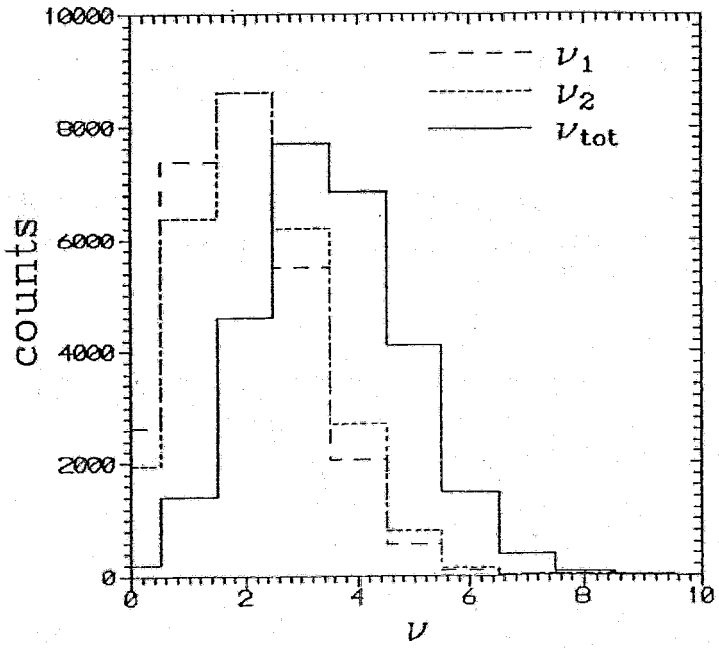

Figure 7: Neutron multiplicty yield for the neutron counter hemispheres and total neutron multiplicity yield

5 Outlook

The detailed data analysis and first physical interpretation is presented by Düring et al. [8]. However, the first results have shown that the mass and energy resolution of

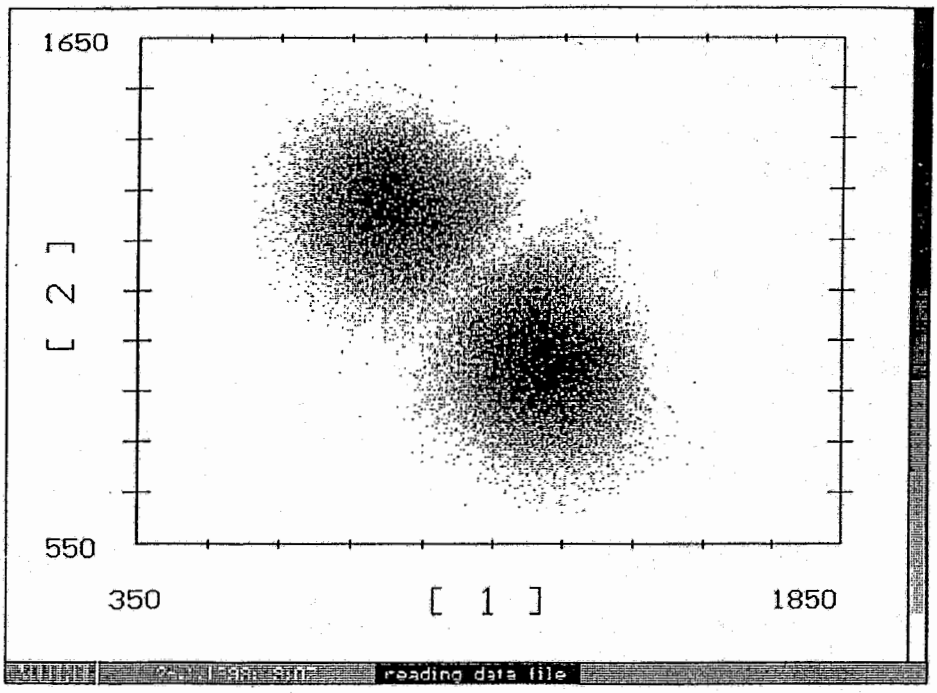

Figure 8: Scatter plot of anode pulses for the thin Cf-source

the fission fragments is influenced by the large values of the energy loss $\Delta E_{loss}/\cos\Theta$. Therefore, a new experiment has been started with a better fission sample, i.e. a ^{252}Cf source with a fission rate of 120 per second on a thin carbon layer of 4.5 $\mu g/cm^2$.

Fig. 8 shows a scatterplot of the anode signals for this new source. One has to note that scattered fragments are nearly absent. In future, we will use this source with a better resolution and try to study the influence of the pulse height defect. Combining the TIC with moduls of a large area neutron detector (LANCER [11]) presently under construction, a new type of correlation experiment will be possible.

This work is supported by BMFT under contract 06 DD 112.

References

[1] O. Buneman, T. E. Cranshaw, and J. A. Harvay, Can. J. Res. A **27**,191 (1949)

[2] E. Segre, Experimental Nuclear Physics, Vol.1, John Wiley & Sons Inc., New York, 1952

[3] H.-H. Knitter, F.-J. Hambsch, and C. Budtz-Jørgenson, Nucl. Phys. A **536**, 221 (1992)

[4] C. Signarbieux, G. Simon, J. Trochon, and F. Brisard, J. Phys. Lett. **46**, 1095 (1985)

[5] C. Budtz-Jørgenson, H. - H. Knitter, Ch. Straede, F. - J. Hambsch, and R. Vogt, Nucl. Phys. A **258**, 209 (1987)

[6] B. Cramer, PHD-thesis (1989), Hahn-Meitner-Institut Berlin

[7] G. Simon, J. Trochon, F. Brisard, and C. Signarbieux, Nucl. Inst. and Meth. **286**, 220 (1990)

[8] A.Ruben, Manual 'The PC-CAMAC Based Twin-Ionization Data Acqusition Program – TIC' (1992)

[9] A.Ruben and H. Märten, Z.Phys. **A 337**, 237 (1990)

[10] I. Düring et al., these proceedings

[11] H. Märten et al., Project LANCER, TU Dresden

Fission of Spin-aligned Projectile-like Nuclei from ^{208}Pb (29MeV/u) + Au

U. Jahnke
Hahn-Meitner-Institut Berlin GmbH, Glienickerstr.100, D-1000 Berlin 39

As has been reported before [1], fission of projectile-like nuclei from the reaction Pb (29MeV/u) + Au is restricted to comparatively low values of the associated neutron multiplicity, $M_n \approx 10$ to 35 (the multiplicity M_n is measured with the ORION neutron tank at GANIL, it is not yet corrected for the detection efficiency of 64%). Fission is thus observed from peripheral reactions only. For still lower multiplicity or more gentle collisions the projectile survives as evaporation residue, for higher $M_n \approx 35$ to 70 it completely disassembles in smaller debries.
In this contribution we report on a futher analysis [2] of the fission decay:

Fission fragments from projectile-like nuclei were observed and their atomic charge Z was determined with a position-sensitive ΔE-telescope in the angular range from 6 to 20 degrees. When plotted in the rapidity versus perpendicular momentum plane the fragments form Coulomb rings about the emission direction of the fissioning quasi-projectile. Fig. 1 exhibits representative examples of these rings for symmetric fission, $Z \approx 40$ and for $Z = 32$ and 48, which corresponds to the half maximum of the Z distribution. Only the two M_n-bins in the middle of the figure where fission dominates exhibit the characteristic sharp circles with the radius decreasing for increasing Z. The lower and the upper M_n-bins have been added in order to demonstrate how these structures fade away when other break-up processes take over.
From these data we deduce two parameters characterizing the projectile-like fragment (PLF) prior to fission, its deflection angle Θ_{PLF} and the absolute value of its velocity v_{PLF} (from the center of the rings) as well as two quantities related to fission, the Z-distribution $d\sigma/dZ$ of the fragments and their relative velocity (from the radius of the rings). The dumb-bell shape of $d\sigma/dZ$ (fig.2) with the broad maximum near $Z = 40$ and the relative velocity, which is consistent with the Viola-systematics, manifest once more the binary character of the fragmentation.
The parameters of the primary reaction, Θ_{PLF} and v_{PLF}, to first order do not depend on the Z-asymmetry of the subsequent fission process, as one would expect (fig.2). But the PLF is slowed down continously with increasing inelasticity or multiplicity M_n. From this reduction of v_{PLF} relative to the beam velocity of 7.3 cm/ns, or more precisely from M_n itself we estimate the average excitation energy of the PLF to be 75, 180 and 275 MeV, respectively, in the three lower M_n-bins. The deflection angle on the other hand does not vary significantly with M_n, it is always slightly inside of the grazing angle of 6.2°.
There are two major conditions in order to observe sharp ring pattern for the fission fragments. The first one is, that the trajectory of the PLF is precisely defined by the dynamics or the experimental selection, which is obviously the case (fig.2). A dispersion in Θ_{PLF} or v_{PLF} would otherwise introduce a smearing of the rings. The se-

cond one is, that the fission fragments are mostly emitted in the reaction plane. This implies that the PLF's are aligned perpendicular to the reaction plane and that their fission decay is strongly anisotropic, i.e. strongly focussed into this plane.
In order to investigate the latter condition the experiment has been simulated by a Monte Carlo calculation for the extreme cases of isotropic emission of the fission fragments in space or in the reaction plane only. From the comparison with the experiment, in fig. 3 for M_n= 25- 34 and Z=32, it seems that the strong spin alignment assumption is indeed closer to the observation.
Given a strong alignment, which has moreover been observed before in reactions with much lighter ions [3], we can in turn estimate the angular momentum of the PLF necessary to produce a sufficient fission angular anisotropy. According to conventional models this anisotropy is controlled by $I^2/2K_0^2$. Assuming values of 150 to 200 for the variance K_0^2 (with a shape parameter J_{sp}/J_{eff}= 1.5 and temperatures T=2 to 3 MeV), we see that spin values of I≈40 to 50 h could produce a sufficiently strong anisotropy to account for the observation. Much lower spin values, on the other hand, would favour the neutron decay and much higher values are also excluded, because the fission barrier approaches zero for 65 to 85 h in the Pb-like nuclei.
In summary we have observed a strong alignment of projectile-like fragments from peripheral reactions of 29 MeV/u Pb with Au. These Pb-like fragments in turn split up into fission fragments which are focussed into the reaction plane. Spin and excitation energy of the projectile-like nuclei are estimated to be 40 to 50 h and 75 to 275 MeV, respectively.

[1] E. Piasecki et al., Phys. Rev. Lett. 66 (1991) 1291
[2] S. Bresson et al., Phys. Lett. B 294 (1992) 33
[3] K. Asahi et al., Phys. Rev. C43 (1991) 456

Fig. 1: Lorentz-invariant cross sections in the rapidity vs. perpendicular momentum plane for Z= 32, 40 and 48 and different neutron multiplicity M_n-gates.

Fig. 2: Recoil velocity v_{PLF}, deflection angle Θ_{PLF} and differential cross section $d\sigma/dZ$ as a function of Z in three different neutron multiplicity M_n-gates.

Fig. 3: Comparison of experimental cross sections (middle) with Monte Carlo simulations for Z=32, M_n= 25- 34 and in-plane isotropic emission (left) or completely isotropic emission (right). The geometric limits of the detector acceptance are indicated by the solid lines.

Fig. 1:

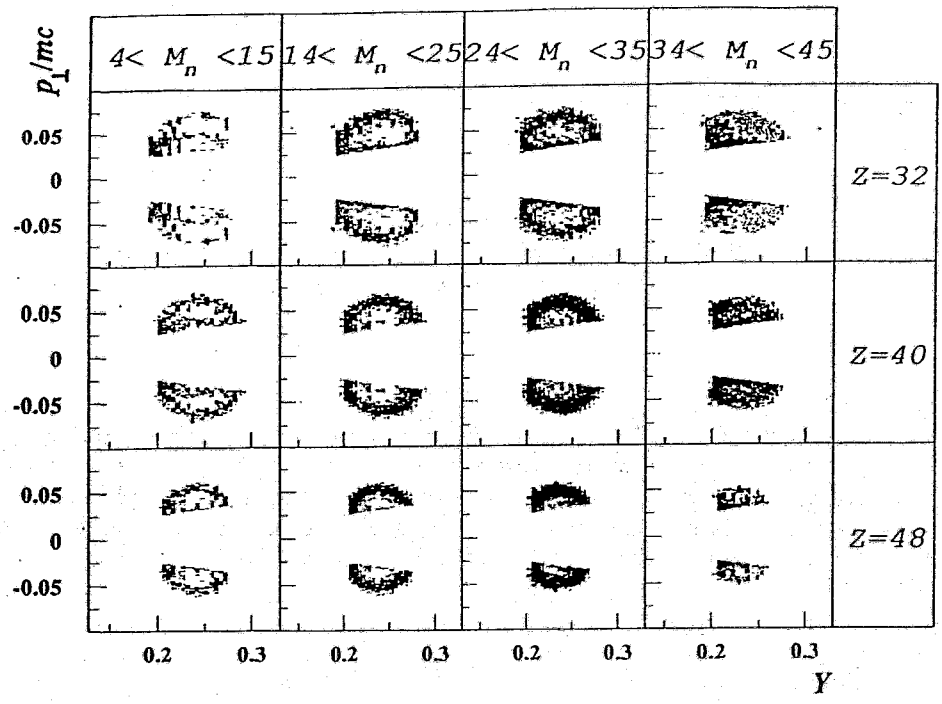

Fig. 2:

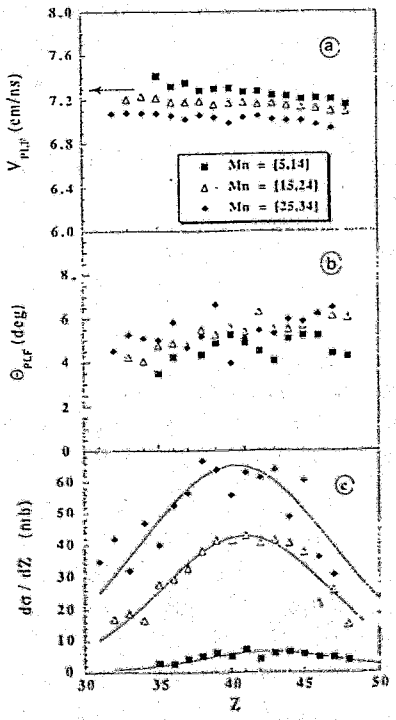

Fig. 3:

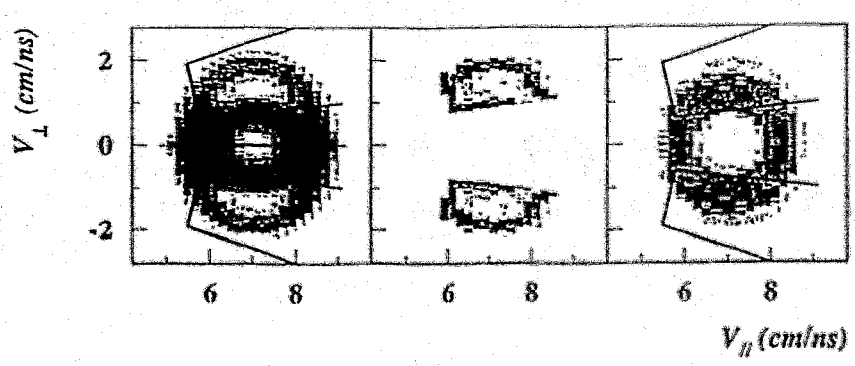

Neutron Emission from Primary Fragments and Mass Determination

D. Volný*, J.Krištiak
Institute of Physics SASc , 842 28 Bratislava , Slovakia
* *Comenius University , Bratislava*

Abstract

In the frame of statistical model with preequilibrium contribution a probability of prompt neutron emission from primary fission fragments has been calculated. The calculation of yields of primary f.f. from experimental values of relevant yields has been performed using these probabilities. An influence of using post-neutron experimental yield of f.f.'s on the determination of mass distribution of primary f.f.'s has been discussed.

1 Introduction

In determining the mass distribution of fission fragments emission of neutrons must be taken into account. This correction depends on the fragments' pre-neutron mass m and kinetic energy E. From the mass and momentum conservation relations follows that pre-neutron masses of the light m_L^* and heavy m_H^* fragments are given by following formula

$$m_L^* = A\frac{E_H}{E_L(1+\xi)+E_H}, \qquad m_H^* = A\frac{E_L}{E_L+E_H(1+\xi)} \tag{1}$$

The correction

$$\xi = \frac{m_H}{m_H^*}\left[\frac{\nu(m_L^*)}{m_L} - \frac{\nu(m_H^*)}{m_H}\right] \tag{2}$$

takes into account the number of emitted neutrons ν from pre-neutron fragments. The ν value is often taken from Apalin et al. [1]. The aim of our calculation was the verification of this method of correction in which the post-neutron yields are used.

In work [2] it was shown that use of post-neutron yields changes for example the value of neutron odd-even effect. To show this, we used a statistical model of de-excitation of primary fragments from fission of ^{235}U. This model enables us to compute the probability of creation of the isotopes (Z,A') from the primary fragment (Z,A) by its de-excitation. Based on the knowledge of these probabilities it is possible to compute (solving the inverse problem) the pre-neutron yields. The comparison between computed and measured values enables us to give answer to our question.

2 Model calculations

The statistical model was used to compute the probabilities of emission of neutrons and protons. The competition of γ-rays was taken into account by the GDR model. In the de-excitation chain of each fragment, the seven nuclei in the following scheme were included:

$$
\begin{array}{lll}
(Z,A) & \rightarrow & (Z-1,A-1) \rightarrow (Z-2,A-2) \rightarrow \\
\downarrow \searrow & & \downarrow \searrow \quad\quad \downarrow \searrow \\
(Z,A-1) & \rightarrow & (Z-1,A-2) \rightarrow \\
\downarrow \searrow & & \downarrow \searrow \\
(Z,A-2) & \rightarrow & \\
\downarrow \searrow & & \\
(Z,A-3) & \rightarrow & \\
\downarrow \searrow & &
\end{array}
$$

The inverse cross sections were taken from [3]. The level densities are given by the formulae for level densities of Fermi gas which is for excitation energies bellow 5 MeV smoothly connected to the formula for level densities with a constant temperature. Parameters for the level densities are taken from [4]. The non-equilibrium contributions are taken into account by the standard exciton model [5].

Distributions in of excitation energy were considered as gaussian. Mean values of this distribution were calculated from the total excitation energy of both fragments $\overline{E}_{exc} = Q - \overline{E}_{kin}$ (Q were taken from [6] and $\overline{E}_{kin}$ from [7]). We assume that both fragments have the same temperature so $\overline{E}_1/\overline{E}_2 = a_1/a_2$, where $\overline{E}_1, \overline{E}_2$ are mean values of excitation energies of given fragments and a_1, a_2 are the parameters of level densities. Widths of these distributions are equal for the light and heavy group. In our calculation it was taken as a free parameter.

The measured yield is the sum of several contributions, which originate on different ways. The proton emision is negligible. Therefore, we can write for each element an independent system of coupled equations.

$$
\begin{aligned}
Y_e(Z,A_1) &= \sum_{A=A_1}^{A_1+C_z} Y_c(Z,A)P(A_1|Z,A) \\
Y_e(Z,A_2) &= \sum_{A=A_2}^{A_2+C_z} Y_c(Z,A)P(A_2|Z,A) \\
Y_e(Z,A_3) &= \sum_{A=A_3}^{A_3+C_z} Y_c(Z,A)P(A_3|Z,A) \\
&\vdots \\
Y_e(Z,A_K) &= \sum_{A=A_K}^{A_K+C_z} Y_c(Z,A)P(A_K|Z,A), \qquad (3)
\end{aligned}
$$

where $A_{i+1} = A_i - 1$, K is the number of isotopes of given element, Y_e, Y_c are experimental and primary yields of fragments, respectively. $P(A_i|Z,A)$ are probabilities of creation of the isotope Z, A_i from the primary fragment Z, A by its de-excitation, $C_z = 4$ is a constant which is given by the maximum number of neutrons which can be emitted from the primary fragment (see scheme).

In this way, we got a system of coupled linear equations with unknown Y_c. This system of equations has, in general, $K + C_z$ unknowns. The real number of unknowns was in our case

usually $K+2$ (sometimes $K+3$) depending on the excitation energies of fragments. These equations are possible to solve by using additional constraints

$$0 < Y_c(Z,A) < 1$$

$$\sum_A Y_e(Z,A) = \sum_A Y_c(Z,A).$$

3 Results and discussion

Results of solving the system of equations are displayed in Fig. 1. We see that in some regions of A the pre-neutron yields of fission fragments are very different from the measured ones. These corrected yields were used for an evaluation of emission of neutrons from primary f.f.

In Fig. 2. we show the influence of the correction to the number of emitted neutrons from individual fragments. We again see that using of corrected yields leads to remarkable corrections in emission of neutrons from individual fragments, e.g. for $A \sim 106, 134$.

The mean number of neutrons $\overline{\nu}$ emitted from a certain mass A is plotted on Fig. 3. This result is equivalent to the used experimental corrections of Apalin et al. The comparison of $\overline{\nu}$ computed from experimental yields with those from corrected (pre-neutron) yields shows great deviation in the region of $A \sim 134$. It indicates that in this region the correction on emission of neutrons should be used carefully, or an iteration method should be used. Our results are obtained on the basis of a limited set of f.f., but in spite of that the results reproduce the basic features of experimental values of $\overline{\nu}$.

In Fig. 4 the influence of pre-neutron mass distribution on the statistical spectra of neutrons and γ-rays is represented.

The results show that description of these spectra in region of higher energies (E > 2 MeV) requires a modification of the standard procedure.

References

[1] V. Apalin, Yu. Gritsuyk, I. Kutikov, V. Lebedev, L. Mikaelian, Nucl. Phys. 71(1965)553

[2] D. Volný, J. Krištiak, S. Gmuca, J. Kliman, Proc. Dynamical Aspects of Nuclear Fission, Smolenice 1991, ed. J. Kristiak, B. J. Pustylnik, p. 301

[3] A. Chatterjee, K. N. H. Murthy, S. K. Gupta, IAEA Vienna, INDC(IND)-27/GJ

[4] A. V. Malyšev, Plotnost urovnej i struktura atomnych jader, Atomizdat Moskva, 1969

[5] S. Gmuca, IAEA Vienna, H4-SMR-284

[6] J. R. Nix, private communication

[7] Y. Nakagome, J. Kanno, J. Kimura, Proc. Physics of Neutron Emission in Fission, Mito 1988, ed. H. D. Lemmel, INDC(NDS)-220, p. 65

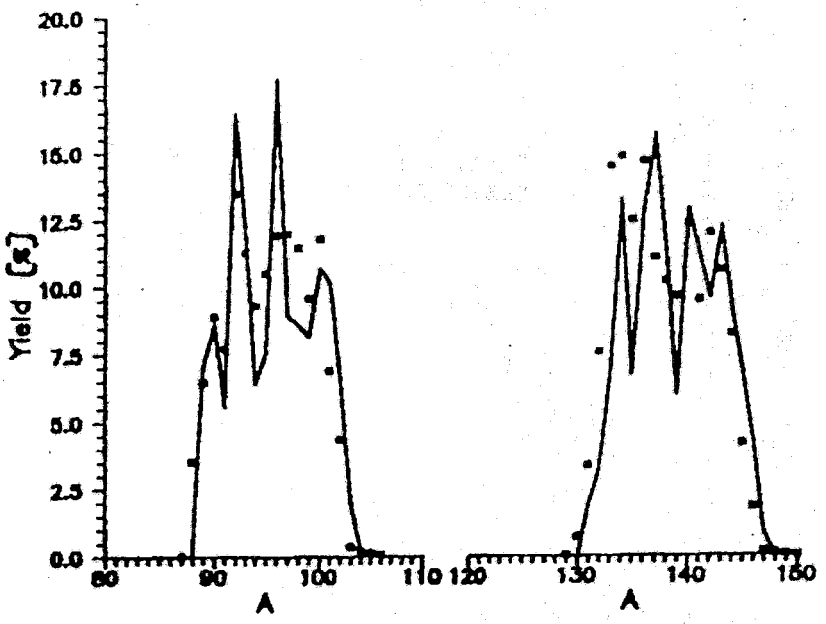

Figure 1: Fragment yields: dots - measured, line - corrected ($\sigma = 2.6$ MeV).

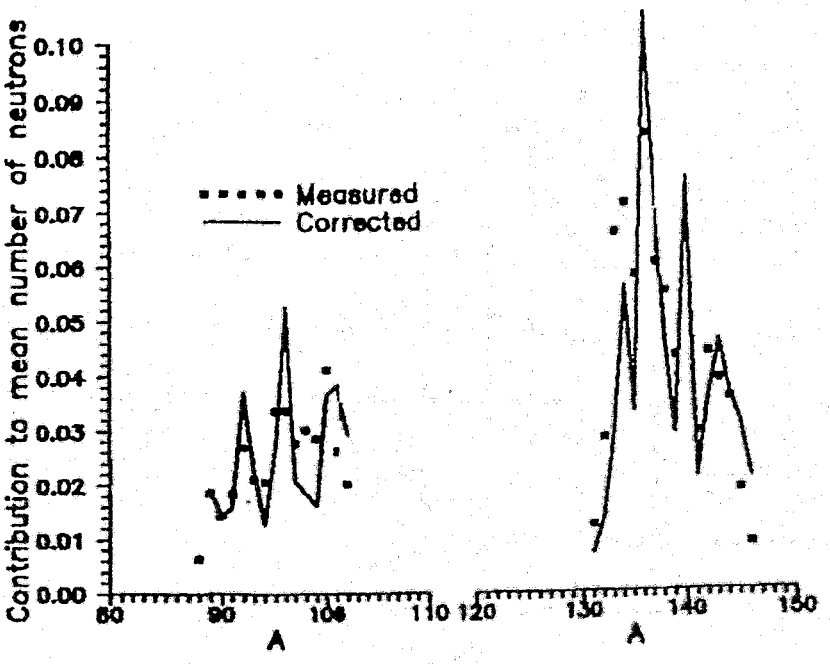

Figure 2: Contribution of neutrons from individual fragments ($\sigma = 2.6$ MeV).

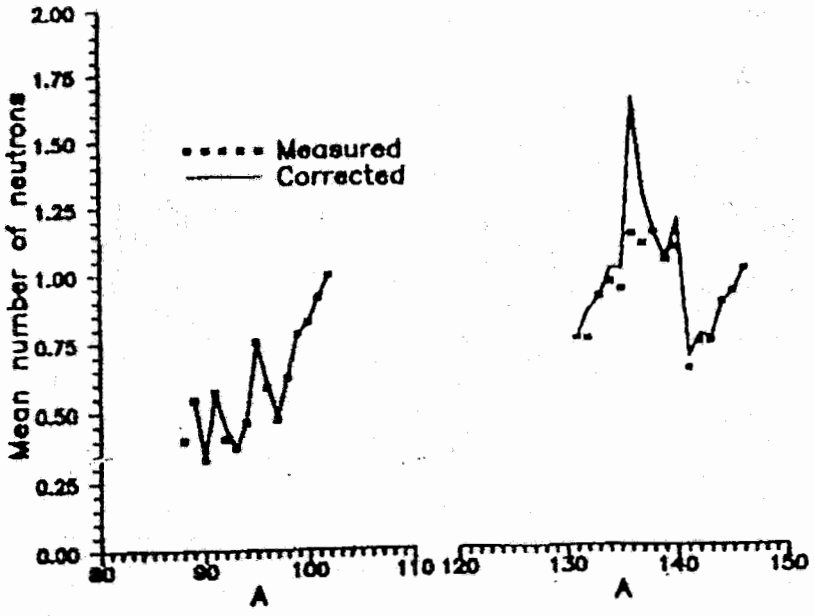

Figure 3: Mean number of neutrons (σ = 2.6 MeV).

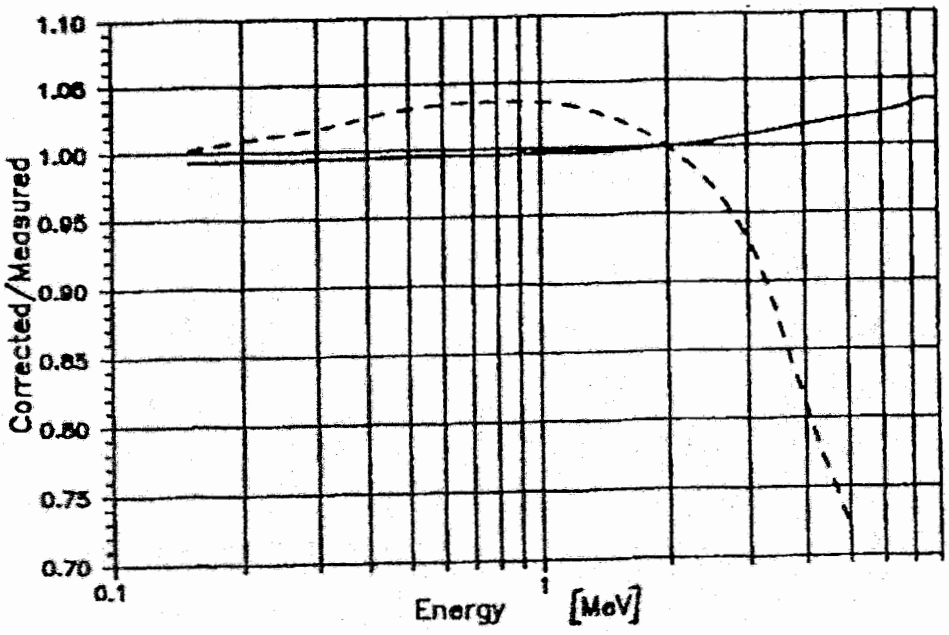

Figure 4: Ratio of spectra (σ = 2.6 MeV): solid line - neutron, dashed line - γ-rays.

γ-Spectroscopy as a means to investigate mass and charge distributions in the fission of actinides

Persyn K., Pommé S., Jacobs E., De Frenne D., Govaert K., Yoneama M.-L.

Nuclear Physics Laboratory
University Gent

Abstract

In this paper we will describe the system set up at the University of Gent to perform g-spectroscopy on Al-catcherfoils as well as on irradiated capsules containing target material. This method is used to study some characteristics of fission fragments: mass and charge distributions, proton odd-even effects,...

1. Introduction

Already some 20 years ago γ-spectrometry on β^--decaying fission products using the catcherfoil method were started at our lab to determine post neutron mass distributions of fission products. This technique has been developed and improved during the past. With this method it is however impossible to detect fission fragments with half lives shorter than 1 min. In former times only very scarce spectroscopic information was available for short-lived fission products. As more data on very short-lived fission products were published, we could determine the yields of these short-lived products, making it possible to deduce not only mass, but also charge distributions. To do so a pneumatic transport system was constructed to perform γ-spectrometry on irradiated actinide target nuclei.
Using γ-spectrometry on catcherfoils and on pneumatically transported actinide targets, irradiated at our new LINAC, it becomes possible to investigate a broad range of fission characteristics (e.g.: mass distribution, proton odd-even effect) close to the fission barrier as a function of the excitation energy.

2. Experimental Set-up

2.1. Bremsstrahlung

All our present experiments are carried out at the 2% duty factor 15 MeV linear electron accelerator of the Nuclear Physics Lab of the University of Gent (MON90). Electrons accelerated to energies between 6.5 and 14 MeV were

converted to bremsstrahlung using a cylindrical carbon (graphite) block with a central conical hole. This configuration is needed to handle the very high power in the electron beam. The bremsstrahlung spectrum for this configuration needed for the calculation of the average excitation energy of the compound nucleus is achieved by performing a Monte Carlo calculation using the EGS4 computer code (NEL85).

2.2. Catcherfoil technique

A holder containing thin circular plates made of the material under investigation (e.g.: ^{235}U, ^{238}U, ^{232}Th) separated from each other by Al-foils is placed in the photon beam. Fission fragments leaving the target are caught in the Al-foils. After an irradiation of one hour these Al-foils are brought to a HPGe-detector, and the γ-spectra from the β^--decaying fission products are recorded during a total time of approximately 5 hours. To include time information (to make identification easier) several consecutive spectra are recorded (see table 1).

Table 1: Time evolution for typical catcherfoil measurement.

Time (from - until in minutes)	Activity
0 - 60	irradiation
60 - 65	cooling down
65 - 85	4 spectra of 5 min. each
85 - 125	4 spectra of 10 min. each
125 - 205	4 spectra of 20 min. each
205- 365	4 spectra of 40 min. each

All these times can of course be adapted to any specific case. As it takes 5 minutes to start the measurements (cooling down of the activity around the accelerator; manually transporting the Al-foils) it is impossible to obtain information on isotopes with a half live shorter than a few minutes. For higher electron energies the electron current of the machine has to be limited in order to keep the dead time in the beginning of the measurement low enough. To obtain sufficient statistics several runs were performed (4 to 7). Afterwards the spectra of these different runs are added before being analysed. If necessary a rescaling is included before adding up the spectra.

2.3. Pneumatic transport system

To obtain information on shorter lived isotopes, a pneumatic transport system was installed. Ni or Al capsules containing the target material (e.g.: ^{235}U, ^{238}U, ^{232}Th) are transported into the bremsstrahlung beam, and automatically returned after being irradiated for 30 seconds. The capsules end up in front of the HPGe detector, and -analogous as with the catcherfoil method- several

consecutive spectra are recorded. These vary in duration from 0.2 s to more than 50 s, a total cycle of 54 spectra being recorded in some 10 minutes (see table 2).

Table 2: Time evolution for typical rabbit measurement.

Time (from - until in seconds)	Activity
0.0 - 30.0	irradiation
30.0 - 31.5	transportation of capsule
31.5 - 32.5	5 spectra of 0.2 s each
32.5 - 34.9	6 spectra of 0.4 s each
34.9 - 39.7	6 spectra of 0.8 s each
39.7 - 49.3	6 spectra of 1.6 s each
49.3 - 68.5	6 spectra of 3.2 s each
68.5 - 106.9	6 spectra of 6.4 s each
106.9 - 183.7	6 spectra of 12.8 s each
183.7 - 337.3	6 spectra of 25.6 s each
337.3 - 644.5	6 spectra of 51.2 s each

We want to stress that in these experiments, contrary to the catcherfoil measurements, the irradiated actinide targets themselves are placed in front of the Ge-detector. To avoid build up of long lived products in the samples, about 15 different samples were used in succession. The limiting factor for the electron current is again the dead time in the first spectra. To obtain enough statistics, over 200 runs are needed.
As the transportation time for the pneumatic transport system is only 1.5 s, yields of nuclei with half lives from 1 second on can be determined. The results of both methods are linked together by calculating the ratio of the yield of some isotopes with intermediate half lives (a few minutes), which can be measured with both methods.

3. Analysis of measurements

The spectra were analysed using the programmes MARKER and CAOS of Westmeier (WES80), which calculate the peak areas. The relative independent and cumulative yields were deduced from these peak areas with a fitting program, designed for this purpose, and in principle able to deal with any arbitrary combination of decay chains. The number of disintegrations $N_k(t_1,t_2)$ of the k-th product in a certain decay chain during a time interval $[t_1,t_2]$ after ending the irradiation of the samples is calculated using:

$$N_k(t_1,t_2)=\sum_{i=1}^{k}\left[\sum_{j=1}^{i}Q_j\prod_{\substack{t=j\\ t\neq i}}^{k}\left(\frac{\lambda_t}{\lambda_t-\lambda_i}\right)\right]\left(\frac{1-e^{-\lambda_i\tau}}{\lambda_i}\right)\left(e^{-\lambda_i t_1}-e^{-\lambda_i t_2}\right)$$

where τ is the duration of the irradiation interval, Q_i the production rate of product i directly from the fission of the studied actinide, and λ_i the decay constant of product i.

The spectroscopic data (half-lives, decay schemes and γ-intensities) were taken from the γ-ray catalogue of Reus and Westmeier (REU83) and from recent Nuclear Data Sheets.

Home-made software was designed to deal with several corrections. For catcherfoil measurements a correction has to be made for the fact that the probability for a fragment to escape from the target (with a thickness larger than the range of the fragments in the target material) to be caught into the Al-foil is proportional to its range in the target material. The calculation of this correction was based on the range data for $^{235}U(n_{th},f)$, measured as a function of the fragment mass by Niday et al. (NID61).

For the fast γ-spectrometry of the other hand we had to correct for the γ-attenuation in the target as well as in the capsules. These corrections were based on the attenuation coefficients of Storm and Israel (STO70). This way the relation between the measured peak area $S(t_1,t_2)$ of a γ-ray peak in each spectrum and the corresponding number of disintegrated products $N_k(t_1,t_2)$ is given by:

$$S(t_1,t_2)=N_k(t_1,t_2).\frac{K.\varepsilon(E_\gamma).I_\gamma}{C_{DT}.C_R.C_A}$$

where K is a normalisation factor, $\varepsilon(E_\gamma)$ is the relative efficiency of the HP-Ge detector for γ's with energy E_γ, I_γ is the absolute intensity of the γ-transition with energy E_γ in the decay of product k and C_{DT}, C_R and C_A are the correction factors for resp. dead time, range and γ-absorption.

Although we measured as many independent and cumulative yields as possible (over 150 γ-peaks from over 70 nuclei in the heavy mass region and over 80 peaks from more than 45 nuclei in the light mass region) not all yields could be measured. The reasons for this can be diverse: γ-intensities not known, small peaks too close to intensive ones, ... All these problems occur far more for peaks in the light mass region, so that we had to restrict ourselves to determining the yields of isotopes in the heavy mass region. But also here we had to calculate some missing yields by means of the fit of a gaussian charge distribution, modulated with an odd-even correction factor, to the other (known) yields of fragments of the same mass chain. These isobaric charge distributions have then the following shape (a formula based on Wahl et al. (WAH88) and Amiel et al. (AMI74)):

$$Y(Z|A) = \frac{\int_0^{E_c} F_p(E).F_N(E).\exp\left[-\frac{(Z-Z_p(E))^2}{2\sigma_Z^2}\right].N(E_e,E).\sigma_F(E).dE}{\sqrt{2\pi}\sigma_Z \int_0^{E_e} N(E_e,E).\sigma_F(E).dE}$$

with Z_P the top, σ_Z the width of the distribution and F_P and F_N the correction factors for respectively the proton and the neutron odd-even effect. We assumed the width parameter the same for all fragment masses and all compound nucleus excitation energies ($\sigma^2(Z|A) = 0.40$). If for some mass chain there were not enough independent or cumulative yields to obtain Z_P, this parameter was fixed at an interpolated value. The size of the odd-even effect is entered iteratively. The thus fitted independent yields are stored in a database, from which it is easy to extract any combination of data (e.g.: mass and charge distributions, odd-even effect, ...).

4. Some results

We have performed these measurements on ^{232}Th, ^{235}U and ^{238}U for several bremsstrahlung endpoint energies. Here we include some typical results for ^{238}U, taken from POM93 and DEF84. Fig. 1 shows the isotopic mass distribution for 6.44 MeV bremsstrahlung induced fission. One can easily see the enhanced yield of even Z elements.

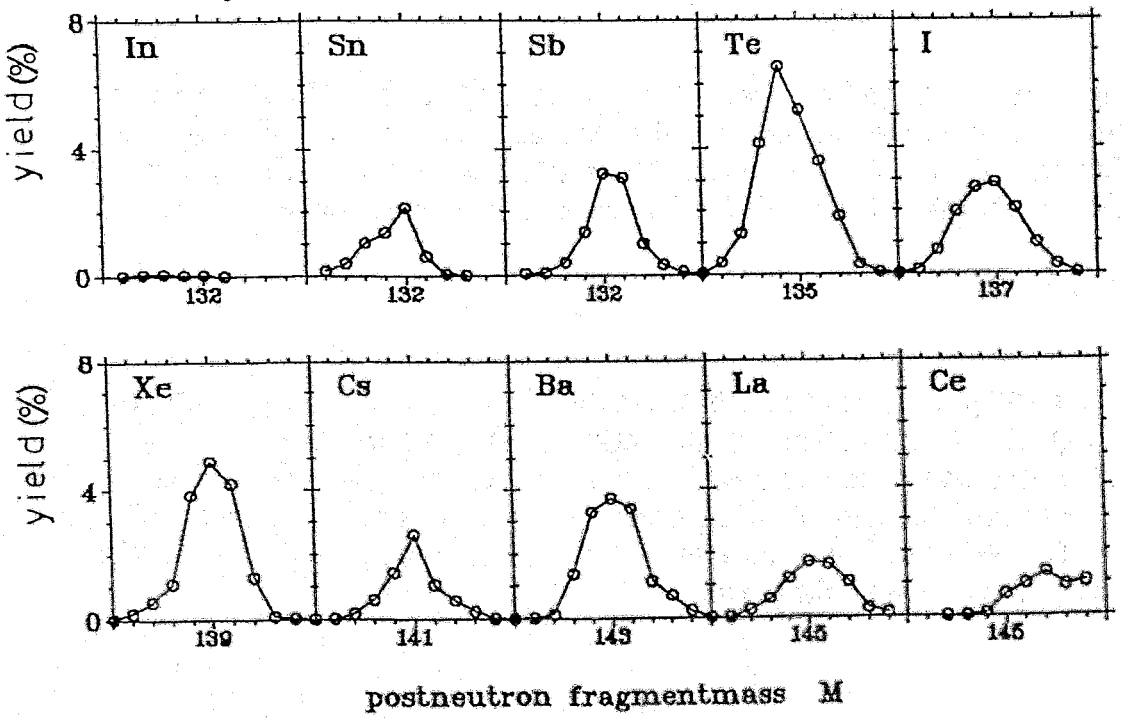

Fig. 1: Isotopic mass distributions for $^{238}U(\gamma,f)$ with 6.44 MeV bremsstrahlung

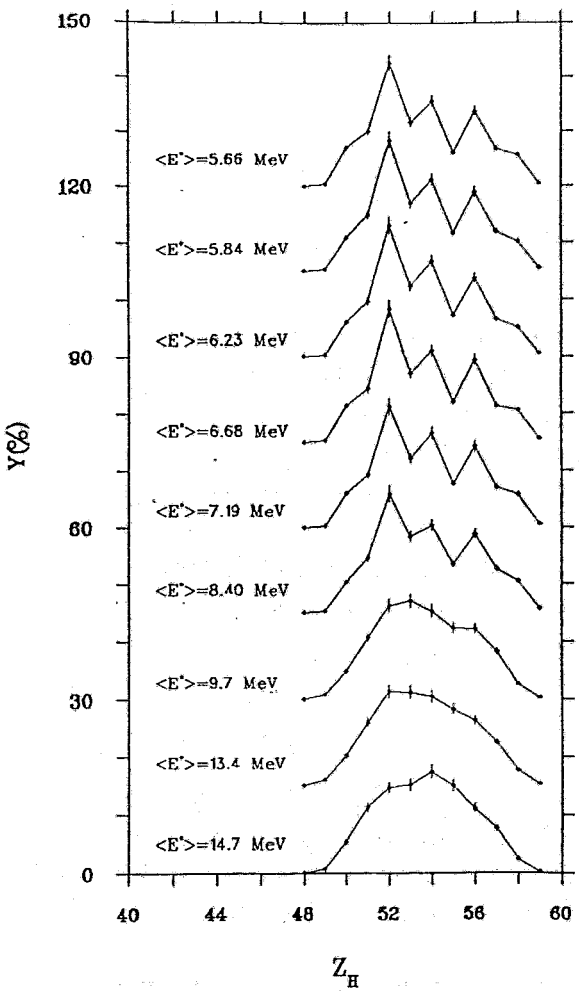

In fig.2 the element distribution for nine different average excitation energies is shown. The clear odd-even staggering for lower energies disappears as the electron energy increases above 8 MeV.
We already calculated the proton odd-even effect for ^{235}U and ^{238}U (calculations for ^{232}Th have only just started). In both cases the odd-even effect remains constant for excitation energies up to ca. 2 MeV above the barrier, and decreases then exponentially to zero. This could indicate that pairs are preferably broken when at the saddle point the energy available above the barrier is larger than the pair breaking gap, and not during the descent from saddle to scission.

Fig. 2: Elemental yields, Y, for 238U(g,f) with 6.12 - 30 MeV bremsstrahlung, corresponding to average compound nucleus excitation energies <E*> between 5.66 and 14.7 MeV. The results at <E*> = 9.7, 13.4 and 14.7 MeV are from DEF84, the others from POM93. Each consecutive curve is shifted over 15%.

5. Conclusion

In the past years a method has been developed and used to investigate mass and charge distributions using g-spectrometric methods on catcherfoils and pneumatically transported actinide targets. The method allowed for the first time a complete study of the fragment characteristics for the photofission of ^{232}Th, ^{235}U and ^{238}U. These have been studied as a function of the excitation energy in the near barrier region.

References

AMI74: S. Amiel and H. Feldstein, Proc. third Intern. Symp on the Physics and Chem. of Fission, Rochester 1974 (I.A.E.A., Vienna, 1974) Vol II, p. 65
DEF84: D. De Frenne, H. Thierens, B. Proot, E. Jacobs, P. De Gelder and A. De Clercq, Phys. Rev. C29 (1984) p. 1908
MON90: W. Mondelaers, Proceedings of the European Particle Accelarator Conference, Nice, 1990, p.526
NEL85: W.R. Nelson, H. Hirayama and D.W.O. Rogers, SLAC-Report-265, 1985
NID61: J.B. Niday, Phys. Rev. 1221 (1961) p. 1471
POM93: S. Pommé, E. Jacobs, K. Persyn, D. De Frenne, K. Govaert, M.-L. Yoneama, Nucl. Phys, to be submitted.
REU83: U. Reus, W. Westmeier, Atomic Data and Nuclear Data Tables 29 (1983) p. 193
STO70: E. Storm and H.I. Israel, Nuclear Data Tables A7 (1970) p. 565
WAH88: A.C. Wahl, At. Data and Nucl. Data Tables 39 (1988) p. 1
WES80: W. Westmeier, private communication

List of spectroscopic data.

^{M}Z(d): Mass and charge of the fission product.
E_γ: Energy (in keV) of considered gamma.
I_γ^{abs}: Absolute intensity
$T_{1/2}$ (d): half life of fission product.
$T_{1/2}$ (m): half life of the immediate predecessor of the fission product.
α: Relative part of the predecessor decaying to the fission product in study.

References are to Nuclear Data Sheets (NDS) or to ref. REU83 (NDT-83).

^{M}Z (d)	E_γ (keV)	I_γ^{abs}(%)	$T_{1/2}$ (d)	$T_{1/2}$ (m)	α (%)	Referentie
$^{83}Se^{g}$	225.2	32.6	22.3 m	13.3 s	23	[NDS-86d]
	356.7	69.9				[NDT-83]
	510.0	42.6				
^{84}Se	408.8	100	3.1 m			[NDT-83]
						[NDS-89a]
$^{84}Br^{g}$	881.6	41.6	31.8 m	3.1 m	100	[NDS-89a]
$^{84}Br^{m}$	424.0	100				[NDS-89a]
	881.6	98				
$^{85}Kr^{m}$	151.2	75.0	4.48 h			[NDT-83]
	304.9	14.0				
^{87}Kr	402.7	49.6	76.3 m	55.7 s	97.4	[NDT-83]
				16.3 s	6.8	
^{88}Br	775.3	63	16.5 s	1.52 s	99.66	[NDS-88c]
^{88}Kr	196.3	26.0	2.84 h	16.5 s	93.6	[NDS-88c]
	834.8	13.0		4.53 s	14	[NDT-83]
	1529.8	10.9				
^{88}Rb	898.0	14.04	17.78 m	2.84 h	100	[NDS-88c]
	1836.1	21.4				
^{89}Kr	220.9	20.1	3.15 m	4.40 s	87.0	[NDS-89d]
	497.4	6.67				
	586	16.64				
^{89}Rb	1031.9	58	15.15 m	3.15 m	100	[NDS-89d]
	1248.1	42.6				
^{90}Kr	539.5	28.6	32.3 s	1.92 s	75.4	[NDT-83]
	1118.7	36.2				
$^{90}Rb^{g}$	831.7	27.8	2.60 m	32.3 s	88.0	[NDT-83]
	1060.7	6.64				
$^{90}Rb^{m}$	831.7	93.9	4.30 m	32.3 s	12.0	[NDT-83]
	1060.7	7.61				
^{91}Kr	506.6	19.14	8.57 s	0.541 s	81.7	[NDS-90d]
						[NDS-80]
^{91}Rb	1137.2	3.88	58.4 s	8.57 s	100	[NDS-90d]
						[NDS-80]
^{91}Sr	749.8	23.6	9.63 h	58.4 s	100	[NDS-90d]
	1024.3	33.4				[NDS-80]
$^{91}Y^{m}$	555.6	94.9	49.71 m	9.63 h	59	[NDS-90d]
						[NDT-83]
^{92}Kr	1218.6	61.6	1.85s			[NDT-83]
^{92}Sr	1383.9	90.0	2.71 h	4.5 s	100	[NDT-83]
	430.6	3.33				
^{92}Y	934.5	13.9	3.54 h	2.71 h	100	[NDT-83]
^{93}Sr	590.2	65.7	7.423 m	5.7 s	97.5	[NDS-88d]
	875.8	23.4		2.70 s	10.4	[NDS-85a]
^{93}Y	266.9	6.8	10.10 h			[NDS-88d]
^{94}Rb	836.9	87.1	2.702 s			[NDS-85a]
^{94}Sr	1427.6	94.2	75.1 s	2.70 s	89.6	[NDS-85a]
				0.38 s	8.9	[NDT-83]
^{94}Y	918.7	56	18.7 m	75.1 s	100	[NDS-85a]
^{95}Sr	685.9	24.0	24.4 s	0.38 s	91.1	[NDT-83]
	826.9	3.04		0.217 s	14.2	
	945.3	2.38				

^{95}Y	954.2	19	10.3 m	24.4 s	100	[NDS-83a] [NDT-83]
^{95}Zr	724.2 756.7	43.7 55.4	64.03 d			[NDT-83]
^{97}Zr	743.4 355.4	94.35 2.378	16.90 h			[NDS-85e]
^{99}Zr	469.3 545.9 594.1	45 38 22	2.1 s	1.51 s	99	[NDT-83]
^{99}Mo	181.1 739.4	6.08 12.1	2.75 d			[NDT-83]
^{99}Te^{m}	140.5	87.7	6.01 h	2.75 d	87.6	[NDT-83]
^{100}Zr	504.5	31	7.1 s	0.94 s 0.735 s	100 100	[NDS-90c]
^{100}Nb	535.7	45.7	1.5 s	7.1 s	100	[NDS-90c]
^{101}Mo	191.9 505.9 590.1 590.9 1012.5	18.8 11.8 5.64 16.35 12.8	14.61 m			[NDS-85c] [NDS-91b]
^{101}Tc	127.2 306.8	2.86 88	14.22 m	14.61 m	100	[NDS-85c] [NDS-91b]
^{102}Tc^{g}	475.2	6.7	5.28 s	11.3 m	100	[NDS-82a] [NDS-91c]
^{103}Tc	343.6 346.4 562.9	4.04 17.5 7.0	54.2 s	67.5 s	100	[NDS-85b]
^{103}Ru	497.1	90.9	39.26 d			[NDS-85b]
^{104}Tc	358.0 535.1	89 16.5	18.3 m	60 s	100	[NDS-84c]
^{105}Ru	316.4 469.4+470	11.1 17.7	4.44 h			[NDS-86c]
	676.4 724.3	15.7 47.3				
^{105}Rh^{g}	306.1 318.9	5.10 19.1	36.36 h	4.44 h (45 s)	72 (+28) (100)	[NDS-86c] [NDT-83]
^{106}Rh^{g}	621.9	9.935	29.80 s	373.59 d	100	[NDS-88a]
^{107}Rh	302.8 392.5	66 8.8	21.7 m	3.75 m	100	[NDS-91a]
^{109}Pd	88.04	3.61	13.7 h			[NDS-84a]
^{127}Sb	473.0 685.7	24.7 35.3	3.85 d	2.1 h 4.4 m	100 100	[NDT-83]
^{128}Sn^{g}	482.3	59.0	59.1 m			[NDS-83b]
^{128}Sb^{m}	753.9 314.0	96 88.3	10.4 m	59.1 m	100	[NDS-83b]
^{129}Sb^{g}	812.8 914.6	43 20.3	4.32 h	7.4 m 2.5 m	100 100	[NDT-83]
^{130}Sn^{g}	779.8	59.1	3.72 m			[NDT-83]
^{130}Sb^{A}	330.9 793.4 839.4	78 100 100	39.5 m	1.7 m	100	[NDS-89e]
^{130}Sb^{B}	793.4 839.4 1017.5	86 100 30	6.3 m	3.72 m	100	[NDS-89e]
^{131}Sn^{A}	798.5 1226.2 450.0	*(86/3)* *(100/3)* *(90/3)*	61 s			[NDT-83]
^{131}Sb	642.3 933.1 943.4	22 25 44	23 m	61 s	100	[NDT-83]
^{131}Te^{g}	149.7	68.9	*(23 m)*	23 m 1.25 d	93.2 22.2	[NDT-83]
^{131}Te^{m}	149.7	20.5	1.25 d	23 m	6.8	[NDT-83]

	852.1	21.0				
^{131}I	364.5	81.2	8.02 d	25 m	100	[NDT-83]
				1.25 d	77.8	
^{132}Sn	246.7	42.2	*(38.3 s)*			[NDT-83]
	340.2	43.2				
	898.5	42.2				
	992.2	38.4				
$^{132}Sb^{A}$	496.5	13	4.2 m			[NDT-83]
	1041.5	18				
$^{132}Sb^{B}$	635.6	10.0	2.8 m	40 s	100	[NDT-83]
	696.8	87.0				
	816.6	11.0				
	973.9	99				
	989.6	15.0				
^{132}Te	228.2	89	3.26 d	4.2 m	100	[NDT-83]
				2.8 m	100	
^{133}Sb	632.4	3.87	2.5 m			[NDS-86e]
	817.8	18.5				
	1096.4	43				
$^{133}Te^{g}$	312.1	62.4	12.5 m	55.4 m	15.	[NDS-86e]
	407.6	27.1		2.5 m	70.	
$^{133}Te^{m}$	647.4	19.3	55.4 m	2.5 m	30.	[NDS-86e]
	863.9	15.6				
	912.7	55.				
	914.6	10.9				
^{133}I	529.9	87	20.8 h	55.4 m	85.	[NDS-86e]
				12.5 m	100	
$^{134}Sb^{A}$	297.0	97.	10.4 s			[NDT-83]
	706.3	57				
	1279.1	100				
^{134}Te	180.9	18.1	41.8 m			[NDT-83]
	201.2	8.76				

	210.5	22.5				
	278.0	21.0				
	435.1	18.7				
	566.0	18.4				
	767.2	29.2				
$^{134}I^{g}$	595.4	11.2	52.6 m	3.69 m	98	[NDT-83]
	621.8	10.6		41.8	100	
	847.0	95.4				
	884.1	64.9				
	1072.6	15.0				
^{135}Te	603.5	37.	19 s	1.71 s	84	[NDS-87b]
	266.8	10.4		0.82 s	24	
^{135}I	1131.5	22.7	6.57 h	19 s	100	[NDS-87b]
	1260.4	28.9				
$^{135}Xe^{g}$	249.8	90.2	9.14 h	6.57 h	83.5	[NDS-87b]
						[NDT-83]
$^{135}Xe^{m}$	526.6	80.5	15.29 m	6.57 h	16.5	[NDS-87b]
						[NDT-83]
^{136}Te	332.6	20.9	*(19 s)*	0.82 s	78	[NDT-83]
	578.6	20.5				
$^{136}I^{A}$	1313.0	*(66.7/1.8)*	83.4 s	17.5 s	99.2	[NDS-87c]
	1321.1	*(24.8/1.8)*				[NDT-83]
$^{136}I^{B}$	197.3	*(78.3/1.8)*	46.9 s			[NDS-87c]
	369.8	*(17.5/1.8)*				
	1313.0	*(100./1.8)*				
^{137}I	1218.0	12.8	24.5 s	2.49 s	97.3	[NDS-90b]
^{137}Xe	455.5	31.2	3.82 m	24.5 s	92.9	[NDS-90b]
^{138}I	588.8	77.4	6.49 s	1.4 s	93.7	[NDT-83]
	875.2	12.8				[NDS-88b]
^{138}Xe	258.4	31.5	14.08 m	6.49 s	90.9	[NDS-88b]
	396.5	6.3				[NDS-82b]
	434.6	20.3				

	1768.3	16.73				
$^{138}Cs^{g}$	462.8	30.7	32.2 m	2.91 m	81	[NDS-88b]
	1009.8	29.8		14.08 m	100	[NDS-82b]
	1435.9	76.3				
$^{138}Cs^{m}$	462.8	18.7	2.91 m			[NDS-88b]
						[NDS-82b]
^{139}Xe	218.6	56	39.68 s	2.29 s	90.1	[NDS-89c]
	296.5	21.7				
^{139}Cs	1283.3	8.3	9.27 m	39.68 s	100	[NDS-89c]
^{139}Ba	165.8	23.7	83.06 m	9.27 m	100	[NDS-89c]
^{140}Xe	805.5	20	13.60 s	0.86 s	90.6	[NDS-87a]
	621.9	8				
	1413.7	12.2				
^{140}Cs	602.3	49	63.7 s	13.60 s	100	[NDS-87a]
^{140}Ba	537.3	24.39	12.752 d	63.7 s	100	[NDS-87a]
^{140}La	328.8	20.6	1.6781 d	12.752 d	100	[NDS-87a]
	487.0	44.3				
^{141}Cs	588.7	5.15	24.94 s	1.72 s	99.96	[NDT-83]
^{141}Ba	190.3	46.3	18.27 m	24.94 s	99.95	[NDT-83]
	277.0	24.0				
	304.2	25.0				
	343.7	14.2				
	647.9	6.01				
^{141}Ce	145.4	48.4	32.50 d	3.92 h	100	[NDT-83]
^{142}Cs	359.6	100	1.70 s	1.22 s	100	[NDS-84d]
	966.9	37.9				
	1326.5	47.5				
^{142}Ba	231.6	12.5	10.6 m	1.70 s	100	[NDS-84d]
	255.3	21.1				
	895.2	14.3				
	1204.3	14.6				
^{142}La	641.2	47.4	91.1 m	10.6 m	100	[NDS-84d]

^{143}Ba	798.7	15.2	14.5 s			[NDS-86a]
	211.5	24.9				
^{143}Ce	293.3	42.8	33.0 h	14.2 m	100	[NDS-86a]
^{144}Ba	430.5	18.3	11.5 s	1.01 s	96.83	[NDS-89b]
	388.2	13.5				
	172.8	15.4				
^{144}La	397.4	9[illegible].3	40.8 s	11.5 s	100	[NDS-89b]
	541.2	39.2				
	844.8	22.25				
^{144}Ce	133.5	11.09	284.893 d			[NDS-89b]
^{145}La	355.8	3.83	24.8 s	4.31 s	100	[NDS-86b]
	447.4	3.22				
^{145}Ce	724.2	59	3.01 m	24.8 s	100	[NDS-86b]
^{146}Ba	140.7	20.2	2.22 s			[NDS-90e]
	251.2	19.6				
$^{146}La^{A}$	258.5	63.7				[NDS-90e]
	409.9	4.33				
	924.6	7.45				
$^{146}La^{B}$	258.5	100	10.0 s			[NDS-90e]
	409.9	87.4				[NDS-84b]
	503.1	27.9				
	514.6	33.5				
^{146}Ce	210.5	4.95	13.52 m	6.27 s	100	[NDS-90e]
	218.2	20.8				
	264.6	8.99				
	316.7	56.2				
^{146}Pr	453.9	48	24.15 m	13.52	100	[NDS-84b]
^{147}Pr	577.9	16.3	13.6 m	56.4 s	100	[NDT-83]
	641.3	19.0				
^{147}Nd	91.1	27.9	10.98 d			[NDT-83]
^{148}Ce	291.7	16.7	56 s	1.05 s	100	[NDS-90a]
$^{148}Pr^{A}$	301.7	61	2.27 m	56 s	100	[NDS-90a]

$^{148}Pr^{B}$	301.7 450.8	95 50	2.0 m			[NDS-90a]
^{149}Nd	114.3 270.2	19.0 10.7	103.2 m	2.26 m	100	[NDS-85d]
^{151}Nd	116.8	43.36	12.44 m			[NDS-88e]
^{151}Pm	340.1	22.5	28.40 h			[NDS-88e]
^{153}Sm	103.2	28.3	46.7 h			[NDT-83]
^{155}Sm	104.3	75.1	22.1 m			[NDT-83]

Channeling of heavy ions: perspectives for precision spectrometry

A.A.Alexandrov, I.A.Alexandrova, Yu.V.Pyatkov, A.I.Slyusarenko,

Moscow Engineering Physics Institute

The ionization chambers have demonstrated impressive results in mass and charge fission fragment (FF) spectroscopy. Nevertheless the semiconductor detectors (SCD) can still be useful in many applications, as in the siliconball [1], detector telescopes in meson physics studies [2], various multistrip systems. There are also still unused but potentially powerful possibilities concerned with channeling.

The channeling effect is known to take place, when the ion moves "slides" along some direction (axis or plane) in the crystal lattice. For fission fragment range of masses and energies the specific energy loss dE/dx in Si crystal is about two times smaller in the channeling mode of motion than that for the ordinary one. This fact results in a significant lesser energy loss due to nuclear collisions together with angular struggling decrease. The range of a particle moving in such an "oriented" direction correspondingly increases . Moreover, the influence of the crystal lattice leads to the auto-focusing of the ion beam on condition of its primary orientation towards the lattice axis (the so-called damping effect) [3].

These and some other rather interesting results were confirmed in the experiments performed at the one-armed MEPhI spectrometer [4]. To observe such an effect one must, however, provide a beam with a rather small angular divergence. The necessary condition for an ion to move in this channeling mode is that the angle between its direction and the crystallographic axis doesn't exceed the value of

appr. $(2*Z_1*Z_2*e^2/d*E)^{1/2}$, where $Z_{1,2}$ - are nuclear charges of ion and crystal matter, d- is the channel diameter and E is the kinetic energy of the incoming ion. These results in about 0.8^o for the mean heavy and 0.6^o for the mean light fission fragment within the <110> axis direction. The experimental curve for the SCD with 50 mkg*cm^{-2} gold surface contact, shown in FIG. 1, correlates well with the estimations. Thus, this condition for channeling is fulfilled in most known mass-separators and TOF spectrometers.

Unfortunately, not all the ions move in such a way. Some of them are scattered by the surface contact or amorphous layer and don't enter this mode at all, while another portion escapes from the channeling mode somewhere near the start. This leads to a rather complex shape of the detector response function, which is formed by overlapping components of "channeled", and " dechanneled" ions. These components however may be well resolved on two-dimensional plot energy - time-of-flight (FIG.2a). For the heavy group of FF the resolution is almost complete (FIG. 2b). The additional criterion to distinguish between these two groups may be the nuclear charge of fragments, as it differs by at least 6 units for dechanneled and channeled ions in the overlapping region. The percentage of the channeled ions amounts up to 85% for a ion-implanted SCD.

Our investigations for separated [5] as well as for unseparated FF, Ni and Al ions [6] confirmed the result of Moak [7] (for ^{127}I ions) that for the channeled particles the pulse height defect extrapolated to the infinite field strength in the detector approaches zero (with an accuracy of 2%). This fact may be put into a basis of non-parametric "absolute" energy calibration for FF [8]. the necessity of a precise calibration been often underlined at a number of related Conferences [9].

The logical consequence of the diminished dE/dx in the channeling mode is the improvement of the energy resolution. This is shown in FIG. 4 for $^{239}Pu(n_{th},f)$ mass-separated FF. The "residual" resolution seems to be governed by recombination losses of charge carriers, mainly at the surface of the detector [10]. The resolution limit can be achieved in case of homogeneous surface, as it was likely to take place in ref.[7] or one can try to "protect" the holes from recombination at the surface by a "frozen" electric field [11]. Taking all this into account, one may hope to obtain the energy resolution of about 200 keV for the heavy group of FF.

The channeling effect may be used as well in specific energy loss measurement for nuclear charge identification. To this end we have tried a thin oriented detector at the MEPhI spectrometer. The detector thickness was chosen so, that in the non-oriented mode only light fragments could pass it. When the detector was rotated, that its crystal axis was parallel to the FF beam, the spectrum shown in FIG. 5 could be observed in the stop E-detector put close in a telescope assembly. When the latter detector was distanced from the thin dE-detector by 90 cm, the difference in count rate was about 10 times (Fig. 6). This drastically decrease of the angular struggling must of course influence the energy struggling as well. Thus an oriented absorber may be useful for charge FF spectrometry.

Summing up, one may note that the possibility of reaching more or less the same values of energy and charge resolution for the heavy FF group as for the light one will make it possible to include the laws of conservation for double-armed measurement interpretation. From our point of view it is desirable to study in details the heavy group FF M-E-Z spectra of actinides with the help of channeling.

1. G.Pausch,W. Bohne, H. Fuchs et al, preprint HMI-P/92/P2-Paul
2. M.Gornov et al, preprint MEPhI 076-83, M. 1983
3. M.A.Kumakhov, G. Shirmer Atomic Collisions in Crystals, M. 1980
4. A.A.Alexandrov,I.A.Alexandrova,A.V.Ermolenko, Nucl.Instrum.Meth., A303(1991)323
5. A.A.Alexandrov,I.A.Alexandrova,S.L.Podshibyakin, Nucl.Instrum.Meth., A312(1991)542
6. A.A.Alexandrov,I.A.Alexandrova, Yu.V. Pyatkov et al,Rad.Effects 124(1992) 191
7. C.D.Moak, J.W.T. Dabbs W.W.Walker, Rev.Sci.Instr.,37(1966)1131
8. A.A.Alexandrov,I.A.Alexandrova,S.L.Podshibyakin Nucl.Instrum.Meth., A302(1991) 478
9. G. Signarbieux, Proc.Int.Workshop Dynamical aspects of nuclear fission, Smolenice 1991,p.19
10. A.A.Alexandrov, V.F. Kushniruk, Yu.V. Pyatkov et al In. Methods of Exper.Nucl.Physics in Studies of Fission Processes and Products, M. 1985 p.33
11. V.K. Eremin, E.M. Verbitskaya, N.B. Strokan, Sov.Jrn.Theor.Phys.,56(10) (1986) 1987
12. A.A. Alexandrov, Yu.V. Pyatkov, A.I. Slyusarenko et al,in.:Experim. Meth.of Low and Middle Energy Nucl. Physics, M. 1986,105

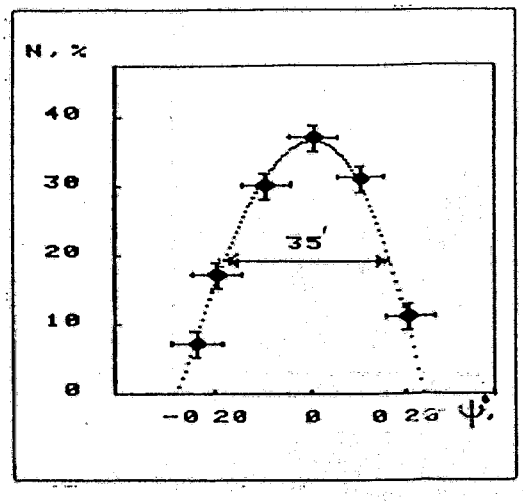

Fig. 1. Yields of the channeling FF for the middle part of the light ion group v.s. angle of detector's <110> crystal axis with respect to the fragment beam.

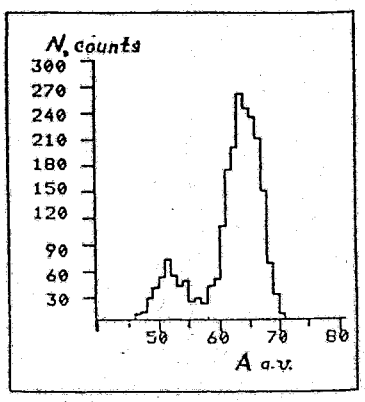

Fig. 3. ^{235}U FF pulse-height spectrum for the middle part of the heavy ion group, presented in fig. 2b at fixed time-of-flight value.

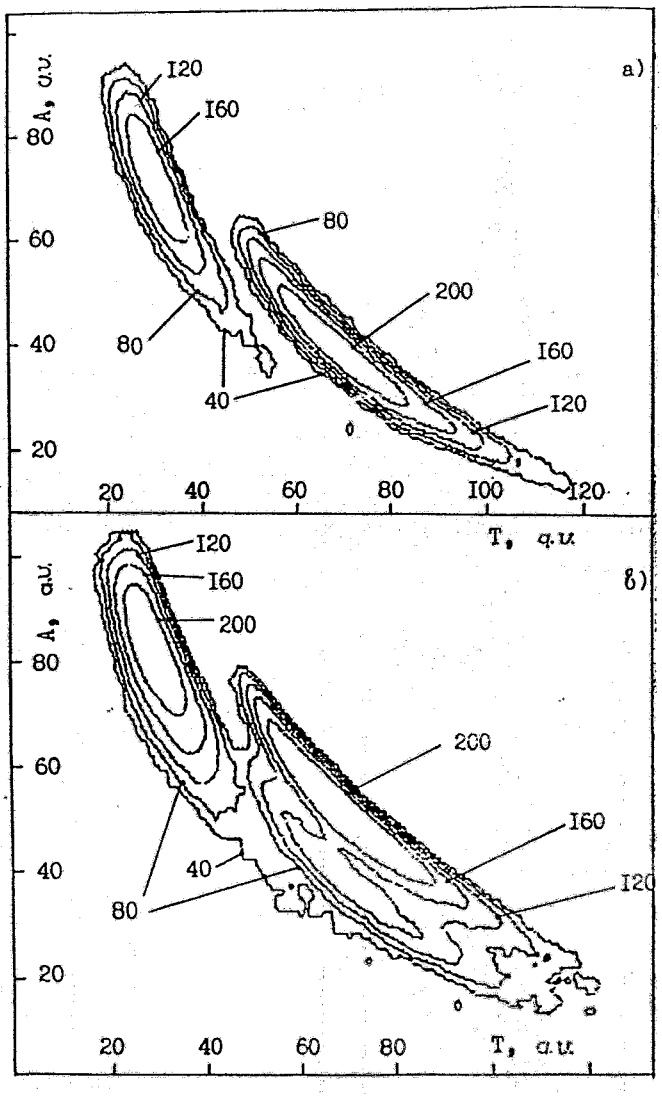

Fig. 2. Yields of FF v.s. time-of-flight (T) and amplitude of the detector signal (A):
a) the angle between FF and detector crystal axis <110> is 4 .
b) the axis <110> is parallel to the FF beam with $\pm 5'$ accuracy.

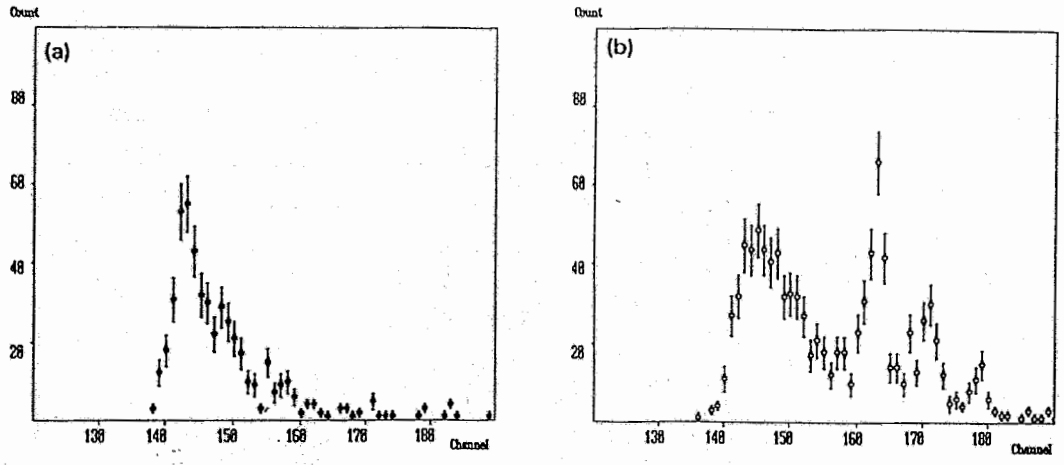

Fig. 4. Pulse-height spectra for $^{239}Pu(n_{th},f)$ FF. The energy difference between neighbouring lines is 3.05 MeV; (a) the angle between FF and detector axis <110> is 3°; (b) the axis <110> is parallel to the FF beam.

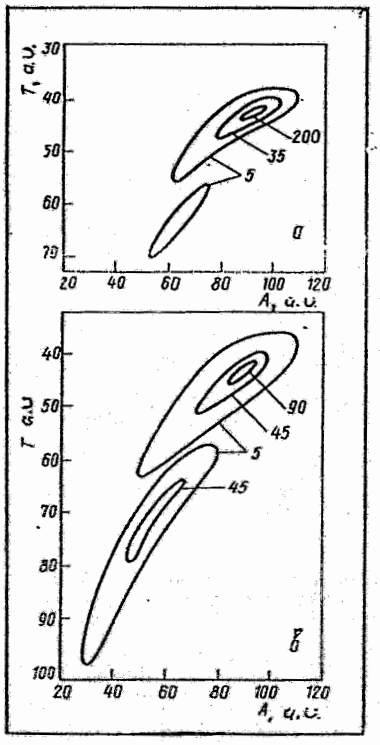

Fig. 5. Two-dimensional plot amplitude - time-of-flight for the Δ E-SCD for nonaligned (a) and aligned detector (b).

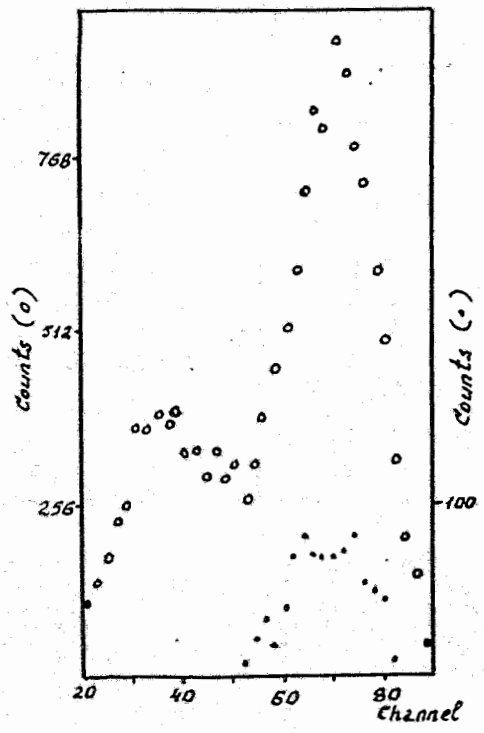

Fig. 6. FF pulse-height spectra Δ E-SCD for aligned o and nonaligned • modes.

High–Energy γ–Rays in Heavy–Ion Fusion–Fission

J. B. Fitzgerald
Max–Planck–Institut für Kernphysik, D-W-6900 Heidelberg FRG

Abstract

Calculations based on energy systematics suggested that, for the system ^{197}Au(^{19}F,f) at 120MeV, fissions with one fragment near ^{132}Sn might show an enhanced high-energy γ-ray yield (E_γ >3MeV). Such a component has now been observed for this system in a measurement with the Heidelberg-Darmstadt Crystal Ball, with a maximal enhancement by a factor of nearly 2 at E_γ=6MeV. Two further reactions with different fragment mass distributions have now been studied to provide additional information on the source of this significant new component of the fragment decay.

Introduction

Recent experimental studies have provided extensive information on the de-excitation of fission fragments from heavy–ion fusion–fission reactions [1]. All of the measured contributions – γ-ray emission (measured for $E_\gamma \leq 3$MeV), neutron evaporation (see also [2]) and fragment TKE – are either constant with mass or rather smooth. However, the calculated energy release, from ground-state mass evaluations, shows a local maximum when the heavy fragment is in the A$\sim$132 region with spherical ground-state configurations (rather than near symmetry, in the A$\sim$100 region of deformation). This poses the question: where does the additional energy release go to, if not neutrons and low-energy γ-decay?

It was proposed [1] that the difference between the observed decay energy (in γ-rays below 3MeV and neutrons) and the values suggested by the calculations might be carried by higher-energy γ-rays. It would be surprising if the γ-ray spectrum above 3MeV showed large variations as a function of mass; the very low-energy part of the spectrum shows small differences in the discrete component (the "E2–bump") related to nuclear structure properties of the fragments, and these differences are well understood. The statistical component however appears to be similar for all masses (up to $E_\gamma \leq 3$MeV). On the other hand, there have been recent direct and indirect indications of possible radiative transitions accompanying large shape changes in fission fragments. In the thermal neutron induced fission of ^{248}Cm [3], "hot" fission events (those with low TKE and long scission configurations) appear to show lower than expected neutron emission, and it has been suggested that the fragments may relax from these highly deformed states to their ground-states without particle emission, the energy released by this relaxation process being carried away by some other, presumably radiative, decay. A more direct indication of strongly fragment mass-asymmetry dependent behaviour of the high-energy γ-ray spectrum was provided by results from an investigation of the spontaneous fission of ^{252}Cf [4],[5]. where an increased so-called "non-statistical" component has been observed at 3-8MeV in the γ-spectrum near symmetric mass splits (A$\sim$126).

Experiment

In order to investigate this surprising possibility, an experiment was performed with the Heidelberg-Darmstadt Crystal Ball 162 element 4π NaI scintillator array, and a complete data analysis has now been carried out. A total

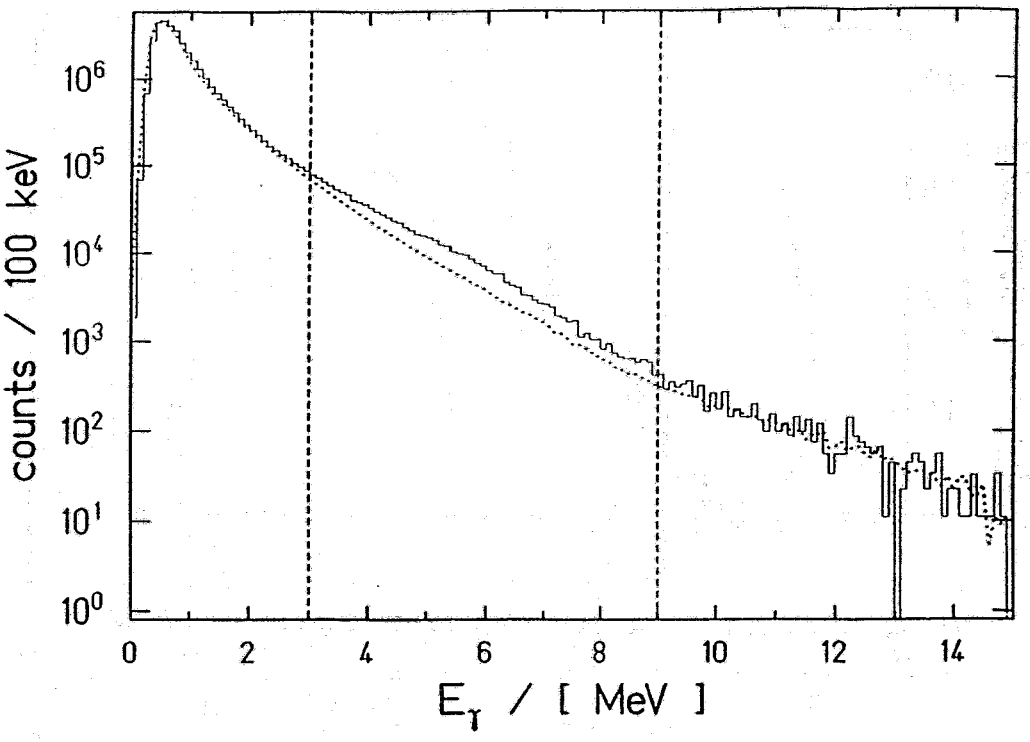

Figure 1: Energy spectrum for γ-rays from $130 \leq A \leq 135$ (solid) and from symmetric mass splits (dotted line)

of 5 million fragment–fragment–γ coincidence events were recorded from the heavy-ion fusion-fission reaction ^{197}Au(^{19}F,f) at a beam energy of 115MeV, with the fission fragments detected in a pair of symmetrically placed position-sensitive parallel-plate avalanche counters (PPAC) for determination of the fragment mass asymmetry. The Crystal Ball was used to record γ-ray spectra up to 20MeV as a function of fragment mass.

The Crystal Ball allows clean separation of neutrons and γ's by time-of-flight. The γ–ray spectra in coincidence with symmetric mass-splits (in the mass region $94 \leq A \leq 119$) and with events with one fragment in the mass region $130 \leq A \leq 135$ are shown in figure 1. The spectra are normalised on the number of fission events in each mass cut, and as expected are rather similar below 3MeV and above 9MeV (the entrance channel GDR region). However, in the region 3–9MeV, the asymmetric masses show clearly enhanced γ-ray intensity.

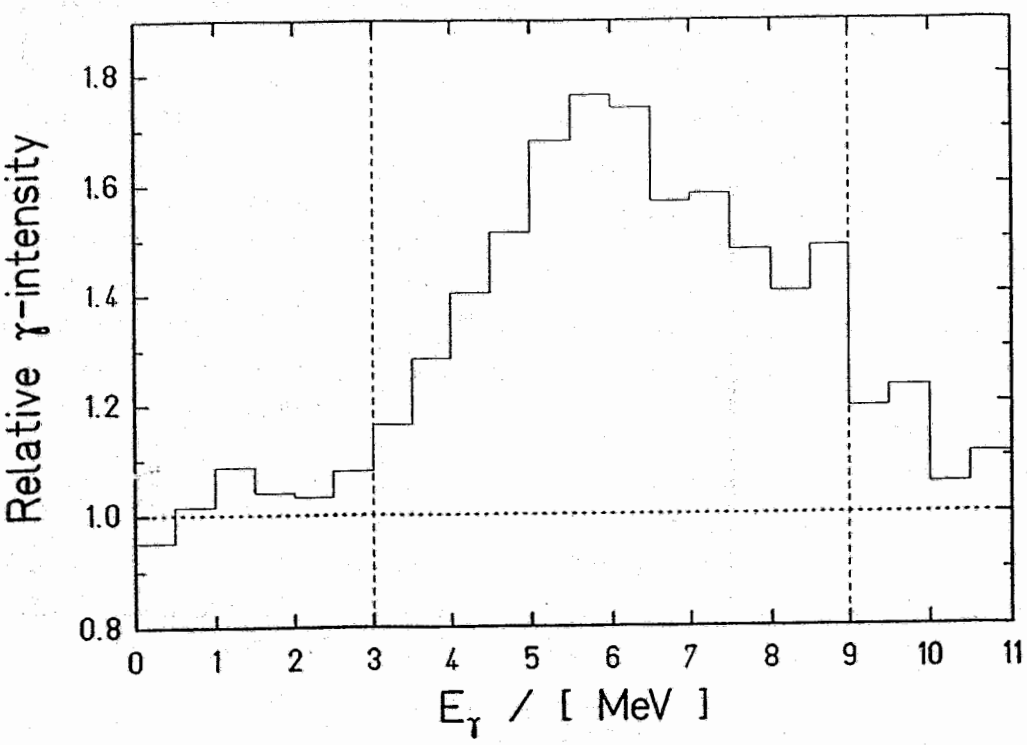

Figure 2: Ratio of γ-yield for $130 \leq A \leq 135$ to yield at symmetry

In total, the yield in this region is increased by 32% for $130 \leq A \leq 135$. Figure 2 shows the ratio of the γ-ray intensity for A$\sim$132 to that for symmetric mass splits as a function of γ-ray energy. The yield at 6MeV is increased by a factor of 1.8, corresponding to a very large enhancement.

The increased yield per fission (i.e. divided by the fragment yield) in the region 3–9MeV (compared to the yield at symmetry) is plotted as a function of fragment mass in figure 3. Since the γ-ray is observed in coincidence with both fragments, and there is no means of assigning it to one or other of the fragments on an event-by-event basis, the yield is plotted against both fragment masses. The observed yield in this "bump" (uncorrected for detector efficiency) reaches a maximum of 6.5 γ's per 100 fissions at A$\sim$132, with a mean energy of nearly 5MeV. Correcting for the Crystal Ball response, and taking account of the broadening introduced by the PPAC mass resolution, suggests a figure of $\sim$15 γ's per 100 fissions (A=132), or around 1MeV per fission on average. If the

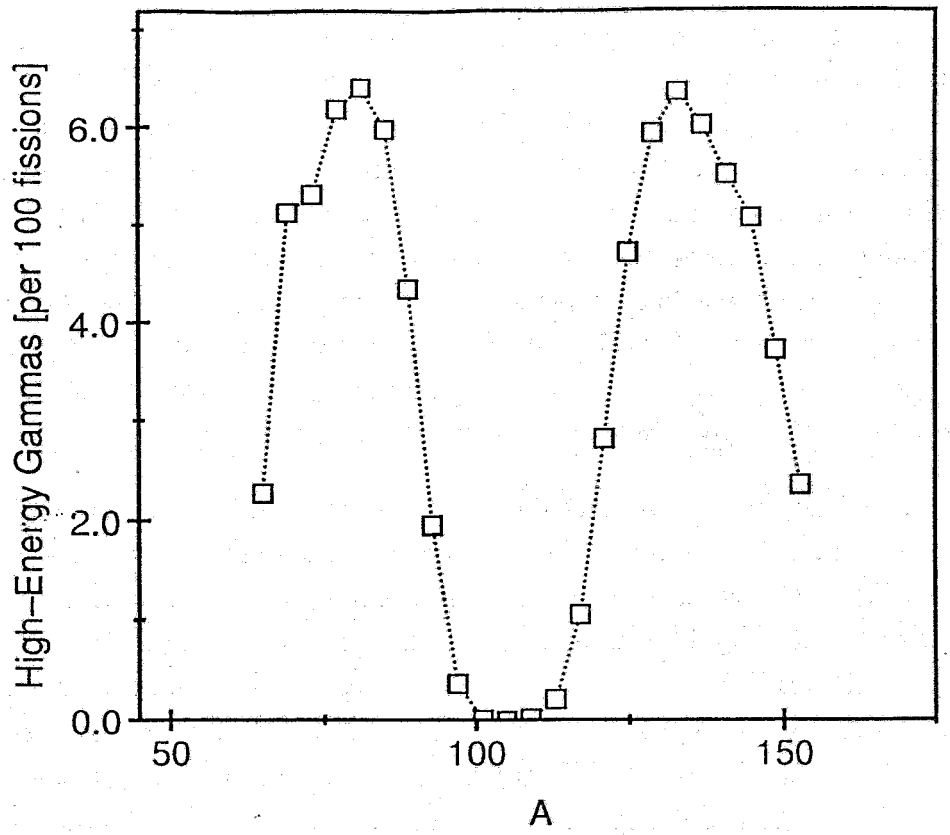

Figure 3: Excess γ-yield (compared to symmetry) per fission vs fragment mass

yield of such γ-rays shows fine structure as a function of fragment mass (or of neutron or proton numbers) then the maximum yield for a given fragment may be even higher. This new component is clearly a very significant contribution to the total fission decay energy.

It should be noted that, by plotting the γ-ray excess yield divided by the fragment yield, mass resolution effects lead to an overestimate of the true γ-yield for very asymmetric fissions (where the mass yield is sharply dropping). If the width of the observed high-energy γ-ray excess distribution as a function of mass (see figure 3) arises only from the fact that the nuclear species emitting these γs cover a wide mass region, then the observed yield divided by the fragment yield gives a true reflection of the relative frequency of emission as a function of fragment mass. If, however, the width observed is due only to detector mass resolution effects (with all the high-energy γ-ray

excess produced by one isotope of one nuclear mass) then the resulting distribution should *not* be divided by the fragment yield curve. Since the yield varies within the region of interest by more than an order of magnitude, the peak position and shape can be significantly distorted by this effect. In fact, the evidence suggests that the resolution of the current experiment is a large contribution to the observed width, but also that many nuclear species are involved in producing this new γ-component, and therefore neither the distribution of the observed total "raw" (i.e. not scaled according to fragment yield) γ excess, nor the excess per detected fragment in each mass bin, is truly representative of the distribution of nuclei responsible.

The difficulty of treating correctly the combination of detector resolution and mass yield effects, and the very different fragment yield curves obtained in heavy-ion fusion-fission (symmetric fission) and spontaneous (asymmetric) fission, make direct quantitative comparisons difficult. However. it is clear that the distribution of the high-energy γ-ray excess yield is very similar, for the heavy fragment only, to that from ^{252}Cf [5], suggesting that this effect is indeed associated with the A$\sim$132 region (rather than, for example, special symmetry properties of the system). Furthermore, in both systems, the total excess yield is around 20 times higher than the yield of any strongly produced product nucleus in the mass region where the "bump" is observed. If only one nucleus were emitting such γ's, this would correspond to $\sim$100MeV per nucleus. A more realistic estimate, assuming 1 γ is emitted per nucleus, suggests that at least 20 isotopes are involved in producing the "bump". In fact more neutron rich products are formed by ^{252}Cf s.f. than by ^{19}F+^{197}Au, indicating that a rather large area of the N-Z plane is responsible. The effect cannot therefore be ascribed to the spectroscopic properties of a single nucleus or even a few nuclei, or to a special proton or neutron number, but is associated with a large range of nuclei.

The mechanism producing such high-energy γ's is unknown, but the data strongly suggest an association with the mass 120–140 region, where a large shape change is undergone on passing from the scission point to the ground-state. Such nuclei also exhibit relatively "hard" shapes or increased "stiffness" at some point during this process, and it has been suggested that this property may be associated with the increased yield of high-energy γ's. Alternative theories have suggested that the emission of the γ-ray is related to vibrations

or oscillations of the combined system following scission [6]. In this model, however, the excess γ yield was predicted at (and symmetically about) half the mass of the fissioning system. The comparison of data from the two systems now investigated does not therefore support this alternative description.

Further Investigations

The observation of this new high-energy γ-ray component in the system $^{19}F+^{197}Au$ has prompted further experimental investigations. The heavy-ion fusion-fission reactions $^{18}O+^{232}Th$ and $^{18}O+^{238}U$, leading to very much heavier compound nuclei and therefore different complementary fragments for any given product nucleus, have been studied, again with the Heidelberg-Darmstadt Crystal Ball in coincidence with parallel-plate avalanche counters for mass determination. The regions of the N-Z plane populated in these fission reactions should also differ from those observed in the reactions $^{19}F+^{197}Au$ and ^{252}Cf; in terms of N/Z ratio the new reactions fall between the two previous measurements. Analysis of the $^{18}O+^{232}Th$ data is at an advanced stage, and the fragment mass yield distribution obtained from the parallel-plate data is in good agreement with expectations. It is hoped that a comparison of the full data set of three heavy-ion fusion-fission reactions will yield more detailed information on this new decay.

Summary

The high-energy γ-ray spectrum associated with fragments in the A$\sim$120–140 region produced in the heavy-ion fusion-fission reaction $^{19}F+^{197}Au$ shows a strong enhancement at 3–9MeV. This new and surprising γ-component corresponds to a contribution of the order of an MeV on average per fission (near A$\sim$132), and the figure may be several times greater for specific isotopes; the present investigation, the first observation of this effect, aimed for high detection efficiency rather than high mass resolution. Further investigations with different compound systems have been carried out in order to gain more information on this new effect. It is hoped that high-resolution (even isotopic resolution) will in the future yield considerable information, including the question of the species responsible for the emission of these γs, and will allow more detailed measurements of the decay energy carried by this component per product nucleus.

References

[1] J.B. Fitzgerald, Proc. 22^{nd} Masurian Lakes Summer School on Nucl. Phys., Piaski (1991) 1 (and references therein)

[2] D.J. Hinde, D. Hilscher, H. Rossner, B. Gebauer, M. Lehmann and M. Wilpert (submitted to Phys. Rev. C)

[3] P. Koczon, M. Mutterer, J.P. Theobald, P. Geltenbort, F. Gönnenwein, A. Oed, M.S. Moore, Phys. Lett. **B191** (1987) 249

[4] P. Glässel, R. Schmid-Fabian, D. Schwalm, D. Habs, H.U. v. Helmolt, Nucl. Phys. **A502** (1989) 315c

[5] A. Wiswesser, Diploma thesis, MPI für Kernphysik Heidelberg (1992)

[6] K. Dietrich and J. Bondorf (to be published)

The Heidelberg-Darmstadt Crystal-Ball-Spectrometer as 4 π - Neutron Detector

Thomas Dörfler, Manfred Mutterer, Peter Singer, J.P. Theobald
TH- Darmstadt, Inst. für Kernphysik

The Heidelberg-Darmstadt Crystal-Ball Spectrometer as 4π - Neutron Detector has been tested [Dör93]. It is shown that an analysis of the events can reduce the cross talk between neighbouring NaJ-detectors. The detection efficiency for neutrons from spontaneous fission of ^{252}Cf is about 55 %. The angular resolution in the Crystal-Ball is ± 9°. The simultaneous measurement of the fission axis allows to decide wether the neutron is emitted from the light- or the heavy fragment.

Construction of the Crystal-Ball

The Crystal-Ball was constructed in the end of the 70-th at the *Max Planck Institute for Nuclear Physics* in Heidelberg. It consist of 162 pentagons and hexagons of thallium-doped NaJ - each with the same solid angle of π/40. The hygroscopic crystals are covered by 0.6 mm thick aluminum sheets. On the top a photo multiplier and a preamplifier is mounted. Putting all detectors together one gets a ball with an inner chamber of 25 cm radius and an effective solid angle of 96% of 4π.

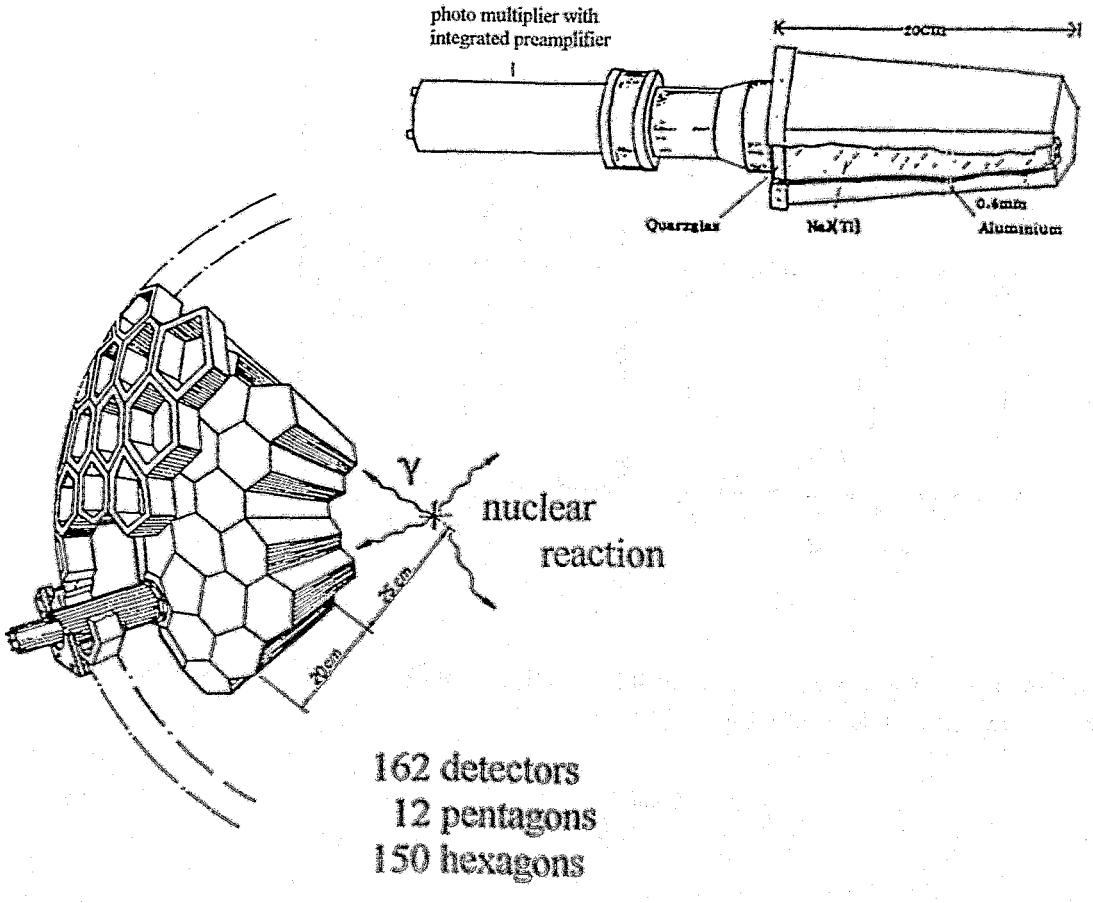

The Crystal-Ball is divided into two halves which can be seperated in order to insert vacuum tight experimental chambers with detector systems. Electronics of Crystal-Ball and experiment are controlled and read out by a CAMAC-Bus. The data recording system is a VAX and allows a rate of events of 1000 per second. The time resolution of the NaJ-detectors is about 3 ns, the dead time 0.5 µs - 1 µs.
Because of the size of the crystals (l = 20 cm) the efficiency for gamma-quanta from ^{252}Cf (sf) is about 90%-95% and for neutrons 50%-70% (depending on energy).

Detection of Gamma-Quanta and Neutrons

A separation of gamma-quanta and neutrons is possible due to the time-of-flight of neutrons over the 25 cm between source and crystals.
The spectra of yield vs. time for ^{252}Cf (sf) (Data from A. Wiswesser, MPI für Kernphysik Heidelberg 1992 [Wis92]), show the prompt gamma-peak and the delayed neutron-hump. The 6 plots are for 6 different regions of energy detected in the NaJ-crystals.

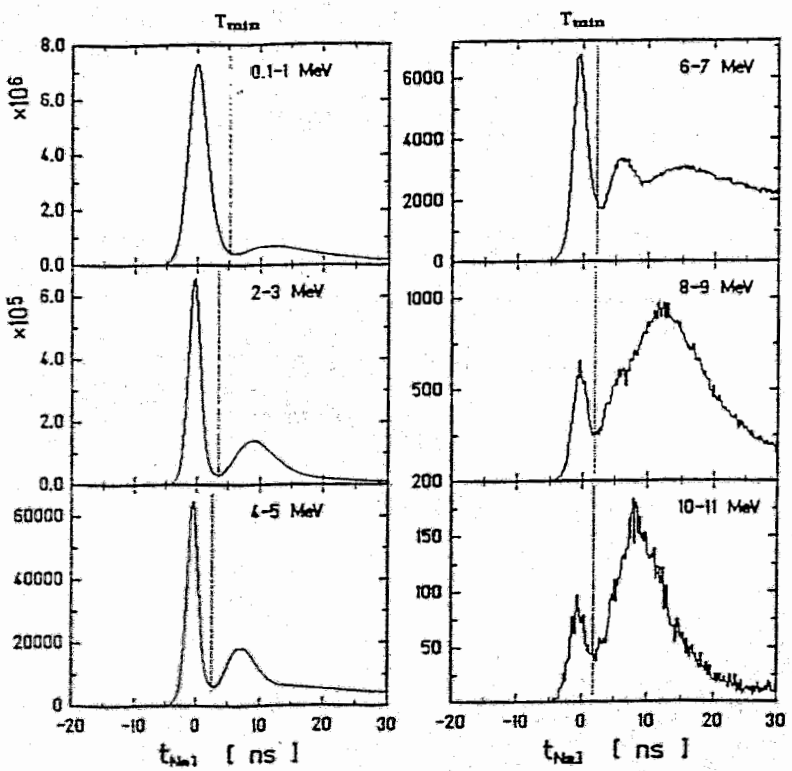

Because of the energy dependence of the response of the NaJ-detectors it is necessary to shift Tmin as function of the detected energy:

$$T\min = 1.5 + \frac{2.9}{\sqrt{E}}$$

For ^{252}Cf (sf) the energy distribution of the neutrons is known [Kle82]. For a transfer into a time-of-flight distribution it is necessary to make assumptions about the mean free path of the neutrons in the NaJ-crystal. (8 - 10 cm : [Sfa88]). In addition one has to take care of a background of delayed gamma-quanta from fission fragments [Ska70] which dominates the yield in the low-energy region and demands an upper time limit $T_{max.}$ For statistics it is no difference, because in a time window from 5 ns to 50 ns are 90 % of the expected neutrons.

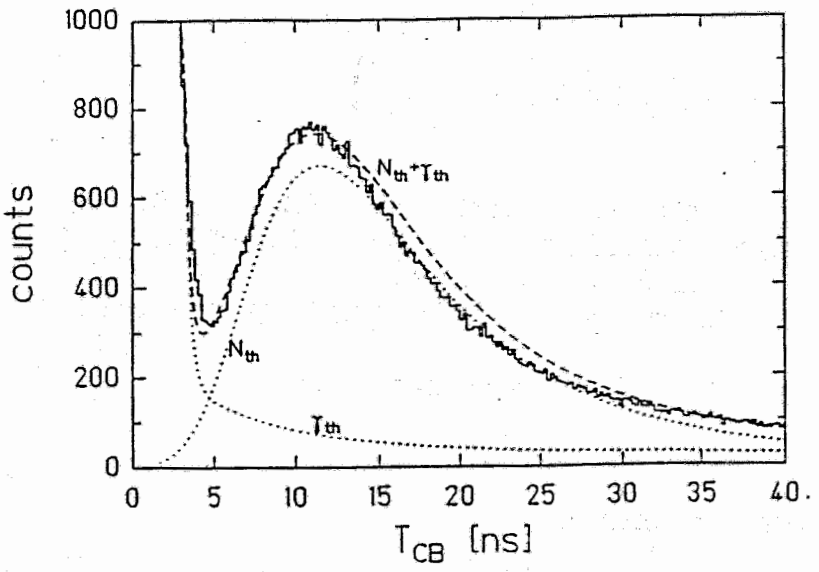

--- Expected time of flight spectra with contribution of delayed γ
__ Measured time of flight spectra

(Figure from R. Schmid-Fabian, Dissertation MPI für Kernphysik 88)

Neutron scattering cross section for ^{23}Na and ^{127}J

The reason for the response of a gamma-detector on neutrons is the scattering cross section of neutrons on ^{23}Na and ^{127}J. There are three different possibilities to produce gamma-quanta with a minimum of 50 keV (detection-limit for electronics):

1. elastic scattering:

Average energy loss for a neutron :

$$\overline{\Delta E} = E^{*}\left(1-\exp\left(-\frac{2}{A+\frac{2}{3}}\right)\right)$$

The kinetic energy of the scattered core has to be converted into gamma rays. The lower energy-limit of the NaJ-crystal for the registration of an event is 50 keV or higher (> 100 keV for the Data from A. Wiswesser).
The resulting limits for neutron energy are 1.5 MeV for scattering on ^{23}Na and 8 MeV for ^{127}J.
Scattered neutrons may be detected in a second NaJ-crystal.

2. inelatic scattering - (n, n'γ) - reactions

The cross section for neutron energies below 1 MeV is low. Above it is constant at 1 barn for ^{23}Na and 2 barn for ^{127}J.
Scattered neutrons may be detected in a second NaJ-crystal.

3. absorption - (n,γ) - reaction

The absorption of neutrons has only for ^{127}J a small contribution on the total cross section for energies below 1 MeV. A (n,γ) - reaction can easily be detected because of the difference between calculated neutron energy and measured γ-energy.

Neutron scattering cross section for ^{23}Na and ^{127}J

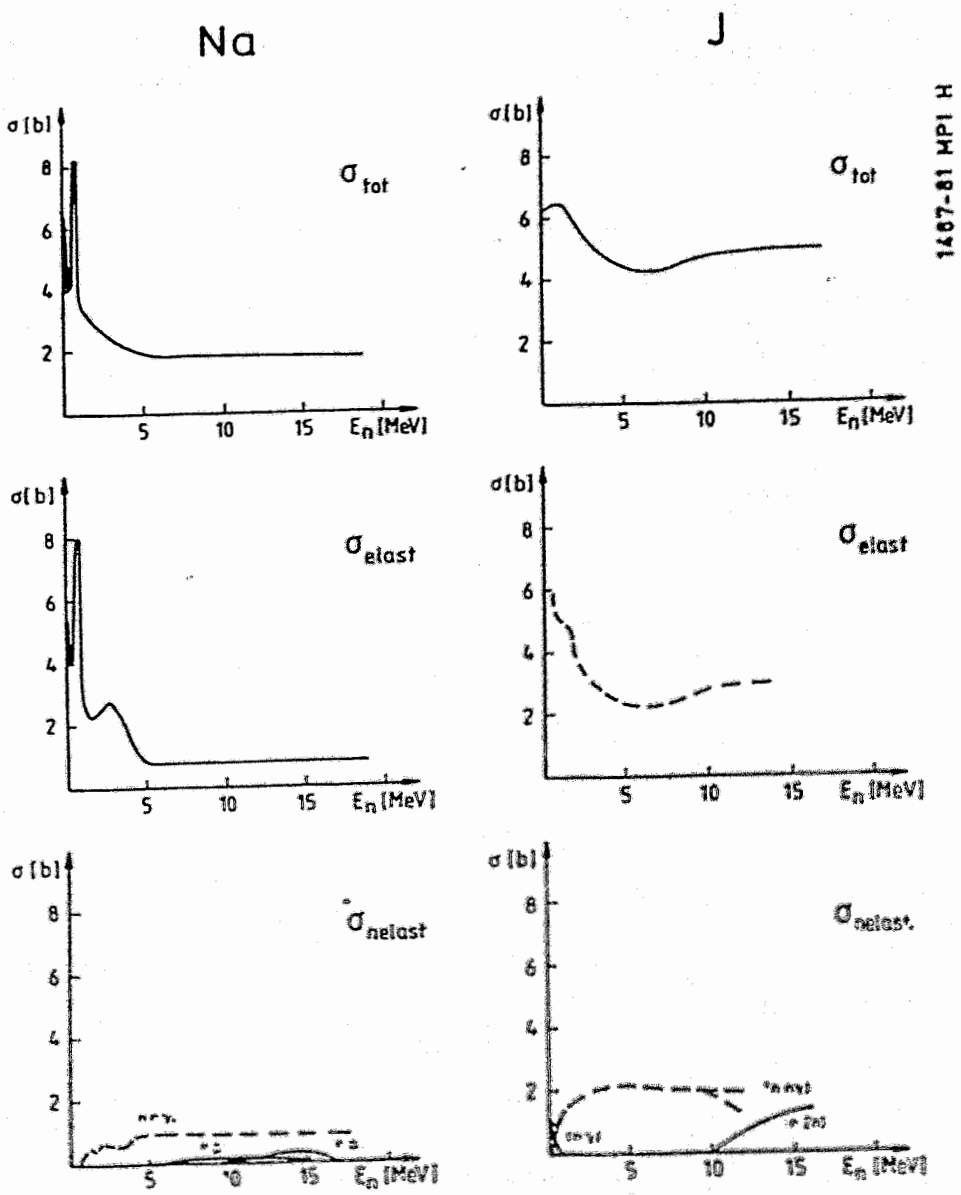

Calculated and measured detection efficiency ε

With the knowledge about the cross sections it is possible to calculate the theoretical detection efficiency for neutrons and to compare it to the measured one. The measured efficiency is deduced from the ratio of measured neutrons to expected neutrons. W. Weiter [Wei81] found that the efficiency depends on the energy threshold of the NaJ-electronics. With 50 keV the efficiency ε is constant at 75 %, with 100 keV ε rises from below 50 % to 70 % and follows the calculated curve for the non-elastic contribution.

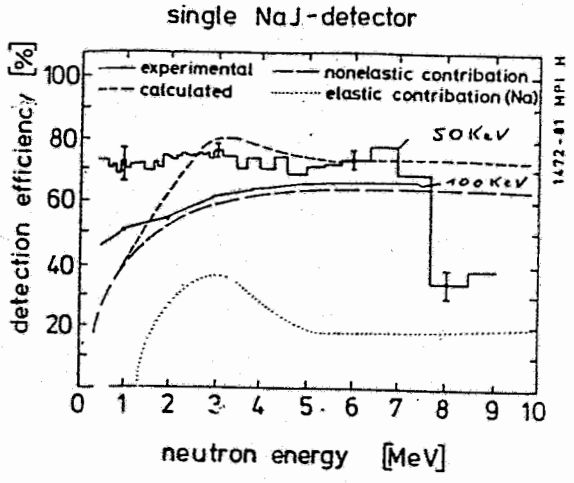

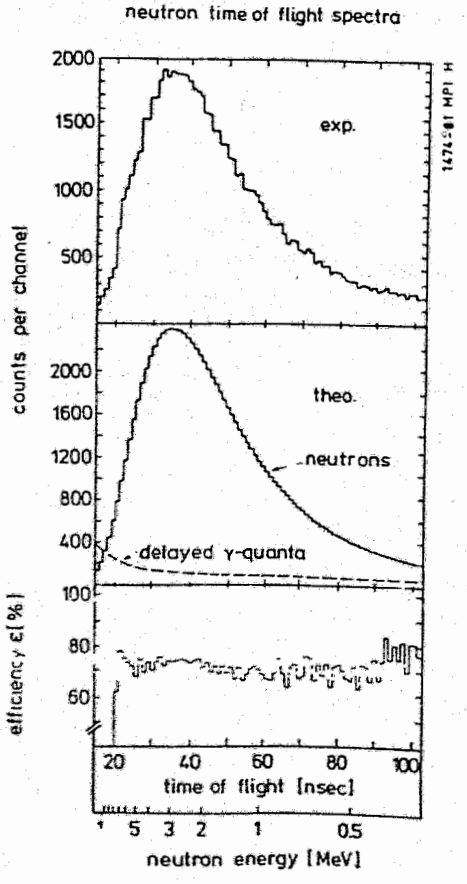

Weiter explained the difference between measured and calculated efficiency in the lower energy region as beeing due to scattering from the sides into the single NaJ-detector.
The comparison of the results for a single NaJ-detector with results from a segment with 22 NaJ-Detectors (central & 2 rings of neighbors) shows this effect of scattering. Weiter measured a efficiency up to 37 % higher. This as "Cross Talk" known effect is with all 162 detectors higher.
The reason for this is the double-detection of scattered neutrons in different NaJ-detectors and cross talk of gamma-quanta.

Suppression of Cross Talk

Because of the cross sections and solid angle of the neighbouring NaJ-Detectors one can estimate, that 90 % of secondary events (cross talk) should measured in next three rings of neighbours. From the rest, scattered neutrons may be suppressed by limiting the Time of Flight to Tmax.
In a Time of Flight window from Tmin = 5 ns to Tmax = 50 ns are 90% of the expected neutrons.

By analyzing energy and time of neighbouring detectors one can eliminate secondary events.
R. Schmid-Fabian [Sfa88] used a cross talk rejection with 2 rings of neighbours for the correction of neutron data from the spontaneous fission of ^{252}Cf. Events in neighbouring detectors within the same time were taken as cross talk of gamma-quanta, events after 1.4-times and 1.8-times time-of-flight as scattered neutrons in the 1.st and 2.nd ring. These factors he deduced from normalizing the average neutron multiplicity to 3.77.

The cross talk rejection we used [Dör93] for the correction of the neutron data from the experiment of A. Wiswesser [Wis92] is valid for 3 rings of neighbours and takes into account of the energy of scattered neutrons. This energy is calculated as difference between energy from time-of-flight calculation and measured energy in the primary detector.

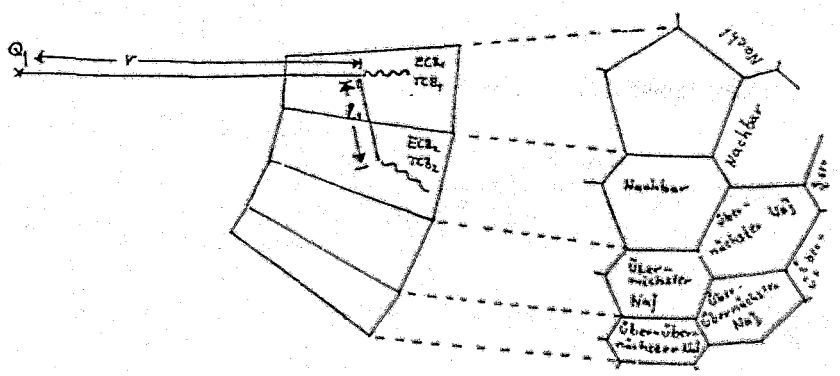

$$\Delta TCB = TCB2 - TCB1$$

$$En = \frac{mn}{2} * v1^2 = \frac{mn}{2}\left(\frac{r}{TCB1}\right)^2$$

$$En' = En - ECB1 = \frac{mn}{2}\left(\frac{li}{\Delta TCB}\right)^2$$

TCB1:		Time of the primary detector
TCB2:		Time of secondary detector
ECB1:		Energy of primary detector
mn	:	Mass of neutron
En	:	Kinetic energy of neutron before scattering
En'	:	Kinetic energy of neutron after scattering
v1	:	Velocity of neutron
r	:	Distance from source to first scattering point
li	:	Distance from first to second scattering point

$$2 * ECB1 / mn = \left(\frac{r}{TCB1}\right)^2 - \left(\frac{li}{TCB1 - TCB2}\right)^2$$

$$TCB2 = TCB1 * \left(1 + \frac{li}{r} * \frac{1}{\sqrt{1 - \frac{2ECB1TCB1^2}{mnr^2}}}\right)$$

Simplification: $(1\text{-}c)^{-1/2} = 1 + c/2$

Time limit within an event is considered as scattered neutron:

$$TCB2 = TCB1 * \left(1 + \frac{li}{r}\left(1 + \frac{ECB1TCB1^2}{mnr^2}\right)\right)$$

Because of the size of the NaJ-Crystals r and li can differ on a wide range. Mean values are:

r = 35 cm 11 = 12.25 cm 12 = 21.35 cm 1 3 = 27.3 cm

Because of the wide range of free paths and the uncertainty of the energy of scattered neutrons the cross talk rejection isn't perfect.
It is not possible to reduce the remaining cross talk in the outer rings of neighbours because of misinterpreting primary events as scattered neutrons.

Results of the Cross Talk Rejection for the example of spontaneous fission of 252-Cf

The following data and figures are based on the evaluation of 10^7 binary fission events from ^{252}Cf (sf), measured by A. Wiswesser [Wis92]. The data reduction has been done by T. Dörfler [Dör93]. Fission products energy and mass were measured by a semiconductor/parallel plate-detector system with a mass resolution of 3 u to 5 u.
Lower energy limit for the 155 used NaJ-detectors was 100 keV. The window for time-of-flight was between 3 to 7 ns (Tmin) and 200 ns (Tmax).

A sensitive method to test the quality of the cross talk rejection is to compare the angle between two neutrons from one fission event.

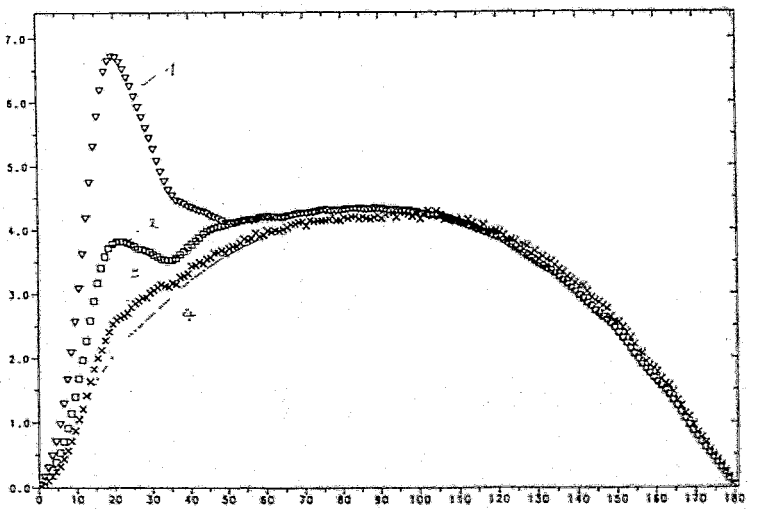

1: uncorrected data
2: cross talk rejection of Schmid-Fabian
3. energy-depended cross talk rejection of this work
4: expected distribution (Monte Carlo Simulation)

The distribution is not normalized. There may be a small fraction of cross talk over all angles.

Neutron multiplicity

The average number of emitted neutrons from the fission of ^{252}Cf (sf) $\overline{\nu} = 3.77$ is a well known number in literature. The neutron multiplicity distribution is given as

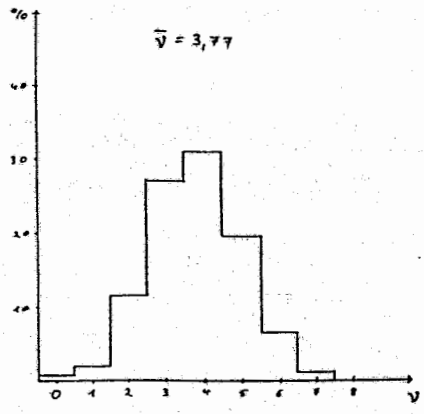

expected distribution

From the data of Wiswesser [Wis92] we found:

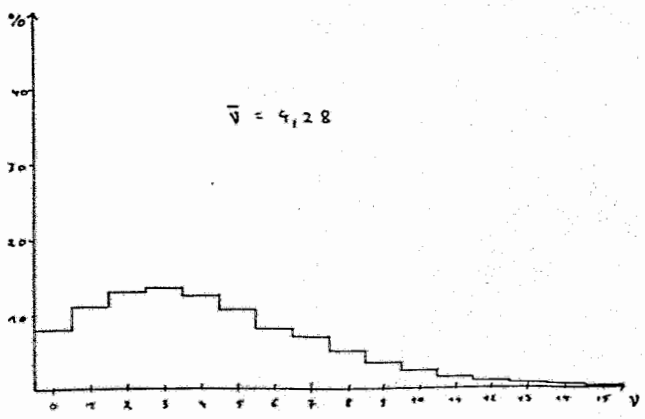

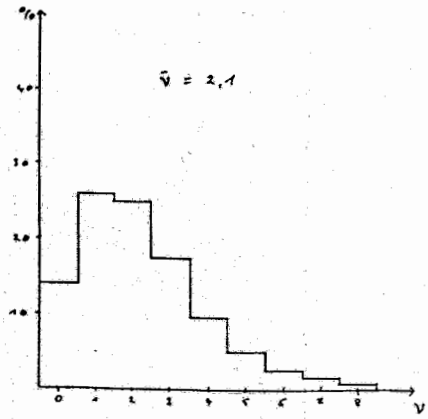

measured distribution before (1) and after cross talk rejection (2)

With an average multiplicity of 2.1 the efficiency can be calculated to be 55 %.

The difference between the measured and the expected distribution originates from the folding with the efficiency matrix.
The vector g(0 .. 7) of the measured multiplicity is the matrix product of the efficiency matrix W(8 x 8) with the vector of the expected multiplicity z(0 .. 7):

$$\begin{pmatrix} g(0) \\ g(1) \\ g(2) \\ g(3) \\ g(4) \\ g(5) \\ g(6) \\ g(7) \end{pmatrix} = \begin{pmatrix} w(0,0) & w(1,0) & w(2,0) & w(3,0) & w(4,0) & w(5,0) & w(6,0) & w(7,0) \\ 0 & w(1,1) & . & . & . & . & . & w(7,1) \\ 0 & 0 & w(2,2) & . & . & . & . & w(7,2) \\ 0 & . & 0 & w(3,3) & . & . & . & w(7,3) \\ 0 & . & . & 0 & w(4,4) & . & . & w(7,4) \\ 0 & . & . & . & 0 & w(5,5) & . & w(7,5) \\ 0 & . & . & . & . & 0 & w(6,6) & w(7,6) \\ 0 & 0 & 0 & 0 & 0 & 0 & 0 & w(7,7) \end{pmatrix} * \begin{pmatrix} z(0) \\ z(1) \\ z(2) \\ z(3) \\ z(4) \\ z(5) \\ z(6) \\ z(7) \end{pmatrix}$$

$$w(n,m) = \binom{n}{m} * \varepsilon^m * (1-\varepsilon)^{(n-m)}$$

The inverse operation should lead from the measured to the "real" multiplicity distribution.

$$\bar{z} = W^{-1} * \bar{g}$$

Unfortunately the rank of this matrix is very high (8) and ε very low. Small distortions of g lead to big differences in z. The unfolding process is very sensible and shows wrong results (e.g. oscillations).

With the known multiplicity distribution for ^{252}Cf (sf)

$$\bar{g} = W * \bar{z}$$

should reproduce the measured distribution:

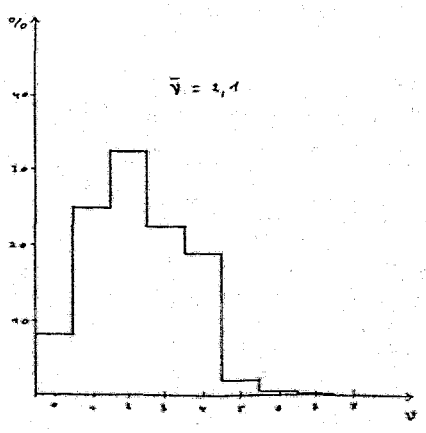

calculated distribution

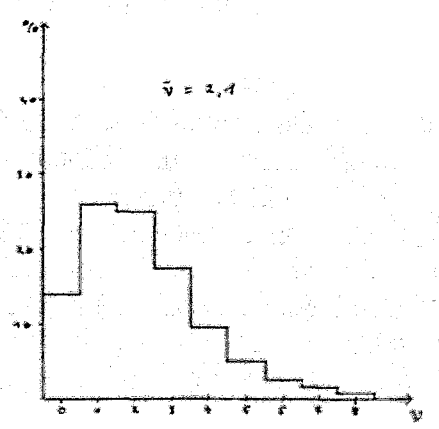

measured distribution

The difference shows, that the unfolding matrix is more complex. Maybe it consists of a efficiency matrix W' and a matrix that describes a small cross talk over all detectors.

Neutron "saw tooth"

The mass dependend neutron multiplicity distribution - known as neutron "saw tooth" is well known in literature.
A comparison with the data from Budtz-Jørgensen, Knitter [Bud88] show differences not only in the extrema, but also in the mass regions from 80 u-100 u and 150 u - 170 u.
These data take care of all measured neutrons within 70° in respect to the fission axis and is not corrected for crossing neutrons - that means neutrons from light/heavy fragment that go to the other hemisphere.

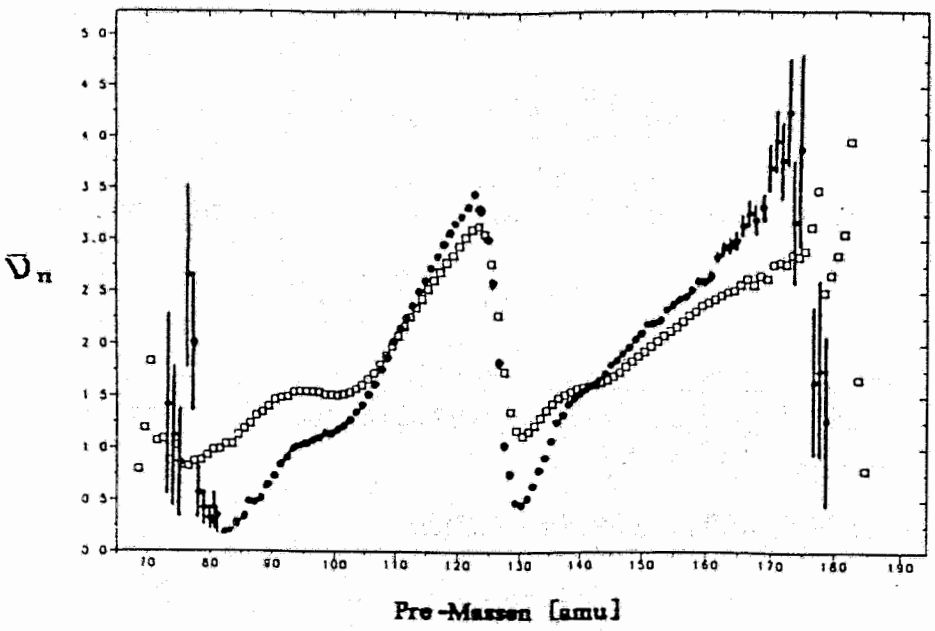

● Data from Budtz-Jørgensen and Knitter
□ Data from this work

The differences in the extrema may be explained by the bad mass resolution. This, however, is not the reason for the differences at the borders. They can be explained by of the angular distribution of the neutrons in the laboratory system and as cross talk through the Crystal-Ball from the side with high/low multiplicity to the other.

The second effect should be reduced by reducing the upper limit for time-of-flight. A second evaluation with Tmax = 50 ns is in preparation.

Conclusions

- Detection efficiency is dependent on the lower energy limit of the NaJ-detectors :

  < 55 % for 100 keV
  > 65 % for 50 keV

- a cross talk rejection can reduce the cross talk of neighbouring NaJ-detectors by a factor 10 ,

- a small cross talk over all detectors has to be taken into account,

- unfolding of multiplicity distributions is difficult.

References

[Bud88] C. Budtz-Jørgensen, H.H. Knitter, "Simultaneous Investigation of Fragments and Neutrons in ^{252}Cf (sf)", Nucl. Phys. **A490** (1988) 307

[Dör93] Th. Dörfler, "Neutronennachweis am Darmstadt-Heidelberger Kristallkugelspektrometer am Beispiel der spontanen Spaltung von ^{252}Cf", Diplomarbeit TH-Darmstadt 1993

[Kle82] H. Klein, "The Neutron Energy Spectrum from the Spontaeous Fission of Cf-252", XII. Int. Symp. on Nucl. Physics, Gaußig 1982

[SFa88] R. Schmid-Fabian, "Messung der spontanen Spaltung von ^{252}Cf am Darmstadt-Heidelberger Kristallkugel-Spektrometer", Dissertation am MPI-Kernphysik, Heidelberg 1988

[SKA70] K. Skarzvag, "Time distribution of Gamma-Rays from spontaneous fission of Cf-252", Nucl. Phys. **A153** (1970) 82

[Wei81] W. Weiter, "Nachweis von Gammastrahlen und Neutronen mit NaJ(Tl)- und BGO-Detektoren und deren Verwendung in einem 4π-Kristll-kugelspektrometer", Diplomarbeit am MPI-Kernphysik, Heidelberg 81

[Wis92] A. Wiswesser, "Messung hochenergetischer Photonen bei der spontanen Spaltung von ^{252}Cf", Diplomarbeit am MPI-Kernphysik, Heidelberg 1992

Neutron Multiplicity Measurements in Correlation with Mass and Energy of Fission Fragments

J. van Aarle, W. Westmeier, R.A. Esterlund, and P. Patzelt
(Institut für Kernchemie, Philipps Universität, D-3550 Marburg)

Abstract:

We have measured the number of neutrons emitted in the spontaneous fission of ^{260}Md and ^{252}Cf, using a large Gd-doped liquid scintillator tank. 1211 ^{260}Md fission events and $1.7 \cdot 10^7$ ^{252}Cf fission events were assayed, and correlations between the number of neutrons emitted by the fission fragments and the total kinetic energy (TKE) released in a particular fission event were investigated. From these correlations, spontaneous fission parameters were derived and compared to exit channel predictions made by Brosa et al. /BRO90/.

Introduction:

In a recent investigation, we measured the number of neutrons emitted in the spontaneous fission of ^{260}Md /WIL90/. We showed that the two different fission channels proposed by Hulet and coworkers /HUL86/ can be clearly separated, using the correlations between the number of neutrons emitted in a particular fission event and both the observed fission fragment masses and the total kinetic energy TKE. The results derived from the ^{260}Md measurements are in agreement with theoretical calculations of Brosa et al. /BRO90/. For the spontaneous fission of ^{252}Cf, Brosa et al. predict six different fission channels /BRO90/, which until now have not all been verified experimentally. Making use of the extremely high counting efficiency of our scintillator tank for neutrons, we should be able to verify whether or not these predicted fission channels do exist.

Experimental:

The neutron detector is a sphere with an outer diameter of 1.06 m, which contains 500 l of a toluene based liquid scintillator (NE 323). The liquid scintillator is doped with ca. 0.4 percent by weight of Gd, which has the largest capture cross-section of all elements for thermal neutrons. Neutrons are thermalized in the scintillator liquid and captured by the Gd, leading to the emission of γ-rays. The scintillator activated by the γ-rays emits light at the violet end of the visible spectrum. To detect these light pulses, 12 large photomultiplier tubes (VALVO XP2041 with a diameter of 12 cm) are mounted symmetrically on the outer surface of the counter. A coincidence of the signals of at least two adjacent photomultiplier tubes is used to distinguish between γ-rays from the neutron capture reactions and the γ-ray background events.

A 12-cm-diameter cylindrical opening through the center of the detector sphere contains an evacuated fission chamber. Fission fragments from ^{252}Cf spontaneous fission are assayed

with two ORTEC surface-barrier detectors having 300 mm^2 active area each. The distance between fission source and fission detectors is set to 13 mm, thus giving an efficiency of ca. 60 % for the detection of fission fragments. The detection of at least one fission fragment opens a 40 μs gate for the registration of fission neutrons.

We assayed coincident fission fragment energies and neutron multiplicities for ca. $1.7 \cdot 10^7$ spontaneous fission events of ^{252}Cf. The neutrons were detected with an efficiency of ca. 85%. The experimental fragment energies E''_1 and E''_2 were corrected for the pulse height defect /WEI86/, yielding secondary energies E'_1 and E'_2. These secondary energies were converted to secondary masses A'_1 and A'_2, which were then converted to primary masses A_1 and A_2, using $\bar{\nu}(A)$ tables from Budtz-Jørgensen and Knitter /BUD88/ and our experimental neutron multiplicity ν_{exp}. The secondary energies E'_1 and E'_2 were also converted to primary energies E_1 and E_2, and thus the total kinetic energy TKE was obtained.

Having these data event by event, we generated three-dimensional plots of both yield vs. fragment mass vs. TKE and $\bar{\nu}$ vs. fragment mass vs. TKE, as well as the concurrent cuts and projections.

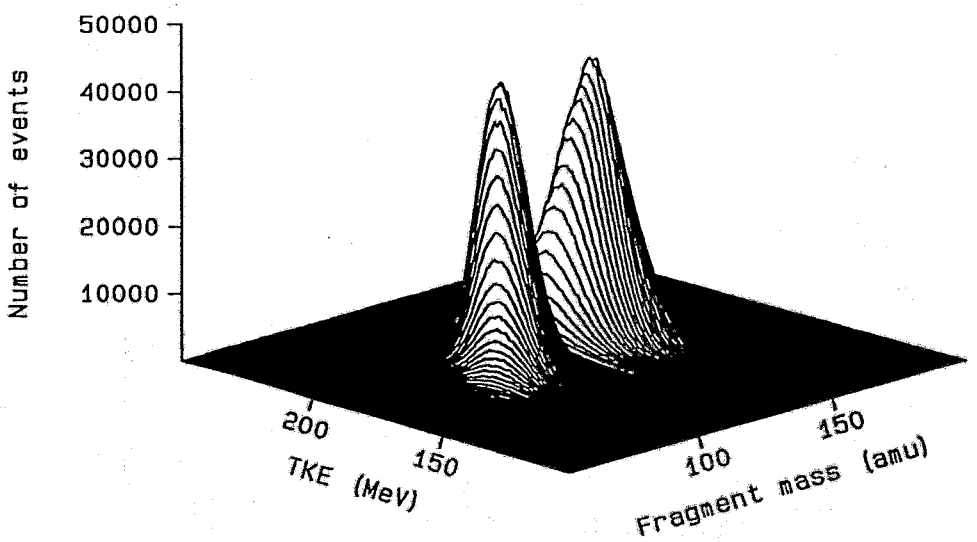

Figure 1: Spontaneous fission of ^{252}Cf: Three-dimensional representation of the fission yield vs. fragment mass vs. total kinetic energy (TKE).

Results and discussion:

In Figure 1, we show the three-dimensional matrix of the number of events as a function of fragment mass and total kinetic energy for the spontaneous fission of ^{252}Cf. The figure covers the assayed range in masses and TKE and shows the well-known double-humped yield distribution. It is obvious that we did not delete any information which might originate from rare fission channels at the flanks of the distribution.

The projection of the data onto the mass axis yields the fission-fragment mass distribution which is given in Figure 2. The shape of the distribution between masses 80 and 172 is consistent with data published earlier by other authors /BUD88, SCH83, WAL77/. The experimental peak-to-valley ratio of 17.0 can be compared to similar values of 15.8 /BUD88/, 13.4 /SCH83/ and 20.7 /WAL77/, respectively. The humps around masses 77 and 175 may possibly originate from the superasymmetric fission channel /BRO90/. The distribution is best fitted with five gaussian functions for both the light and heavy mass regions. The positions of four gaussian functions are in good agreement with the average masses $<A_H>$ of four of the six fission channels predicted by Brosa et al., namely the three standard channels as well as the superasymmetric fission mode. The remaining two fission modes (supershort and superlong) are both expected to have average masses around $<A_H> \approx 127$ and are probably included in the fifth component. Table I shows positions, standard deviations and intensities of the gaussian functions in comparison with theoretical fission mode calculations of Brosa et al. /BRO90/. Similar experimental data on the average fragment masses $<A_H>$ and standard deviations σ_A based on measurements outlined by Budtz-Jørgensen and Knitter /BUD88/ are also given by Brosa et al. /BRO90/.

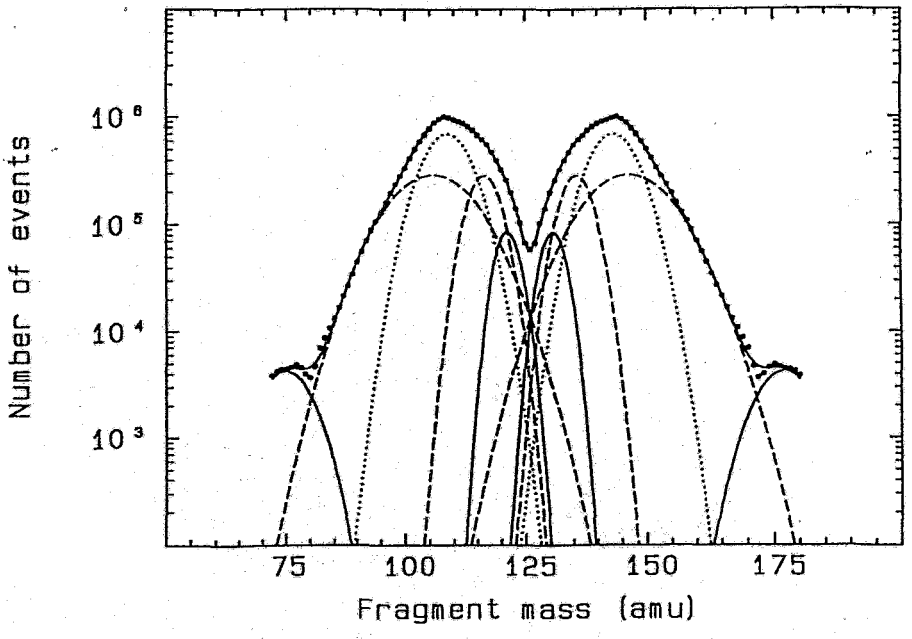

Figure 2: Fission-fragment mass distribution from the spontaneous fission of ^{252}Cf. The gaussian functions show the resolution according to the three standard channels, the superasymmetric channel and a fifth component near mass symmetry, which might be a mixture of the supershort and the superlong fission channel. For details, see text.

The fission-fragment mass distributions were determined for all experimental neutron multiplicities (ν_{exp} = 0 to 9). From the resolution of the mass distributions for each neutron multiplicity ν_{exp}, we obtained the areas of the gaussian distributions and derived the neutron multiplicity distributions due to the various exit channels. The uncorrected (without background, deadtime and efficiency corrections) neutron multiplicity distributions are shown in Fig. 3.

Table I: Intensities (I), positions ($<A_H>$) and standard deviations (σ) of various fission channels connected with the spontaneous fission of ^{252}Cf from this work compared with theoretical calculations ($<A_H>_t$, σ_t) of Brosa and coworkers /BRO90/.

Fission channel	I (%)	$<A_H>$ (amu)	$<A_H>_t$ (amu)	σ_A (amu)	σ_t (amu)
Standard I	13.5 ± 0.5	135.6 ± 0.2	134.9	3.86 ± 0.15	3.13
Standard II	48.2 ± 1.1	143.3 ± 0.1	142.5	4.81 ± 0.10	5.00
Standard III	35.0 ± 1.2	146.3 ± 0.3	148.5	7.90 ± 0.20	7.13
superasymm.	0.3 ± 0.1	177.0 ± 1.2	178.6	4.27 ± 0.90	0.37
superlong	3.0 ± 0.2	130.7 ± 0.2	127.5	2.4 ± 0.1	12.6
supershort			126		1.8

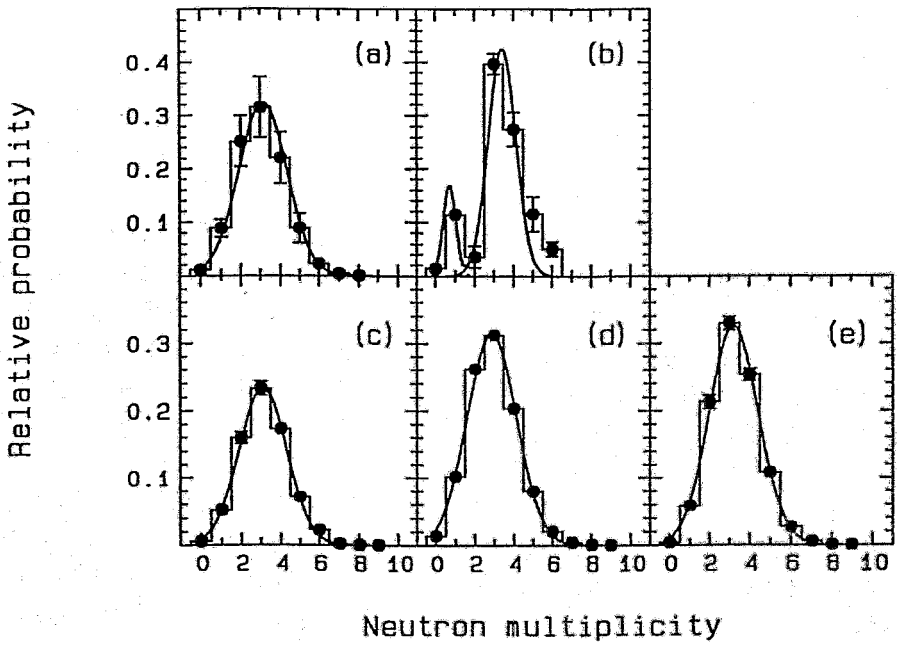

Figure 3: Uncorrected neutron multiplicity distributions from the resolution of the mass distributions of experimental neutron multiplicities $\nu_{exp.}$ (a) shows the distribution for the superasymmetric channel, (b) depicts the distribution of the component near mass symmetry. (c), (d) and (e) show the distributions for the standard channels I, II, and III, respectively.

Part a shows the neutron multiplicity distribution of the superasymmetric fission channel. In parts c, d, and e, the same distributions for the standard fission channels are depicted. Part b shows the distribution for the fifth component near mass symmetry. It consists

of two well-resolved distributions, which are probably due to the supershort (low neutron multiplicities) and the superlong (higher neutron multiplicities) fission channels. The figure shows uncorrected neutron multiplicity distributions. The gaussian functions in all multiplicity distributions are given to guide the eye. From these distributions, we calculated the corrected average neutron multiplicity values $\bar{\nu}$ given in Table II, and compared them with the theoretical predictions of Brosa et al. /BRO90/. Since the theoretical values of $\bar{\nu}$ have uncertainties of ca. ± 1 neutron, the data from these calculations may be considered to be in good agreement with our results.

Table II: Average neutron multiplicities $\bar{\nu}$ of predicted exit channels in the spontaneous fission of ^{252}Cf from this work, compared with theoretical calculations ($\bar{\nu}_t$) of Brosa and coworkers /BRO90/. Data are corrected for background, deadtime and detector efficiency.

Fission channel	$\bar{\nu}$	$\bar{\nu}_t$
Standard I	3.8 ± 0.2	2.5
Standard II	3.5 ± 0.2	3.5
Standard III	3.9 ± 0.2	
superasymm.	3.8 ± 0.2	3.6
superlong	4.2 ± 0.2	6.5
supershort	0.9 ± 0.2	0.1

The $\bar{\nu}$(A) systematics given in /BUD88/ and our experimental ν_{exp} have been used to calculate the partial neutron multiplicities of the light and heavy fragment masses, and thus to correct the secondary masses for neutron emission. From these partial neutron multiplicity data, we iteratively obtained a three-dimensional array of the average neutron multiplicity $\bar{\nu}$ as a function of fragment mass and total kinetic energy. We show this matrix in Figure 4. The well-known sawtooth structure of the average neutron multiplicity $\bar{\nu}$ as a function of the fragment mass is found for all values of TKE, and the variation of $\bar{\nu}$ with TKE shows the same dependence as published earlier by Budtz-Jørgensen and Knitter /BUD88/. In addition, the figure shows some interesting structure. In the mass and TKE region where the superasymmetric fission channel is expected (<A> ≈ 73 amu and <A> ≈ 179 amu with <TKE> ≈ 140 MeV), a third and a fourth sawtooth appear. In the mass region $120 \leq A \leq 130$ amu with TKE values around 230 MeV, we find higher values of $\bar{\nu}$ than expected from theoretical calculations /BRO90/. Fission events in this mass and TKE region are probably due to the supershort fission channel as proposed by Brosa et al., and a very low average neutron multiplicity of ca. 0.1 neutrons per fission is proposed for this fission mode /BRO90/, in contrast to experimental findings.

Since we have measured the total number of neutrons emitted in a particular fission event, we sorted all events in which a given number of neutrons is emitted for the TKE and mass distributions. We also calculated the partial number of neutrons emitted by the light and heavy fragments to correct the secondary fragment masses for neutron evaporation. With these data, we separated fragment mass distributions for a given experimental neutron multiplicity ν_{exp} and the concurrent partial neutron multiplicities. As an example, we show in Figure 5 the mass distributions for partial neutron multiplicities of spontaneous fission events

with a total number of three detected neutrons. The mass distributions with open squares connected by the solid line originate from events where no neutron was emitted by the light fragment (lefthand side, $\nu_L=0$), and all three neutrons were emitted by the heavy fragment (righthand side, $\nu_H=3$). The mass distributions with open circles and a dashed line stem from events where one neutron was emitted by the light fragment, and two neutrons came from the heavy fragment. The distributions with closed squares and a dotted line originate from fission events where the light fragment emitted two neutrons, whereas one neutron was emitted by the heavy fragment. The distributions with closed circles and a solid line originate from events where all neutrons were emitted by the light fragment. The same mass distributions for partial neutron multiplicities were determined for all experimental neutron multiplicities ν_{exp}.

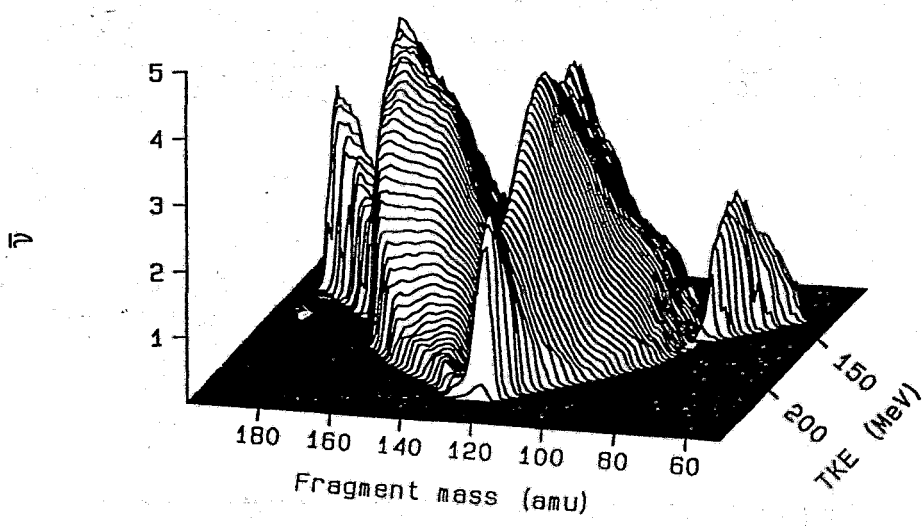

Figure 4: Spontaneous fission of ^{252}Cf: Three-dimensional representation of the average neutron multiplicity $\bar{\nu}$ vs. fragment mass vs. total kinetic energy (TKE).

The observation that the average light fragment mass increases with the partial neutron multiplicity ν_L (for a given ν_{exp}) is consistent with predictions of Brosa et al., and is easily understood in terms of the random neck rupture model /BRO90/. In Figure 6, we show, for the light fragment, the average mass as a function of the partial neutron multiplicity for experimental neutron multiplicities higher than $\nu_{exp}=0$. One observes that the average fragment mass increases with increasing partial neutron multiplicity. One also observes that the neck volume (defined as the difference between two adjacent average mass values) decreases from ca. 10 amu (emission of the first or second neutron) to a value of ca. 3 amu (when the partial neutron multiplicity ν_L approaches the experimental neutron multiplicity ν_{exp}).

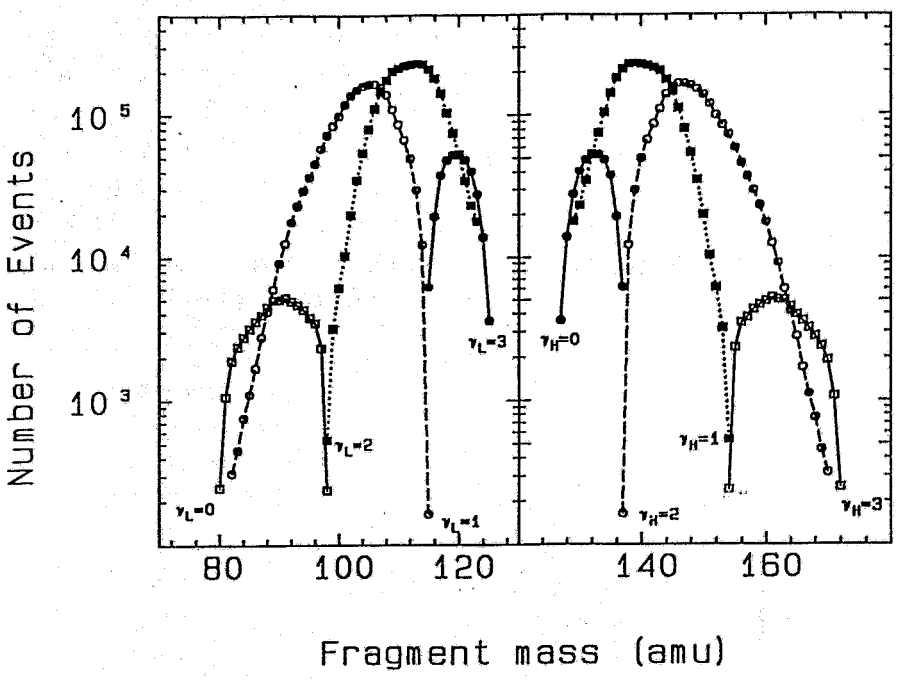

Figure 5: Mass distributions for partial neutron multiplicities derived from fission events with a total number of three detected neutrons.

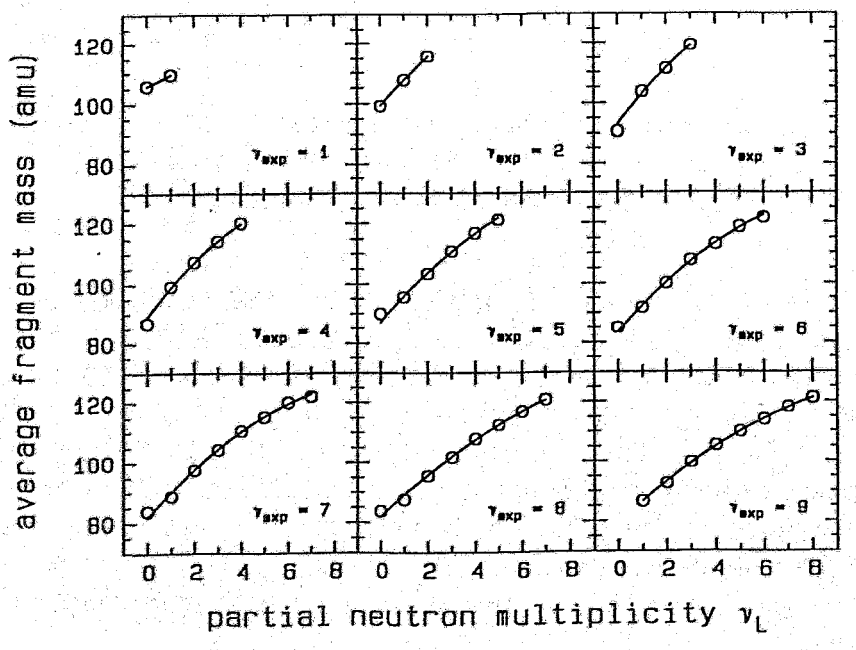

Figure 6: Average mass of the light fragment as a function of the partial neutron multiplicity (lines to guide the eye).

As the light fragment mass increases with the partial neutron multiplicity, the mass split becomes more symmetrical. For a given deformation (i.e. neutron multiplicity), this will affect the total kinetic energy released in the fission process. Figure 7 shows the TKE as a function of the partial neutron multiplicity of the light fragment ν_L. For the first emitted neutron, the increase in TKE is ca. 16 MeV, because there is also a large increase of the average mass (see Figure 6) and thus the mass split becomes more symmetrical. For the second and the third emitted neutron, the increase in mass is smaller and the increase in TKE is only ca. 7 MeV for the second and ca. 3 MeV for the third neutron emitted by the light fragment.

From Figure 6, we derived the increments of the number of neutrons emitted by either the light or the heavy fission fragment. To understand this dependence, we schematically show in Figure 8 the prescission shape (part a) and the preferred scission configurations (parts b to e) of a ^{252}Cf nucleus, for the case where a total number of three neutrons is emitted from the fission fragments.

In spontaneous fission, the excitation energy of the fission fragments comes from the deformation of the scissioning nucleus. The number of neutrons emitted from the fission fragments is correlated with the excitation energy. The higher the excitation energy of a fission fragment, the greater the number of neutrons emitted from this fragment, and vice versa. This implies that the total number of neutrons emitted in a particular fission event is directly connected with the deformation of the nucleus at scission. Therefore, the shapes of scissioning ^{252}Cf nuclei which lead to different total numbers of emitted neutrons must also differ.

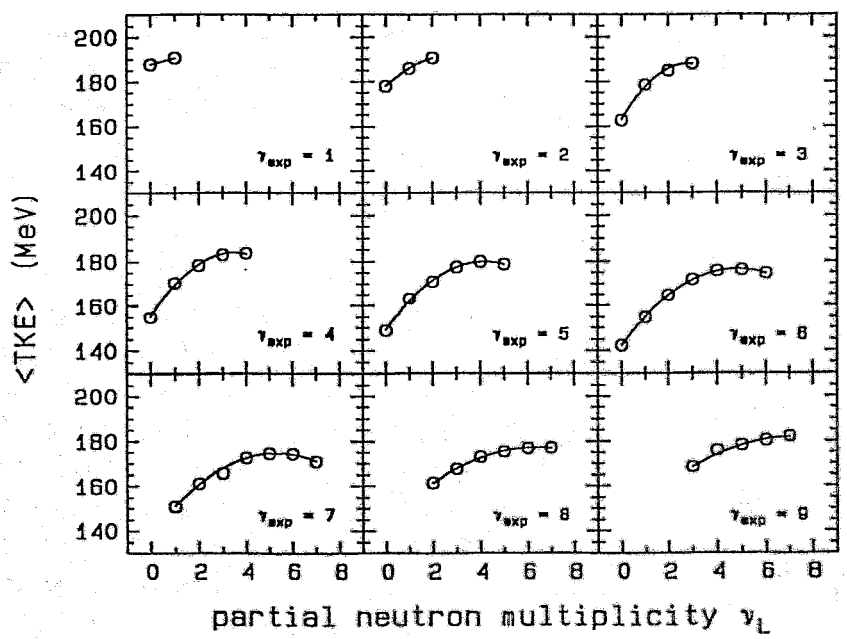

Figure 7: Total kinetic energy (TKE) as a function of the partial neutron multiplicity of the light fragment ν_L for the case of a total number of three detected neutrons.

The head ends of the nucleus shown in Figure 8a are schematically indicated by the numbers 90 and 132 for the light and heavy fragment masses, respectively. The vertical lines

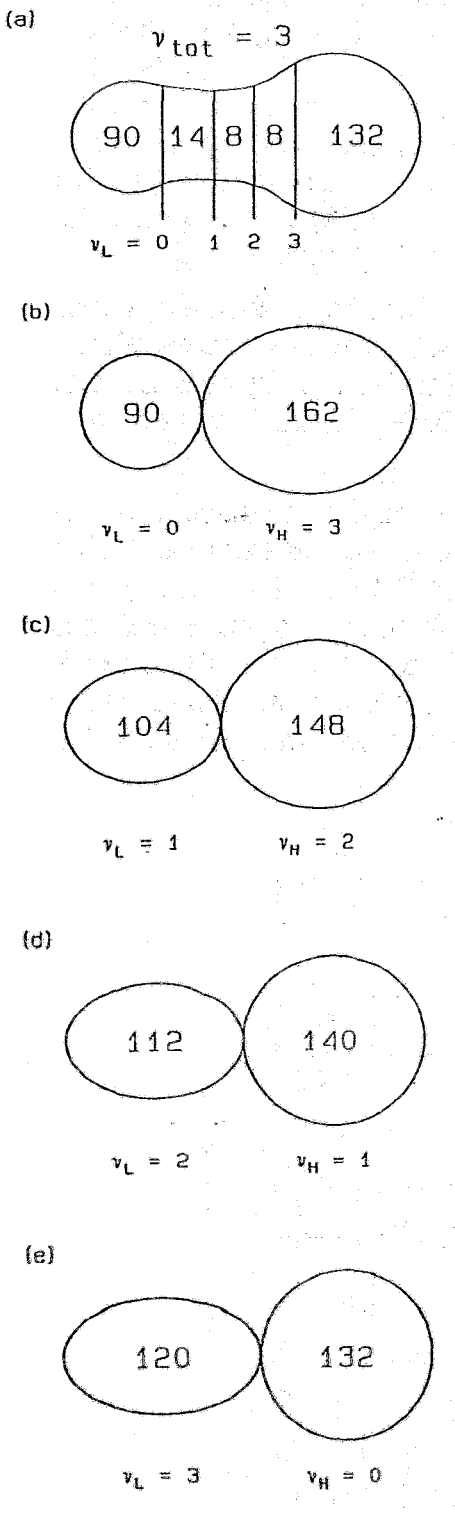

Figure 8:

Schematic shape of a ^{252}Cf nucleus, when three neutrons are emitted by the fission fragments. The figure also shows the four preferred scission configurations (parts b to e). See text for more details.

schematicaly depict various locations in the neck where the nucleus might finally break up and scission occurs. If the neck ruptures close to the one end with the average mass of 90 amu (part b), this light fragment has a nearly spherical shape and therefore its deformation energy is too small to emit a neutron ($\nu_L = 0$). If the light fragment is formed with an average mass close to 104 amu (part c), its shape is somewhat deformed, and the deformation energy is high enough to allow the emission of one neutron ($\nu_L = 1$). Raising the average mass of the light fragment by an additional 8 amu to a value of 112 amu (part d), the fragment shape is even more deformed, and two neutrons are emitted from the light fragment ($\nu_L = 2$). Figure 5 shows that this neck rupture configuration is mostly preferred in spontaneous fission events with a total number of three emitted neutrons. If the light fragment emits all three neutrons ($\nu_L = 3$), nearly the entire neck remains with this fragment and the deformation energy reaches its maximum value (part e). The average mass of the light fragment is ca. 120 amu. This schematic description is in agreement with the sawtooth structure of the $\nu(A)$ distribution. The average neutron multiplicity emitted from the light fragment reaches its maximum value near 120 amu, whereas for the corresponding heavy fragment mass near 132 amu, the average neutron multiplicity has its minimum value.

Summary:

From the mass distributions of partial neutron multiplicities originating from fission events with a given number of neutrons (see Figure 5), we schematically derive various prescission configurations of the ^{252}Cf nucleus (see Figure 8). The differences in these prescission configurations originate mainly from the length of the neck, and thus determine the deformation of the fission fragments after the neck ruptures. The deformation according to these schematical prescission configurations can be expressed in terms of both TKE and mass increments (see Figures 6 and 7). With these data, it may be possible to calculate the actual prescission shape of a ^{252}Cf nucleus for any given number of total or even partial neutron multiplicity.

References:

/BRO90/ U. Brosa, S. Grossmann and A. Müller, Phys. Rept. **197** (1990) 167

/BUD88/ C. Budtz-Jørgensen and H.H. Knitter, Nucl. Phys. **A490** (1988) 307

/HUL86/ E.K. Hulet, J.F. Wild, R.J. Dougan, R.W. Lougheed, J.H. Landrum, A.D. Dougan, M. Schädel, R.L. Hahn, P.A. Baisden, C.M. Henderson, R.J. Dupzyk, K. Sümmerer, and G. Bethune, Phys. Rev. Lett. **56** (1986) 313

/SCH83/ R. Schmidt and H. Henschel, Nucl. Phys. **A395** (1983) 15

/WAL77/ P.L. Walsh and J.W. Boldeman, Nucl. Phys. **A276** (1977) 189

/WEI86/ E. Weissenberger, P. Geltenbort, A. Oed, F. Gönnenwein, and H. Faust, Nucl. Instr. Meth. Phys. Res. **A248** (1986) 506

/WIL90/ J.F. Wild, J. van Aarle, W. Westmeier, R.W. Lougheed, E.K. Hulet, K.J. Moody, R.J. Dougan, E.-A. Koop, R.E. Glaser, R. Brandt, and P. Patzelt, Phys.Rev. C **41** (1990) 640

MULTI-FOLD CORRELATIONS BETWEEN $^{252}Cf(sf)$ FRAGMENTS AND FISSION NEUTRONS/γ-RAYS

I. Düring[1], M. Adler[1], H. Märten[1], A. Ruben[1]
B. Cramer[2], and U. Jahnke[2]

[1]Technische Universität Dresden
Institut für Kern- und Atomphysik
Mommsenstrasse 13, D-O-8027 Dresden, Germany

[2]Hahn-Meitner-Institut Berlin
Glienicker Str. 100, D-W-1000 Berlin 39

Abstract

Direction-sensitive spectroscopy of fission fragments (twin ionization chamber with Frisch grids) was combined with the measurement of neutron multiplicity distribution P(ν), average total γ-ray energy (2x2π Gd-loaded scintillator) as well as energy and angular distribution of neutrons and γ-rays. Based on the careful account for necessary corrections, scission configurations given by mass asymmetry, elongation (total kinetic energy of fragments), and shape asymmetry (ν_1/ν_2) can be studied exclusively in correlation with differential distributions of emission products. The scheme for correcting the neutron multiplicity distribution including its separation into the contributions from the complementary fragments is presented in detail. The mass yield for extreme $\bar{\nu}_1/\bar{\nu}_2$ ratios show fine structures indicating the cold shape-asymmetric fission.

1 Introduction

Beside the specification of scission point configurations by mass and charge asymmetry (A_1/A_2 and Z_1/Z_2, respectively) and elongation (measured as total kinetic energy TKE of the fragments), the shapes of the nascent fragments define the energetical conditions at scission point essentially. The only one corresponding observable is the number of neutrons emitted from the individual fragments as a measure of (asymptotic) fragment excitation energy released after dissipation of fragment deformation energy after scission. First attempts in this field by Alkhazov et al. [1] hint at unusual effects.

In order to make this option accessible, a twin ionization chamber TIC [2] was combined with the 2x2π Gd-loaded scintillator tank [3] at Hahn-Meitner-Institut Berlin. In addition, differential characteristics (energy and angular distributions) of emission products have been measured by the use of a NE213 n/γ detector and a ΔE-E-telescope.

In this paper, we will restrict to the determination of the neutron multiplicity distribution from individual fragments characterized by A and TKE. The analysis of the data involves several corrections to be considered carefully in order to obtain reliable results. Besides the account for detector efficiency, background, and cross talks the measured neutron multiplicity distributions from the two hemispheres of the scintillator tank have to be unambigiously transformed (and separated) to the actual distributions of the complementary fragments. This requires the use the fragment-neutron angular correlation.

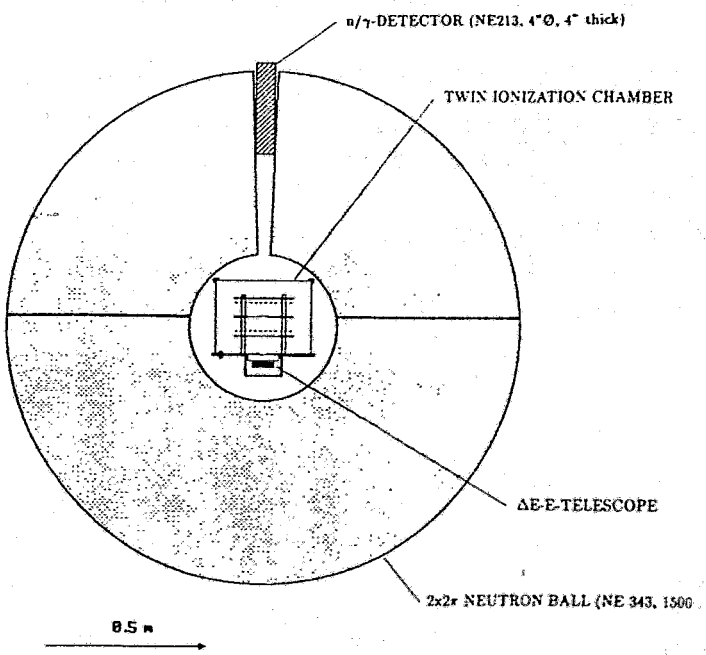

Figure 1: Cross-section of the axially symmetric experimental set-up.

2 Experiment

The experimental set-up is schematically shown in Fig. 1. From the anode (energy) signals corrected for energy loss and Frisch grid inefficiency the fragment kinetic energies $E_{k,i}$, the total TKE = $E_{k,1}$ + $E_{k,2}$, and the preliminary masses $A_1/A_2 = E_{k,2}/E_{k,1}$, $A_1 = 252\,(1+E_{k,1}/E_{k,2})^{-1}$, $A_2 = 252$ - A_1 are deduced. The fragment angle Θ is measured triple by: (i) drift times (time difference between cathode and anode signals, (ii) grid signals (positive amplitude of the bipolar signals are proportional

to $cos\Theta$), and (iii) sum signals of anode and grid pulses [4]. Version (iii) yields the best angular resolution [2]. The cathode time signal is also used as START for the neutron time-of-flight measurement. In addition, the light output and pulse-shape amplitude of the n-γ-detector pulses are collected. The γ-flash (as a measure of total γ-ray energy) registered by the neutron sphere is well separated (in time) from the neutron events appearing within about 40 μs after fission due to capture by Gd nuclei. Neutron events from both hemispheres as well as the total number are scaled. In addition, cross talks (coincidence between both hemispheres within a 25 ns window), the background rate, and pile-up events (i.e. further fission event within the 40 μs counting interval) are marked. The experiment involves multiple calibrations, e.g. $^{252}Cf - \alpha$-line measured at higher CH_4 pressure in the TIC, and a continuous stability check.

3 Data Analysis and Corrections

The TIC data analysis and correction is described elsewhere [2].

Correction for cross talks: Cross talks CT disturb the separation of the total neutron number into the individual numbers emitted from both complementary fission fragments remarkably. Their rate is proportional to ν_{tot}. The necessary elimination of events marked as CT requires a first correction of the yield Y(A,TKE) by the CT efficiency deduced from the measured data directly by calculating the ratio of the yields without/with CT. It is represented in Fig. 2.

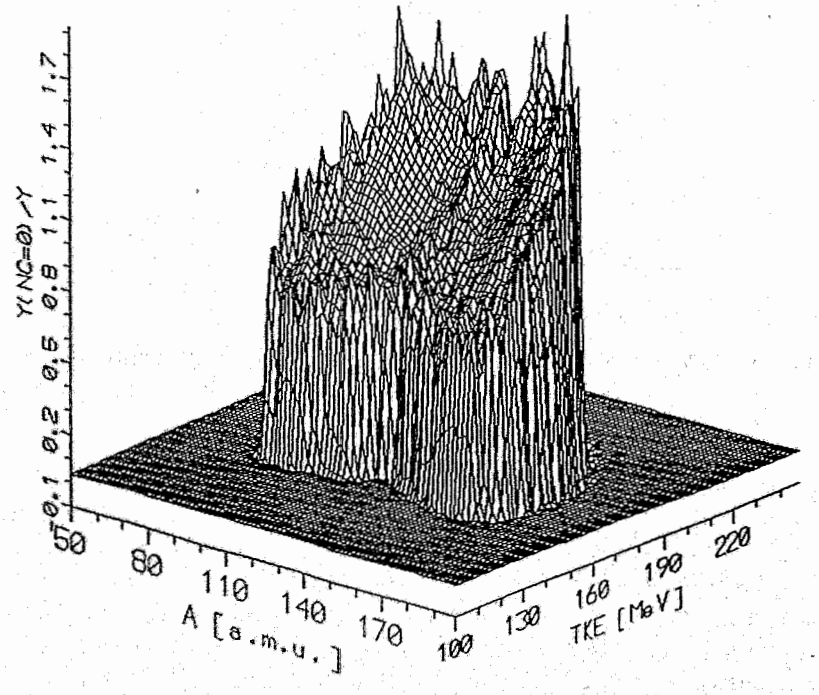

Figure 2: Ratio of the non-cross talk rate to the total one (renormalized).

This result has been well reproduced on the basis of a neutron transport calculation in connection with the description of the neutron angular distribution (code MCNP [5]) as f(A,TKE) within a complex statistical model [6] to fission neutron emission.

Angle cone selection: The separation of the neutron numbers counted to neutron multiplicities from the light and heavy fragment is only possible if utilizing the fragment-neutron angular correlation. This requires the selection of a fragment direction cone close to the sample plane normal. In the present work the $cos\Theta$ interval considered has been set to 0.85 - 1.0 (31.8 deg). Here, the mass and energy resolution is best due to the rather small energy loss of the fragments ($\sim cos^{-1}\Theta$).

Correction for counting efficiency: The relation between the measured (M_i) and the real (Q_k) multiplicity distribution is given by

$$M_i = \sum_{k=i}^{k_{max}} A_{ik} Q_i, \tag{1}$$

where A_{ik} is the efficiency matrix

$$A_{ik} = \binom{k}{i} \epsilon^i (1-\epsilon)^{i-k}. \tag{2}$$

The inverse matrix method based on

$$Q_i = \sum_{k=i}^{k_{max}} A_{ik}^{-1} M_k \tag{3}$$

fails in the case of low efficiencies and/or poor statistics. Therefore, we make use of an iteration procedure [7]

$$Q_i^{(s+1)} = Q_i^{(s)}[1 - \sum_{k=0}^{n} A_{ki}(1 - \frac{M_k}{\sum_{i=0}^{n} A_{ki} Q_i^{(s)}})], \tag{4}$$

$$Q_i^{(0)} = \frac{1}{n} \quad ; \quad \forall i. \tag{5}$$

in order to avoid arbitrary fluctuations in the case of rare events.

Foreward/backward correction: The neutron angular distribution for given A_1/A_2 and TKE is a superposition of the contributions from both fragments. The neutrons emitted at laboratory system (LS) angles $\Theta \geq 90$ *deg* are detected in the opposite hemisphere of the 2x2π neutron counter. This effect is corrected on the basis of statistical model calculations [6] leading to the double-differential LS emission probability N(E,Θ). The integral emission probability

$$I_{\Theta_1}^{\Theta_2} = \int_0^\infty dE \int_{\Theta_1}^{\Theta_2} 2\pi N(E,\Theta) sin(\Theta) d\Theta \tag{6}$$

is used to deduce the intensity ratio

$$\beta(A,TKE) = \frac{I_{90}^{180}(A,TKE)}{I_{0}^{90}(A,TKE)} \tag{7}$$

as the basis for the corresponding correction leading to the final neutron multiplicity distribution for each fragment at given A and TKE. Eq. (7) is only exact for a fragment direction identical with the sample plane normal. The full analysis accounts for the fragment angle cone mentioned above. Fig. 3 represents β calculated for an approximative center-of-mass (CMS) spectrum $\phi(\varepsilon) \sim \sqrt{\varepsilon} exp(-\varepsilon/T)$ as function of the average spectrum "temperature" T and the characteristic CMS-LS-transformation parameter $E_f = E_k/A$. Note that T = f(A,TKE) has to be considered exclusively. It is deduced from the measured neutron multiplicity, which is transformed into an average excitation energy via energy balance of fragment de-excitation.

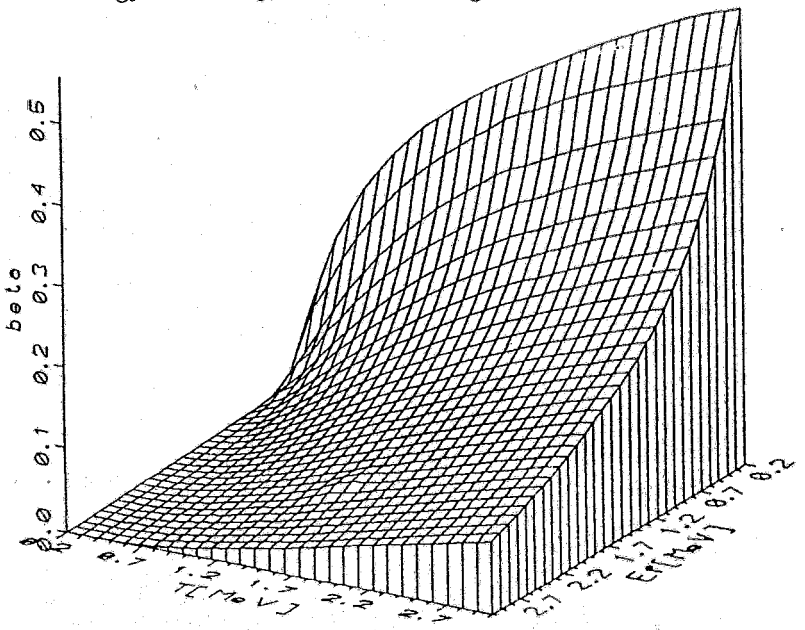

Figure 3: Foreward/backward correction factor β as function of average spectrum temperature T and $E_f = E_k/A$.

Analysis of neutron and γ-ray spectra: Neutron time-of-flight spectra for given $cos\Theta$ are transformed into the energy distribution taking into account the detection efficiency, which can be easily determined by analyzing the integral neutron spectrum with regard to the $^{252}Cf(sf)$ standard. This method yields an effective matrix including the correction for scattering effects. The angular distributions of γ-rays is measured as function of response energy. Their analysis is performed with account for the γ-ray response matrix of the NE213 detector calculated by Monte Carlo technique. An adequate model calculation (statistical model of γ-ray emission and VMI - variable moments of inertia - model to account for transitions within the rotational band) will give information about the average angular momentum of fission fragments for given scission configuration.

4 First Results

The $\bar{\nu}$(A) curve (Fig. 4) demonstrates the influence of the corrections discussed above obviously. Here, the superasymmetric fission mode yielding a triple saw-tooth curve $\bar{\nu}$(A) is evident (cf. [8]).

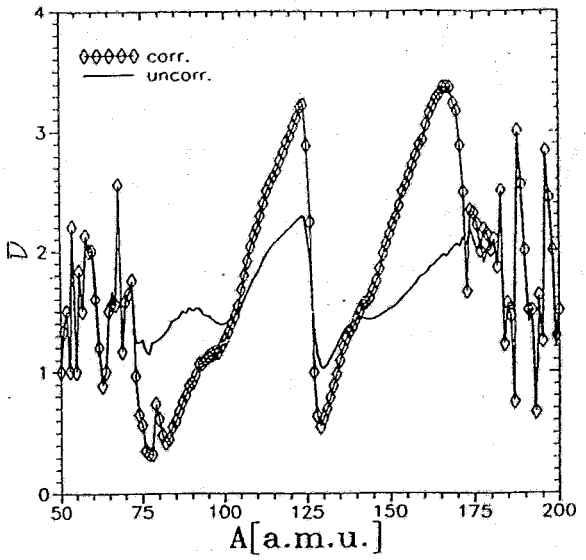

Figure 4: Average neutron multiplicity as function of fragment mass.

The full dependence of $\bar{\nu}$ on A and TKE is represented in Fig. 5. $\bar{\nu}$ and TKE for given A are clearly anticorrelated. This is a consequence of energy conservation (Q = TKE + TE^*).

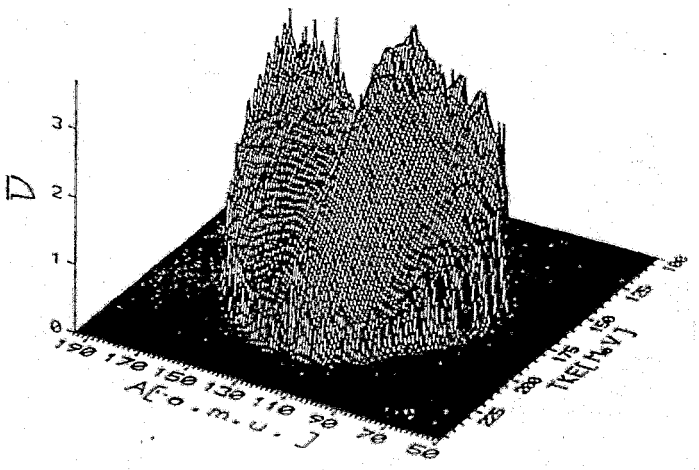

Figure 5: Average neutron multiplicity as function of A and TKE.

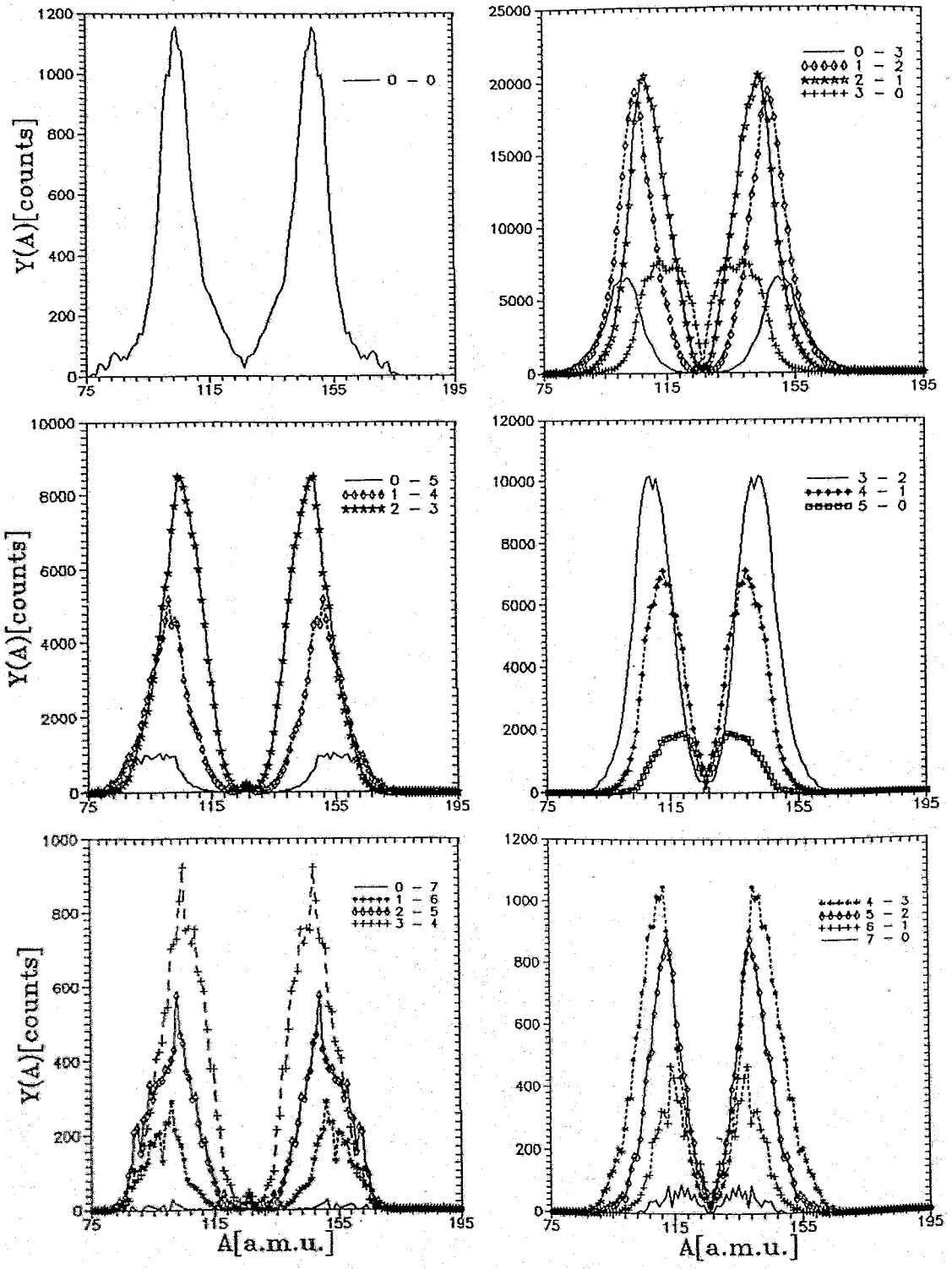

Figure 6: The fragment mass distribution for fixed combinations of neutron multiplicities ν_1/ν_2 (parameter).

The mass distributions for fixed ratios ν_1/ν_2 are of special interest. Figure 6 shows a selection of the results obtained. The fine structure effects for extreme multiplicity ratios are predominantly due to a proton odd-even effect because of the typical A dependent period of about 5 a.m.u. As an example, the mass distribution for $\nu_1/\nu_2 = 0/5$ is represented in Fig. 7, where the charge numbers according to the unchanged charge distribution (UCD) are also indicated. Our data confirm the first experimental indications of a shape-asymmetric cold fission measured by Alkhazov et al. [1] *qualitatively*.

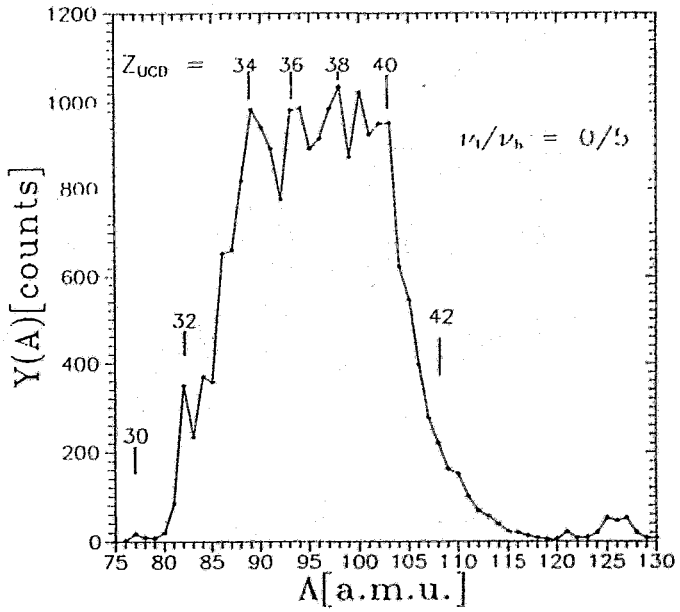

Figure 7: Fragment mass yield for fixed $\nu_1/\nu_2 = 0/5$.

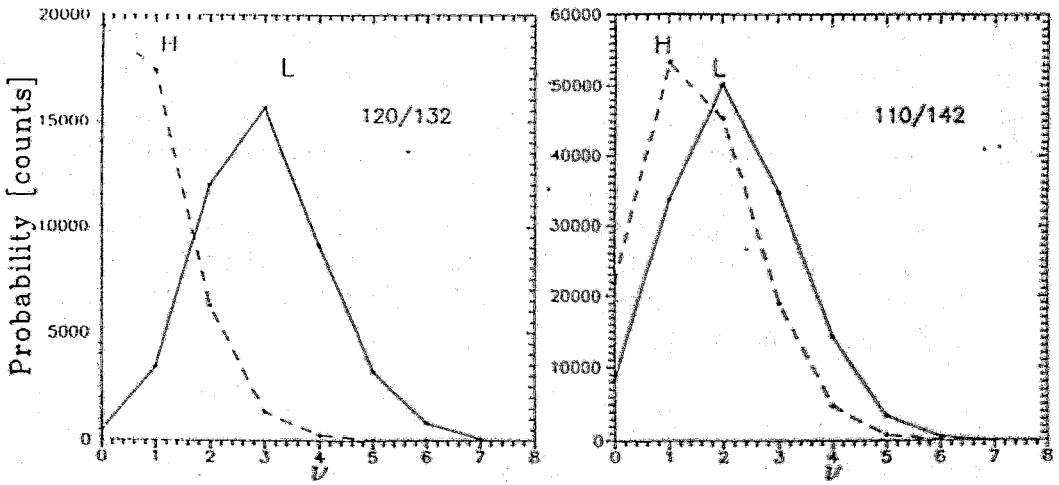

Figure 8: Neutron multiplicity distributions for the fragment pairs with $A_1/A_2 = 110/142$ and 120/132.

Some typical (one-dimensional) neutron multiplicity distributions are shown in Fig. 8. The two-dimensional distribution $P(\nu_1, \nu_2)$ as represented in Fig. 9 for the symmetric

mass split can be understood as an qualitative indication of the potential energy surface at scission depending on the typical individual deformations of the complementary fragments. Obviously, mass-symmetric fission is predominantly shape-asymmetric.

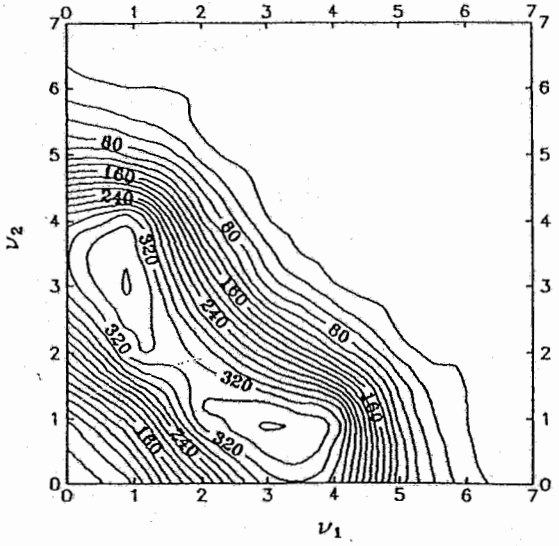

Figure 9: Two-dimensional neutron multiplicity distribution for the symmetric mass split 126/126.

5 Summary and Outlook

In the present work, we presented first (preliminary) results of a fission correlation experiment combining the measurement of the fragment distribution in A, (Z), TKE, and angle with the determination of integral characteristics (neutron multiplicity and average γ-ray energy) and the spectroscopy of related emission products (neutrons, γ-rays, and charged particles. In particular, the fragment distributions for fixed (individual) neutron multiplicities indicate unusual fission modes (cold compact, cold deformed, cold shape-asymmetric). The further analysis of the multi-fold data will include higher-order correlations, e.g. regarding the spectroscopic emission characteristics of neutrons and γ-rays.

ACKNOWLEDGEMENT
The very fruitful contacts and encouraging discussions with Prof. Gönnenwein (U Tübingen) and his group are greatfully acknowledged.

This work is supported by BMFT under contract 06 DD 112.

References

[1] I.D. Alkhazov, A.V. Kuznetsov, and V.I. Shpakov, Proc. Int. Conf. on "Fiftieth Anniversary of Nuclear Fission", Leningrad, Oct. 16-20, 1989 (at present, only available as report)

[2] A. Ruben et al., these proceedings

[3] B. Cramer, PHD-thesis (1989), Freie Universität Berlin

[4] C. Budtz-Jørgensen, H.-H. Knitter, Ch. Straede, F. - J. Hambsch, and R. Vogt, Nucl. Phys. A **258**, 209 (1987)

[5] J.F. Briesmeister (Ed.): "MCNP - A General Monte Carlo Code for Neutron and Photon Transport", Los Alamos Report LA-7396-M (1986)

[6] K. Arnold, I. Düring, H. Kalka, H. Märten, A. Ruben, and D. Seeliger, Nucl. Phys. A **502**, 325c (1989)

[7] G. Ingold, PhD Thesis (1984), Freie Universität Berlin

[8] C. Budtz-Jørgensen, H.H. Knitter et al., Nucl. Phys. A **490**, 307 (1988)

COMBINED INVESTIGATIONS OF HEAVY NUCLEUS FISSION IN THE REACTION WITH SLOW NEUTRONS

A.M. Gagarski[1], S.M. Kalebin[3], Yu.E. Penionjkevich[4], G.A. Petrov[1], A.K. Petukhov[1], V.P. Pikul[7], L.B. Pikelner[5], Yu.S. Pleva[1], Yu.V. Pyatkov[2], O.A. Shcherbakov[1], V.I. Shpakov[6], G.V. Valski[1]

[1] PNPI -Petersburg of Nuclear Physics Institute, Gatchina 188350, Russia
[2] MEPI -Moscow Engineering and Physical Institute
[3] ITEP -Institute of Theoretical and Experimental Physics, Moskow
[4] LNR -Laboratory of Nuclear Reactions JINP, Dubna
[5] FLNP -Frank Laboratory of Neutron Physics, JINP, Dubna
[6] RI -Khlopin Radium Institute, Sankt-Petersburg
[7] NPI -Nuclear Physics Institute of Uzbek Academy of Sciences

1 INTRODUCTION

Present stage ot the experimental and theoreticl investigations of heavy nucleus fission process consists in study of the excited and deformed nuclear system movement from the top of fission barrier towards scission point where the fissioning system is separated into two fragments with different masses and charges.

The ultimate aim of such investigations consists in working out complete theory of this complex reaction in nuclear physics. The main aim of the modern experiment in fission physics consists in the collecting of the information about masses, charges, excitation and kinetic energies, and angular momenta of fission fragments as well as secondary neutron and γ-ray characteristics.

Keeping in mind the great importance of fission reaction in the modern atomic energetics such elaborate investigations acquire great practical significance because they create conditions for carrying out the calculations with the precision which is now necessary for practice.

The search and development of the some new ways and passibilities for fission process investigations are the important addition to the multiparameter fission experiments. Such an interesting new possibility for fission study can be provided by the space parity violation experiments in neutron induced fission.

It seems interesting and fruitful to use a possibility of the combined investigation of fission and heavy ion reactions with the same compound systems and fragments (or projectiles) of these reactions.

We are planning to study mainly the slow neutron induced fission of some heavy actinides. Such a choice of the type of induced fission reaction is conditioned by the existence in PNPI rather good neutron sousces such as stationary research reactor WWR-M (18 MW), neutron time-of-flight spectrometer GNEIS and, in the nearest future, research reactor PIK, which can give the possibility to achieve a good statistical accuracy in multiparameter experiments.

2 INVESTIGATION OF THE CORRELATED DISTRIBUTIONS OF FRAGMENT MASSES, CHARGES, VELOCITIES AND KINETIC ENERGIES IN THE HEAVY NUCLEUS FISSION INDUCED BY THERMAL NEUTRONS (PNPI, MEPI, JINR(LNR), NPI)

Studies of the single or the few parameter distributions of fission fragments (for example M; Z; E_{kin}; M and Z; M, E_{kin} and V etc.) formed a main part of all experiments in fission physics during more than a fifty years history. But the rather rich information obtained as a result of such investigations turned out to be insufficient for the creation of a complete theory of the fission process.

Very important step on the way of collection of the essential information about fission process has been done in ILL (Grenoble) where highly sophisticated and interesting installations such as "Lohengrin" mass-separator and "Cosi Fan Tutte" spectrometer was put into operation 20 yaers ago [1]. But one can obtain information complete enough practically only for one of two fission fragments because of the low coincidence counting rate ("Cosi Fan Tutte" spectrometer). So, only the most probable magnitides of the main fission parameters for the second fragment can be used in the analysis. To overcome this shortage, the possibility and the expediency of the constructing and use of the twoarm fission fragment spectrometer with the thin fissile target situated near reactor core have been analyzed in our work [2].

Now the spectrometer of this type is under construction. The electromagnetic mass separator is planned to be used on one side of two-arm fission fragment spectrometer. Time-of-flight spectrometer with the precise ionization chamber [3] is planned to be used on the second side of this instrument. To achieve a high acceptance of the fission fragments and to obtain a high coincidence counting rate of fission events, the electrostatic guides for the charged fission fragments will be used to transport charged heavy ions from the target towards the end detectors.

The precise information about the mass and kinetic energy and charges for one of the fragments can be obtained in the arm of electromagnetic mass separator. The masses and kinetic energies of the complementary fragments are obtained from the correlated measurements of the fragment velocities and kinetic energies by the time-of-flight spectrometer. The nuclear charges for the fragments with well defined masses and energies can be extraced from the measurement of the ion ranges in precise ionization chamber. In some experiments the oriented semiconductor detectors will be used instead of the ionization chamber to decrease ionization defect due to atomic collisions.

Several versions of this complex instrument use are planned. For example, at first two time-of-flight spectrometers with the precise ionization chambers will be combined into a two-arm instrument. Such a combination is being tested now on the tangential channel of WWR-M reactor. Besides, the separate employment of each arm of the instrument is possible.

A scheme of the electromagnetic mass separator constructed is presented in Fig. 1.

The distinctive feature of this scheme consists in the complete decoupling of two main elements of the separator (sector electrostatic analyzers $E_{1,2,3}$ and magnetic analyzer M) by means of the electric quadrupole lenses Q_i and hexapole lenses S_i. This circumstance

gives a possibility to change very flexibly the main parameters of the mass separator (mass resolution $M/\Delta M$ and acceptance F) within the following intervals:

$$\frac{M}{\Delta M} = 1000 \quad F = 2.5 \cdot 10^{-4}$$
$$\frac{M}{\Delta M} = 20.000 \quad F = 1.7 \cdot 10^{-6}$$

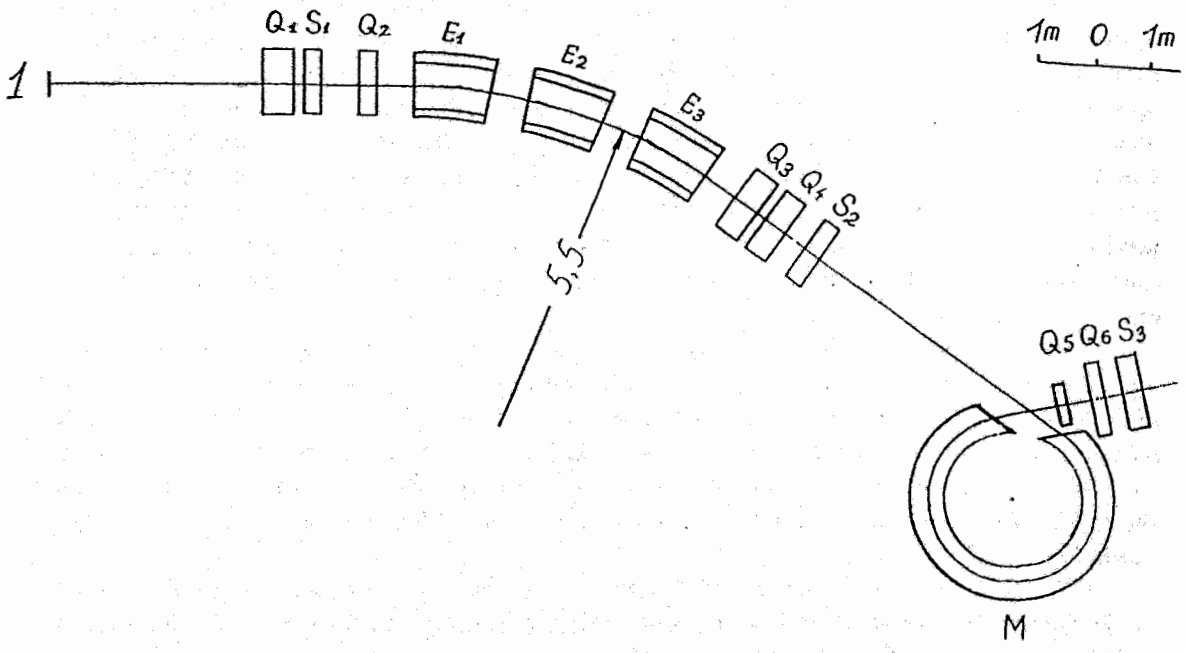

Figure 1: Scheme of the electromagnetic mass separator: 1 - fissile target, 2 - fragment detector, Q - quadrupole lenses, S - hexapole lenses, E - electrostatic analizer, M - magnetic analizer

The scheme of the acting model of two-arm time-of-flight spectrometer installed at the tangential neutron channel of WWR-M reactor is shown in Fig. 2. Some details of this model are shown in the Figs. 3 and 4. The main parameters of this spectrometer obtained in the course of the test measurements are shown in comparison with those of "Cosi Fan Tutte" in the following table

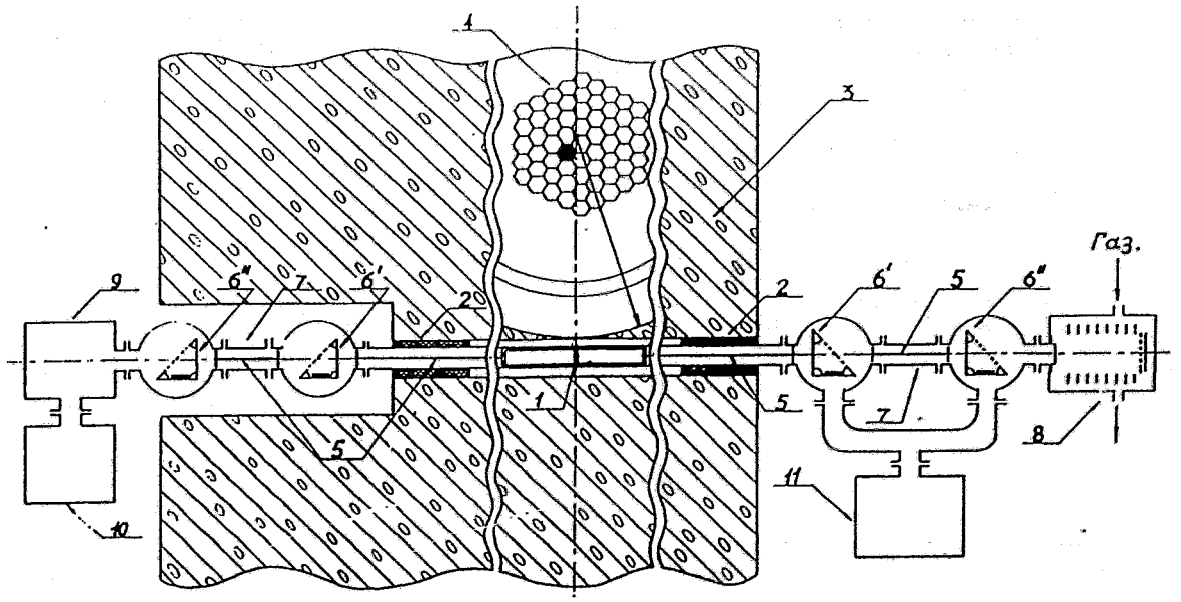

Figure 2: Scheme of the acting model of two-arm time-of-tlight spectrometer with the fissile target situated near the WWR-M reactor core: 1 - fissile target, 2 - reactor radiation shield, 3 - biological shield, 4 - reactor core, 5 - ion quide, 6 - time pick-off detectors, 7 - vacuum tubes, 8, 9 - ionization chambers, 10, 11 - vacuum pumps

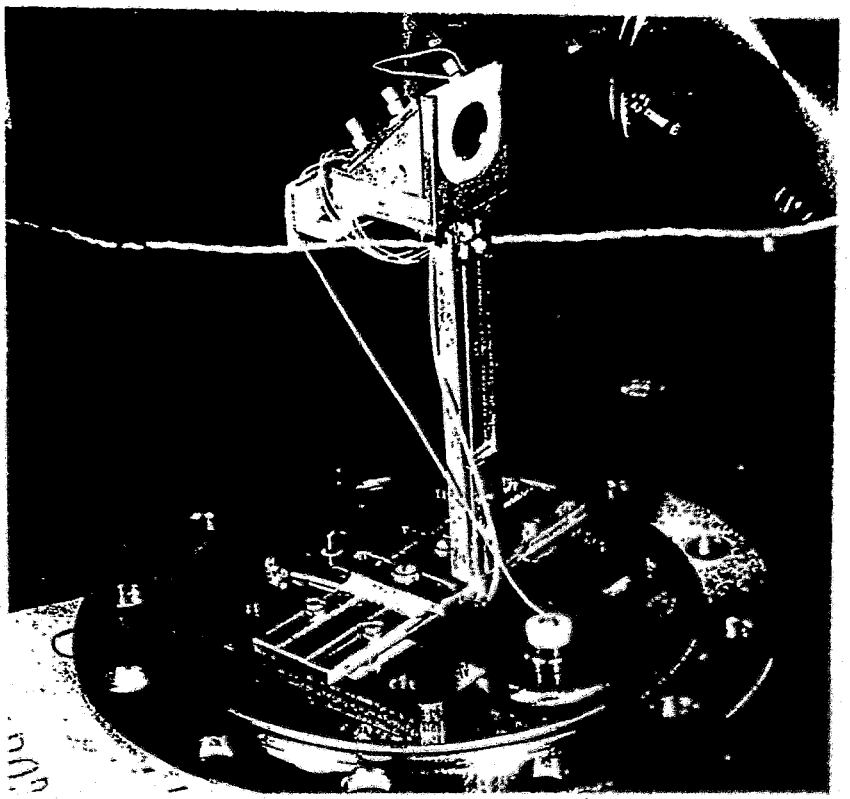

Figure 3: Pick-off detector of the two-arm spectrometer for fission fragments.

Characteristics (*)		Cosi Fan Tutte	Model on WWR-M
Neutron flux on the target	$[\frac{n}{cm^2} \cdot s]$	$5 \cdot 10^9$	$\simeq 10^{12}$
Single counting rate	$[\frac{c}{s}]$	2.5	$\simeq 1000$
Coincidence counting rate	$[\frac{c}{s}]$	< 0.1	> 20
Time resolution	$[ps]$	100	88
Mass resolution	$[a.m.u.]$	0.7	$\simeq 1$

(*) Parameters of ^{235}U targets and the size of the time-detectors werevery close in both installations.

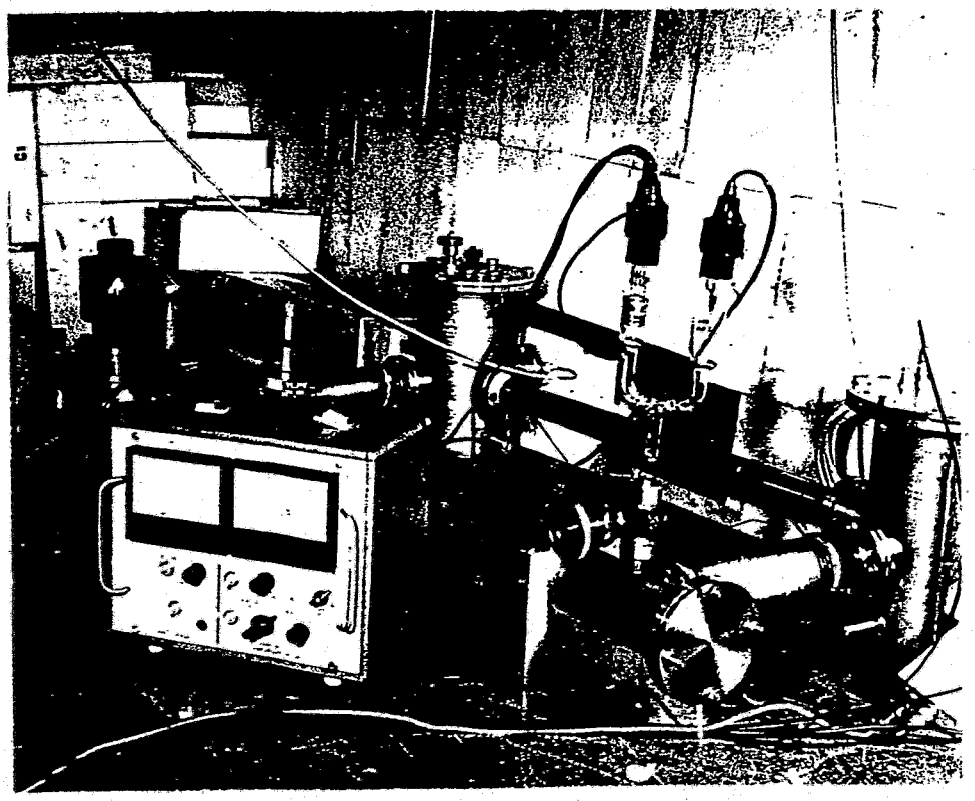

Figure 4: One of the outside parts of two-arm spectrometer situated at through-going neutron channel of WWR-M reactor (Pick-off detector chambers with the ion guide tube are seen).

Now it is claer that the coincidence counting rate of the fission events in principle may be increased hundreds times due to increase of neutron flux and by using time pick-off detectors with greater area without any visible aggravation of the mass and energy resolution. So, even the model of two-arms time-of-flight spectrometer will make it possible

to obtain the rich information about both fission fragments simultaneously.

The analysis of such an information for many fissile isotopes of Th, U, Pu, Am, Cm, Bk, and Cf will give a possibility to check various theoretical models of fission dynamics and will help to answer such important questions as

- viscosity of nuclear matter on the way from the top of the berrier to scission point;
- nature of compact and deformed cold fragmentation processes;
- dynamics characteristics of fissioning nuclear system near the scission point.

References

[1] Neutron Research Facilities at the ILL High Flux Reactor, Edition of ILL (1983)
[2] G.A. Petrov, L.A. Popenko, Preprint LNPI N423 (1979)

3 MEASUREMENTS OF THE SECONDARY NEUTRON MULTIPLICITIES FROM THE FRAGMENTS WITH THE DEFINITE MASSES, CHARGES AND TOTAL KINETIC ENERGIES IN THE THERMAL AND RESONANCE NEUTRON FISSION (PNPI, RI, MEPI)

Investigations of this type are interesting for obtaining the information about excitation energy distributions for the fission fragments with fixed masses, charges, and total kinetic energies. In principle, this information can be extracted on the average from precise measurements described above using the simple equation of the reaction energy balance:

$$(M + m_n) \cdot c^2 + E_n = (M_1 + M_2) \cdot c^2 + (\nu_1 + \nu_2) \cdot c^2 + (E^k_{M_1} + E^k_{M_2}) + \sum_{\nu} E^k_{n\nu} + \sum_{\gamma} E_\gamma$$

Here
- $M_{1,2}$ - fragment masses after neutron emission,
- m_n - neutron mass,
- $\nu_{1,2}$ - numbers of secondary neutrons,
- $E^k_{M_1}, E^k_{M_2}$ - fission fragment kinetic energies,
- $E^k_{n\nu}, E_\gamma$ - neutron and γ-ray energies.

In the neutron multiplicity measurements the information of this type can be obtained practically with a precision restricted only by the fluctuations of $(\sum E^k_{n\nu} + \sum E_\gamma)$ value.

So, these measurements are an important addition to the precise measurements of fragment masses, charges, and total kinetic energies particulary in a course of the joint analysis of the results for the same fissioning nuclei.

For the first time, the pioneering measurements of this type have been carried out in

the Khlopin Radium Institute by Shpakov et al. [1] for spontaneous fission of ^{252}Cf.

Exclusively interesting results have been obtained in these measurements. It seems perspective to carry out the measurements of secondary neutron multipliciteis in the fission of some nuclei induced by thermal and resonance neutrons ($E_n \leq 10 \div 20eV$).

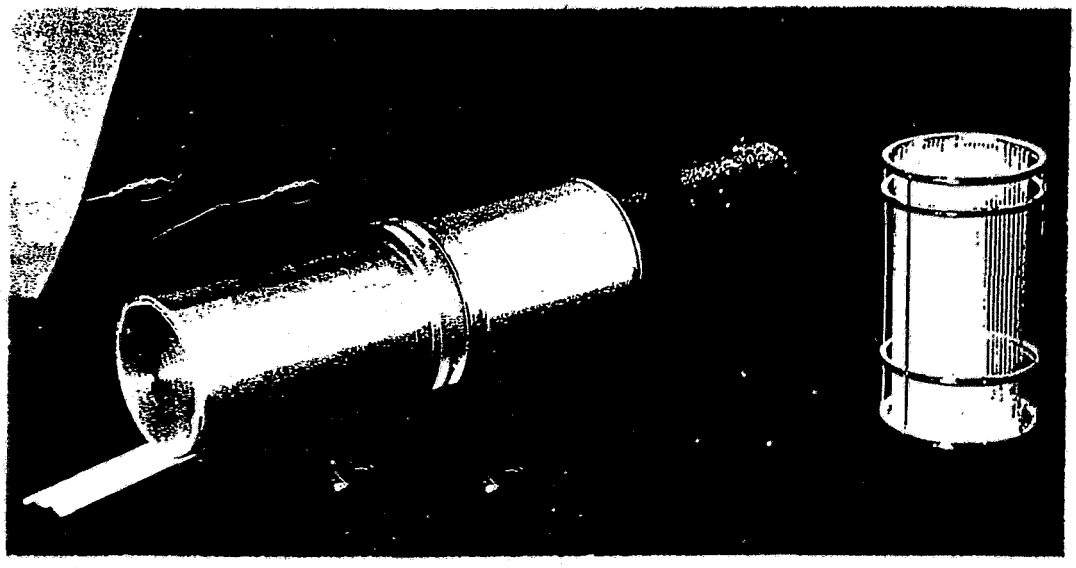

Figure 5: General view of 4π-detector module together with the ^{6}Li glass plate assembly.

At the first steps of these investigations, which we are planning to begin at WWR-M reactor, the modernized installation of the Radium Institute will be used. This set-up consists of two semisperical tanks with the Gd loaded liquid scintillator and with the intermediate shield against rescattering of the neutrons from one tank to another. The drawback of this facility is a long dead time ($\geq 20\mu s$), the very high γ-ray background, and the impossibility to measure the neutron angular correlations and energies.

Just because of these shortcomings we are planning to construct a new 4π- detector of secondary fission neutrons and γ-rays consisting of many modules with different kinds of operation depending on the aims of the experiments.

The main module for the neutron multiplicity measurements will contain the water as a neutron moderator and a number of ^{6}Li glass plates inserted into the water for neutron absorption with a high efficiency (Figs. 5, 6). The main estimated characteristics of such a module are shown in the Fig. 7.

Neutron energies for each number of neutron multiplicity can be estimated by the special module inserted between the main modules using time-of-flight method. In the case of the γ-ray energy and multiplicity measurements, the BGO crystal modules are planned to be used.

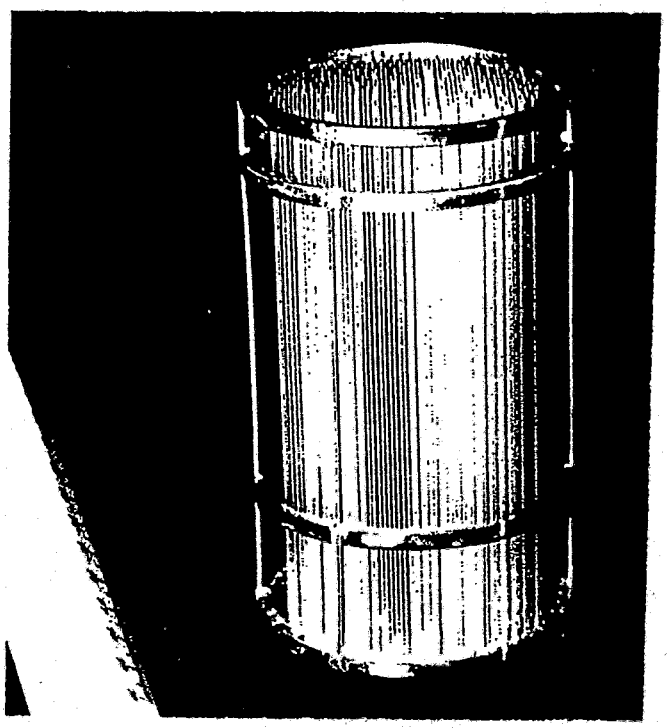

Figure 6: Preliminary assembly the ^{6}Li glass plates ($5 \times 0,5 \times 150mm$).

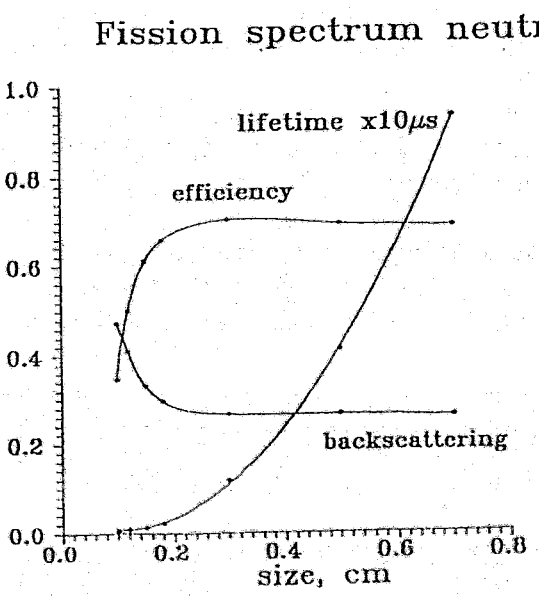

Figure 7: Dependence of some neutron detector characteristics on the size of ^{6}Li glass-water cell.

In all cases the precise back-to-back ionization chamber will be used for the identification of fragment masses, charges, and total kinetic energies.

The scientific program of the investigations consists in the comparative measurements and analysis of the multiparameter data for the fission of some nuclei induced by thermal and resonance neutrons.

References

[1] I.D. Alkhazov et al., Sov. Nucl. Phys. 47, 1214 (1988), and
Proc. XV^{th} Int. Symp. on Nucl. Phys., Nuclear Fission, Gaussig, GDR, 168 (1985)

4 THE INVESTIGATIONS OF THE SPACE PARITY VIOLATION EFFECT IN POLARIZED SLOW NEUTRON FISSION OF HEAVY NUCLEI AND P-EVEN EFFECTS CONNECTED WITH P-ODD EFFECT (PNPI, FLNP JINR)

Introduction

Effect of space violation in the fission reaction displays itself in the experiment as an appearance of the angular distribution asymmetry of the light (heavy) fission fragment emission relatively to the neutron polarization direction [1].

Simultaneously the different P-even asymmetries of the angular distributions of fission fragments can be observed in the neutron fission. These asymmetries are the so-called forward-backward asymmetry $(\vec{p}_n \cdot \vec{p}_f)$ and left-right asymmerty $(\vec{\sigma_n}[\vec{p}_n \times \vec{p}_f])$. Here $\vec{p}_n, \vec{\sigma_n}$ and $\vec{p}_f$ are unit vectors of the momentum and polarization of neutron and momentum of the light (heavy) fission fragments.

These P-even effects are well known and understandable interference effects. The investigations of these effects together with P-odd asymmetry effect $(\vec{\sigma_n} \cdot \vec{p}_f)$ of space parity violation are very useful because of some similarities in the formation machanisms in fission process [2,3].

In this way the important information can be obtained not only about different manifestations of P-odd NN-interaction in complex nuclei and reactions but also about some details of fission reaction and properties of the compound states in the fissile nuclei.

4.1 MEASUREMENTS OF THE AVERAGE VALUES OF P-ODD ASYMMETRY COEFFICIENTS IN THERMAL POLARIZED NEUTRON FISSION OF HEAVY NUCLEI (PNPI)

At present the existence of the P-odd effect of space parity violation in fission process is observed in neutron fission of six elements, namely ^{229}Th, $^{233,235}U$, $^{239,241}Pu$, and ^{241}Am [1,4].

An remarkable feature of the obtained results is that the absolute values of P-odd asymmetry coefficients $\tilde{\alpha}_{nf}$ are equal to $\simeq (1-5) \cdot 10^{-4}$ for all cases and the signs of these effects are the same for four nuclei in six ones studied. In this connection the supposition

appeared that the values of P-odd asymmetry coefficients are not obeyed the law of the random fluctuation as expected in the statistical model of the parity mixing of the compound nucleus states [2,3]. The understanding of the reasons of such possible correlations in sign and magnitude seems to be very important not only for the search of P-odd effects but for the investigations of fission reaction ifselfes. Additional information about this phenomenon can be obtained from the measurements of the P-even asymmetry coefficient magnitudes and signs for the same fissile nuclei.

The most perspective isotopes for future investigations are shown in this table.

	^{232}U	^{238}Pu	^{237}Np	^{242m}Am	^{243}Cm	^{247}Cm	^{249}Bk	^{251}Cf
$\sigma_f[b]$	75	16.5	0.02	7000	620	82	550	2850
I	0^+	0^+	$\frac{5}{2}^+$	5^+	$\frac{5}{2}^+$	$\frac{9}{2}^+$	$\frac{7}{2}^+$	$\frac{1}{2}^+$

It is important to emphasize the special interest of P-odd effect observation in subbarrier fission (for example in ^{237}Np) because of the possibility of existence of the specific barrier enhancement machanism for P-odd effect [5,6].

It is very interesting to measure P-odd effects for some fissile isotopes of Cm and Cf because a sharp decrease of P-odd effect in the ^{245}Cm fission seems to be observed in our work [4].

If this effect will be confirmed in future experiments such an information can be the first indication of special role of the pear shape deformation of fissioning nucleus near the top of external fission barrier in P-odd effect formation.

Measurements planned can be carried out on the vertical neutron channel of the WWR-M reactor or at special polarized neutron beam PN-7 in ILL.

References

[1] G.U. Danilin, Sov. Usp. Fiz. Nauk, 131, 329 (1980)
[2] O.P. Sushkov, V.V. Flambaum, Usp. Fiz. Nauk, 136, 4 (1982)
[3] V.E. Bunakov, V.P. Gudkov, Nucl. Phys, A401, 93 (1983)
[4] G.A. Petrov, Lectures on VI^{th} Int. School on Neutron Physics, Dubna 1, 221 (1991)
[5] V.V. Vladimirski, V.N. Andreev, JETP, 41, 663 (1961)
[6] A.P. Budnik, N.S. Rabotnov, Phys. Lett. 1346, 155 (1973)

4.2 INVESTIGATIONS OF THE MASS AND CHARGE DEPENDENCIES OF P-ODD AND P-EVEN ASYMMETRY COEFFICIENTS OF FRAGMENT EMISSION IN THE THERMAL POLARIZED NEUTRON FISSION (PNPI)

In accordance with the present-day theoretical ideas P-odd and (P-even) asymmetry coefficients ($\bar{\alpha}_{nf}, \bar{\alpha}^{Tr}_{nf}$) have not to depend on the properties of the fission reaction final products (fragments) [1,2]. This is the case because different fission fragments in fact are not fission reaction channels. In fission the real reaction channels are so-called Bohr's transition states.

The only experimental support of this theoretical assumption [1,2] is based on our

work [3]. But this work was carried out with rather poor mass resolution ($\Delta M \sim 6-8$ a.m.u.) and not sufficient statistical accuracy.

Now our result can be improved in statistics about ten times and the mass resolution about $\Delta M \leq 3-4$ a.m.u. can be archived. We plan to develop and to use a new method of the fragment mass and charge identification based on the registration of γ-lines characteristic of the fission fragment γ-ray spectrum. Using this method it will be possible to measure P-odd (P-even) effect coefficients for individual elements (fission fragments). The main difficulty when using this identification method in the P-odd (P-even) effect studies consists in the necessity of precise spectroscopic measurements at the counting rate as high as $(10^5 - 10^6)s^{-1}$. But now such a difficulty can be overcome.

The carrying out of these investigations may prove to be a crucial test to confirm one of the main theoretical assumption about special role of the transition states in P-odd (P-even) effect formation mechanism and about the stage of formation of the observed mass distribution.

References

[1] O.P. Sushkov, V.V. Flambaum, Usp. Fiz. Nauk, **136**, 4 (1982)
[2] V.E. Bunakov, V.P. Gudkov, Nucl. Phys. **A401**, 93 (1983)
[3] A.Ya. Alexandrovich, G.A. Petrov et al., Sov. Nucl. Phys. **v.39**, p.805 (1984)

4.3 THE STUDY OF AVERAGING LAWS FOR VALUES OF P-ODD AND P-EVEN EFFECTS IN THE FISSION OF HEAVY NUCLEI INDUCED BY RESONANCE NEUTRONS

(PNPI, JINR(FLNP), ITEP)

The modern theoretical descriptions of P-odd and P-even asymmetries of the fission fragment angular distributions induced by slow neutrons are based on the assumption about the accidental nature of the fluctuations of physical values involved in corresponding equations for asymmetry coefficients [1,2]:

$$W(\Theta,\varphi,\xi) \sim 1 + \bar{\alpha}_{nf}(\vec{\sigma_n}\cdot\vec{p_f}) + \bar{\alpha}^{lr}_{nf}\cdot(\vec{p_f}\,[\vec{p_n}\times\vec{\sigma_n}]) + \bar{\alpha}^{fb}_{nf}(\vec{p_n}\cdot\vec{p_f}),$$

$$\bar{\alpha}_{nf}(E_n) \simeq Q'_{sp}\cdot\sqrt{\frac{\Gamma^f_p}{\Gamma^f_s}}\cdot Re\{\frac{<p|V_{sp}|s>}{(E-E_p)+\frac{i\Gamma_p}{2}}\cdot\exp(i\Delta\varphi'_{sp})\},$$

$$\bar{\alpha}^{lr}_{nf}(E_n) \simeq Q_{sp}\cdot\sqrt{\frac{\Gamma^f_p\Gamma^n_p}{\Gamma^f_s\Gamma^n_s}}\cdot Im\{\frac{(E-E_s)+\frac{i\Gamma_s}{2}}{(E-E_p)+\frac{i\Gamma_p}{2}}\cdot\exp(i\Delta\varphi_{sp})\},$$

$$\bar{\alpha}^{fb}_{nf}(E_n) \simeq Q_{sp}\cdot\sqrt{\frac{\Gamma^f_p\Gamma^n_p}{\Gamma^f_s\Gamma^n_s}}\cdot Re\{\frac{(E-E_s)+\frac{i\Gamma_s}{2}}{(E-E_p)+\frac{i\Gamma_p}{2}}\cdot\exp(i\Delta\varphi_{sp})\},$$

In these equations justified to the simplest approximation when only two isolated compound states with opposite parities are mixed, the following notations are introduced:

$\vec{\sigma_n}, \vec{p}_n, \vec{p}_f$ - unit vectors of neutron polarization, and neutron and fission fragment momenta (of the separated mass group), respectively
Q'_{sp}, Q_{sp} - spin factors;
$\Gamma^n_{s,p}\Gamma^f_{s,p}$ - neutron and fission widths of the mixing compound states;
E_s, E_p - energies of the mixing s, p-states;
V_{sp} - single-particle operator of waek NN-interaction;
$\Delta\varphi_{sp}$ - phase differences of the mixing s- and p-compound states.

When the effects are averaged over sufficiently wide neutron energy range ($\Delta E \gg \Gamma$), within the framewoork of theoretical ideas [1,2] accidental fluctuations of the absolute values and signs of the effect values around zero average one are expected. However, there are other theoretical approaches for description of P-odd and P-even effects in nuclear reactions (e.g.[3]) based on the so-called valence mechanism which leads to some correlations for values and sings of the effects and to the deviation from the statistical law.

The study of the role of these two probable mechanisms in the formation of P-odd effects in the complicated nuclear systems and processes is the principal task of the research of space parity violation phenomena and the fission process itselfes.

To archieve this aim, the following experiments are planned:

1. Measurements of the average values of P-odd asymmetry coefficients such as $(\vec{\sigma}_n \cdot \vec{p}_f)$ and $(\vec{\sigma}_n \cdot \vec{p}_n)$ in the different fissile systems and in the wide energy range of polarized resonance neutrons $E_n \leq 100$ eV.

2. Comparative measurements of the P-even forward-bachward asymmetry coefficients such as $(\vec{p}_n \cdot \vec{p}_f)$ for different fissile nuclei (e.g. $^{233,235}U$, ^{239}Pu) in the wide energy range of resonance neutrons $E_n \leq 140$ eV.

3. Comparative measurements of the energy dependence of different P-even asymmetry coefficients for angular distributions of fission fragments $\bar{\alpha}^{lr}_{nf}$ and $\bar{\alpha}^{fb}_{nf}$ in the vicinity of a few strong p-wave resonances.

The latter experiments are dedicated to detailed check of the existing theoretical description of P-odd effects in nuclear fission. As well known, in the (n,γ)-reaction some difficulties of the joint description of these effects were noted, which were not solved up to now [4].

The experimental studies mentioned above are planned to be carried out at the neutron time-of-flight spectrometer GNEIS(PNPI), IBR-30 reactor (JINR FLNP) and with the use of multirotor mechanical chopper-monochromators system manufactured at ITEP (see Capter 4.4).

References

[1] O.P. Sushkov, V.V. Flambaum, Usp. Fiz. Nauk. (Sov.), **136**, 4 (1982)
[2] V.E. Bunakov, V.P. Gudkov, Nucl. Phys. **A401**, 93 (1983)
[3] D.F. Zaretzki, V.K. Sirotkin, Sov. Yad. Fiz., **37**, 607 (1983)
[4] V.P. Alfimenkov et al., Short reports of JINR N 10-85, 19, Dubna (1985)
[5] V.P. Alfimenkov et al., Sov. Nucl. Phys., **52**, 927 (1990)

4.4 NEUTRON BEAM MULTIROTOR MECHANICAL MONOCHROMATOR CHOPPER SYSTEM (PINP, ITEP)

This multipurpose set-up is intended to obtain high intensity of the pulsed of pseudo monochromatic neutron beam in eV-energy range. The width of the separated energy interval ΔE depends on the average value of energy range and the rotation frequency of mechanical rotors having the magnetic support. Every rotor has 10 rectangular slits with the symmetry axes lying in the horizontal plane which is orthogonal to the rotation axis.

An average energy E_0 of separated interval ΔE can be changed by the proper set of the phase differences for the synchronously resolving rotors. Inside of separated interval ΔE, the neutron energies can be measured using time-of-flight method with energy resolution δE depending on the rotation speed and the flight path length.

Using a number of identical rotors (up to 6) situated at given distances one by one, it is possible to shape neutron beam having a rectangular cross-section and very low γ and neutron background with energies beyond of separated intervall ΔE. This chopper system will be installed at the radial neutron channel GEK-1 of the PIK-reactor.

The acting model with 4 rotors was installed now at the horizontal neutron beam of the WWR-M reactor.

The main calculated parameters of the neutron chopper are given in the Table. The general layout of the set-up together with the neutron polarizer (this version of arrangement will be used for P-odd and T-violating effects research in separated neutron resonances) is shown in the Fig. 8. In the pictures 9, 10 and 11 some parts of the experimental set-up at the horizontal beem of the WWR-M reactor are shown.

size of slit cm^2	number of slits	frequency Hz	E eV	Δ E eV	δ E eV	$I_n(\Delta E)$ $\frac{n}{cm^2}\cdot s\cdot\Delta E$	$I_n(\delta E)$ $\frac{n}{cm^2}\cdot s\cdot\delta E$
			1	0.16	0.05	$2.3\ 10^6$	$7\cdot10^5$
0.8×3	10	250	3	0.30	0.09	$1.5\ 10^6$	$4.5\ 10^5$
			10	0.54	0.17	$8\cdot10^5$	$2.5\cdot10^5$

The quantities δE and I_n are given for the flight path length of 9 m and resonance neutron flux at the bottom of GEK-1 channel of the PIK-reactor $\Phi_n = 6\cdot10^{13} n/cm^2\cdot s\cdot eV$.

The experimental set-up described above can be effectively used in all cases when there is a need to carry out the measurements in comparatively narrow energy range (e.g. the research of fission parameters or a search and measurements of P- and T-nonconservation effects in separate neutron resonances and etc.)

In the low energy range this st-up can complete successfully with such powerful neutron sources as IBR-30 or LANSCE:

$$\left.\begin{array}{lrcll} IBR-30: & \Phi & \simeq & 3\cdot10^5\frac{1}{E_n}\cdot\frac{n}{cm^2}\cdot s\cdot eV & [1] \\ LANSCE: & \Phi & \simeq & 1.7\cdot10^6\frac{1}{E_n}\cdot\frac{n}{cm^2}\cdot s\cot eV & [2] \\ ROTOR: & \Phi & \simeq & 1.4\cdot10^7\frac{1}{E_n}\cdot\frac{n}{cm^2}\cdot s\cdot eV & \end{array}\right\} for\, E_n \le 10eV$$

References

[1] V.V. Golikov et al., Preprint JINP-3-5736, Dubna (1971)

[2] S.A. Wender, P.W. Losowski, NIM, B24/25, 879 (1987)

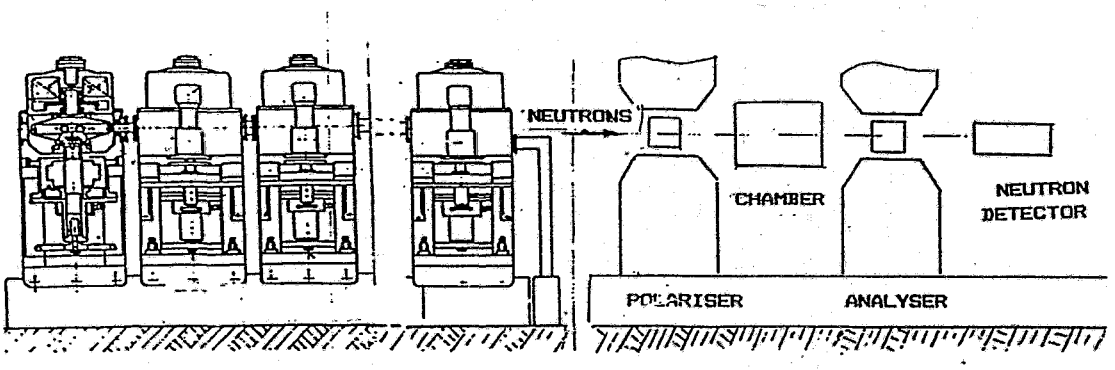

Figure 8: General scheme of the multirotor chopper-monochromator with neutron polarizer-analizer systems.

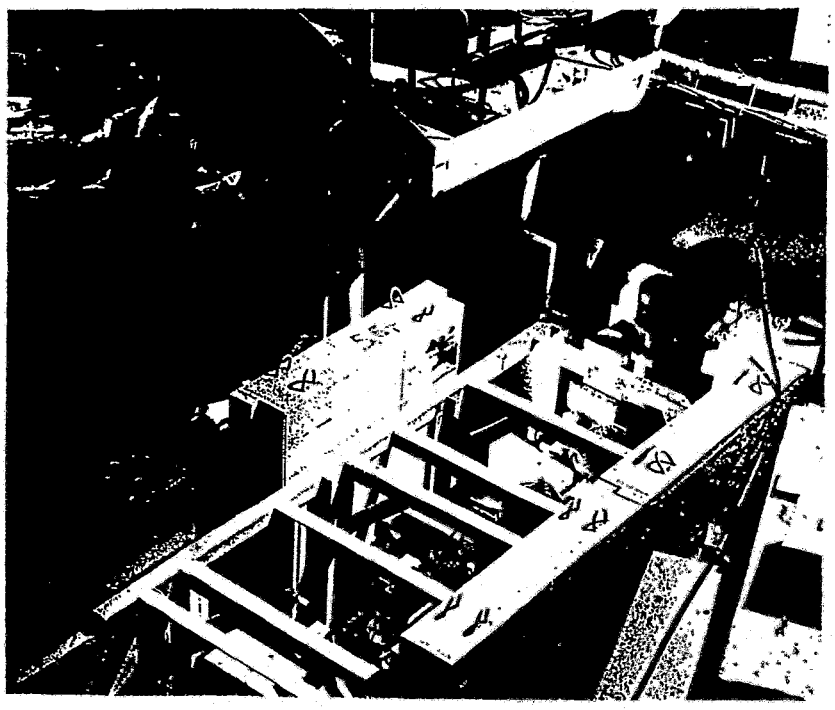

Figure 9: Acting full-scale model of the multrotor chopper-monochromator of resonance neutrons situated at the horizontal neutron beam of the WWR-M reactor.

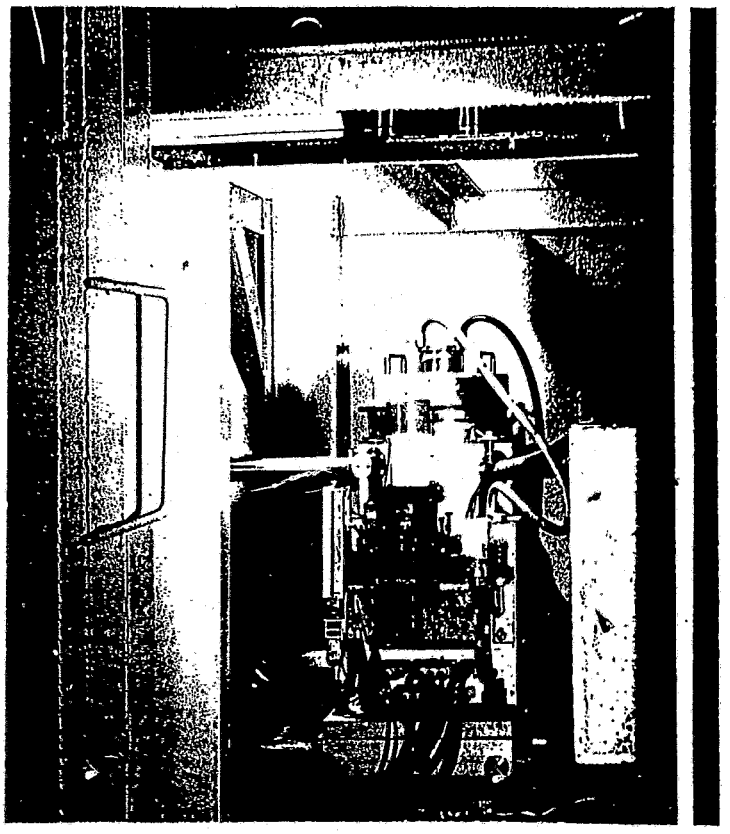

Figure 10: One of the modules of the multirotor system at the neutron baem of WWR-M reactor.

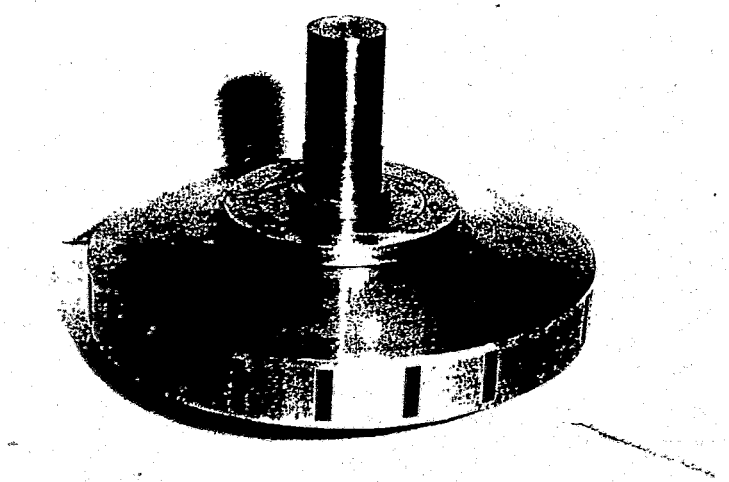

Figure 11: Chopper rotor with 10 through-going reectangular slits.

5 STUDIES OF THE FISSION PROCESS OF HEAVY NUCLEI INDUCED BY RESONANCE AND FAST NEUTRONS USING THE TIME-OF-FLIGHT TECHNIQUE (PNPI, JINR(FLNP), PI)

Introduction

Up to now, one of the most interesting and at the same time the least studied phenomenon is a problem of the channel nature of neutron induced fission of heavy nuclei. Nowadays, a hypothesis about the existence of comparatively small number of transition states (fission channels) first advanced by A. Bohr [1] is developed further into the Brosa's model [2]. Within the framework of this model many experimental facts obtained recently were explained successfully. Nowadays, the connection between these two fission models is the object of theoretical research. However, unsolved as before is a question about the influence of fission channels on such fission characteristics as the energy and multiplicity of fission γ-quanta and the multiplicity of prompt fission neutrons. Besides a problem mentioned above, the experimental studies of these characteristics enable one to obtain information about the fission process dynamics and its energy balance as well as the spectroscopy data about highly excited states of heavy nuclei at normal (in the 1-st potential well of the two-humped fission barrier) and large (in the 2-nd well) deformation.

The utilization of the time-of-flight technique in conjunction with high intensity pulsed neutron sources gives an opportunity to carry out investigations with resonance neutrons within a wide energy range (up to 500 eV for fissile nuclei). The measurements of the characteristics mentioned above for neutron resonances which are in fact nuclear states with determined spin and parity, enable one to ascertain unambiguously the connection between these characteristics and the quantum numbers of fission channels.

To solve the problems enumerated above, one has a need for new experimental data for a large number of fissile (by thermal and resonance neutrons) nuclei as well as for even-even actinides. At present, the available data are restricted by ^{235}U, ^{239,241}Pu only. Furthermore, these data are somewhat contradictory by character, and their accuracy is not high enough. Actually, an analogous information for even-even actinides is absent in the resonance energy range.

Within the framework of this problem, we are going to carry out the following experimental studies.

5.1 MEASUREMENTS OF THE VARIATIONS OF THE FISSION γ-QUANTA TOTAL ENERGY AND THE MULTIPLICITY OF PROMPT FISSION NEUTRONS FOR EVEN-ODD FISSILE NUCLEI ($^{233,235}U$, $^{239,241}Pu$) INDUCED BY RESONANCE NEUTRONS WITH ENERGIES UP TO 500 eV

Besides the information about the height and structure of fission barriers, the spectra of transition states, the experimental data may be obtained about the structure of highly excited nuclear states at excitation energies $B_n - 3MeV < E^* < B_n$ as well as about the nature of γ-transition between them (the so called "compound-compound" transitions). Particularly interesting is the information about the probability of (n,γ f)-reaction [3] obtained from these data. As the detector for fission γ-quanta and prompt neutrons we are going to use the large 200-liter Gd-loaded liquid-scintillator tank at the neutron time-of-

flight spectrometer GNEIS [4] in Gatchina and the analogous technique at IBR-30 pulsed reactor in Dubna (fig.12).

5.2 MEASUREMENTS OF THE VARIATIONS OF THE MULTIPLICITY AND TOTAL ENERGY OF FISSION γ-QUANTA AND THE MULTIPLICITY OF PROMPT FISSION NEUTRONS FOR EVEN-EVEN HEAVY NUCLEI ($^{236,238}U$, $^{238,240}Pu$ etc.) INDUCED BY RESONANCE ($E_n < 2$ keV) AND FAST NEUTRONS ($E_n \simeq 1$ MeV)

In this case, the maesurements with resonance neutrons give opportunity to study the subthreshold fission characterized by strong influence of the class-II compuond states (in the 2-nd potential well) on the properties of fission channels. The measurements with fast neutrons in the near threshold vibrational resonances could help to understand the nature of the class-II states associated with these resonances and that of the corresponding fission channels.

5.3 MEASUREMENTS OF THE FISSION CROSS SECTIONS, THE MASS AND ENERGY DISTRIBUTIONS OF FISSION FRAGMENTS FOR HEAVY NUCLEI WITH FAST NEUTRONS IN THE ENERGY RANGE UP TO 100 MeV

A few experiments of the types enumerated above were already carried out at our TOF-facility GNEIS or are in progress [4,6].

References

[1] A. Bohr, Proc. Int. Conf. Peaceful Uses of Atomic Energy, (Geneva 1955), Vol. II, UN, N.Y., p.220 (1956)
[2] U. Brosa, S. Grossmann, A. Müller, Phys. Rep. 197, 167 (1990)
[3]O.A. Shcherbakov, Sov. J. Part. Nucl. 21(2), 177 (1990)
[4]N.K. Abrosimov et al., Nucl. Instr. Methods, A242, 121 (1985)
[5]V.S. Masterov, N.S. Rabotnov, Sov. Nucl.Phys. 49, 940 (1989)
[6]O.A. Shcherbakov, Preprint LNPI-1664, Leningrad (1990)

ACKNOWLEDGEMENT

The authors of this paper acknowledge the support of the BMFT (Bonn) for attending the conference.

One-armed fission fragment time-of-flight spectrometer with fissile target near the reactor core

A.A.Alexandrov, S.L.Podshibyakin, Yu.V.Pyatkov, A.I.Slyusarenko, A.N.Shemetov, R.A.Shehmametiev

Moscow Engineering Physics Institute

The general scheme of the one-armed time-of-flight spectrometer at the research MEPhI reactor [1] is shown in FIG.1. The fissile target 1 is located facing the reactor core center close to the bottom of the vertical evacuated beam tube 2. The tube is 7.3m long with inner diameter 23 mm. The thermal neutron flux at the target position is about $3.7*10^{11}$ $n*cm^{-2}s^{-1}$ with the cadmium ratio >=400. The installation efficiency is increased by an electrostatic particle guide (EPG) system, which is provided by a tubular coaxial capacitor formed by the tube wall and a thin metal wire electrode stretched along its axis. When the central electrode is at -2.5 kV potential to the tube wall, the efficiency ratio of the spectrometer is about 50 times the geometrical one and amounts to $1.5*10^{-6}$. For a typical target of 50mkg ^{235}U one can detect about 35 events per second.

The fragment mass is obtained by fission fragment time-of-flight between two microchannel plate time pick-off detectors (TPD) 4,7 and its kinetic energy, which is measured by a semiconductor detector (SCD) 8 or a gas ionization chamber (GIC). The detector chamber 6 is used for setting up the additional TPD when measuring the spectrometer time resolution by the method described in [1]. Such a concept of the spectrometer assembly provides the possible statistics increase compared with the well-known "Cosi Fan Tutte" installation.

The spectrometer application range was substantially broadened by including the nuclear charge measurement. This is done by means of the gas ionization chamber, similar to one described in ref.[2].

The entrance window is manufactured from polypropilen with the thickness of 40 $mkg.cm^{-2}$, while hexan at 75 torr is used as a working gas. The electrical field strength is about 6 V/(cm*torr). The time dependence of chamber characteristics without gas change is shown in Fig.2,3. The nuclear charge of the fission fragment is determined by the measurement of its range in the chamber. This range is derived from the following equation (taking into account very small angular divergence of the fragment beam)

$$R=L-v*t,$$

where L is the distance between the Frish grid and the entrance window, v- is the electron drift velocity and t is the measured time difference between the signal from the second TPD and the chamber anode signal. The charge calibration is based on the Bohr-Willer relationship [3]

$R=b(E*M)^{1/2}*Z^{-2/3}$. (E,M,Z- fragment energy, mass and charge).

We have assumed this relation to be valid with possible mass-or-energy dependent corrections, therefore

$$t=a+b(E^*M)^{1/2}*Z^{-2/3}+c^*M+d^*E$$

The last member of this equation happened to be negligible and was later omitted. The coefficients a,b,c were obtained by seeking the minimum of the least-squares functional [4]

$$F=\sum_{i,j}(<t>_{EiMj}-a-b(EiMj)^{1/2}*<Z^{-2/3}>_{EiMj}-cMj)^2/DISP(<t>),$$

where $<t>_{EiMj}$ was the mean t value for given fragment mass and energy. The $<Z^{-2/3}>_{EiMj}$ values were determined with the independent yields data from ref.[5]. The summation was made for the set of {Ei} values of ref.[5] and for all masses of the light group.

The mass and energy calibration were performed as described by us in [6] by the minimization of the difference between the measured integral mass spectrum and the known one for $^{235}U(n_{th},f)$ fission, assuming the parameterization suggested by Shmitt[7].

Though this procedure happened to be adequate for semiconductor detectors, we had to introduce an additional correction for fragment energy measured with the GIC:

$$E'=E+a^*(E-<E>),$$

where <E> is the mean energy for a given mass, and a is about 0.1. The quality of mass and charge spectra obtained for $^{235}U(n_{th},f)$ fission is demonstrated by Fig.4-6, where cold fragmentation region spectra together with the measured dependence of proton odd-even effect vs. energy are presented.

This spectrometer provided the performance of fine structure investigations in fission fragment spectra for $^{233,235}U$, ^{242m}Am,^{249}Cf fission with thermal neutrons at a relatively low-power reactor. The necessary statistics is about 10^6-10^7 events. Some most interesting results are shown in Fig.7-9. The comparison of cold fragmentation mass spectra of $^{242m}Am(n_{th},f)$ with $^{241}Am(2n,f)$ data from ref.[8] is important for studying the spin dependence of fission parameters. A special type fine structure in the form of linear ridges was first found in mass-energy spectra for $^{233,235}U$ [9] (Fig.8), these ridges seem to be coupled with neutron evaporation from fragments [10]. We consider it rather interesting that the cold fragmentation spectra for ^{249}Cf fission (Fig.9) demonstrate the peculiarity of CF for practically one and the same fissile system at different initial deformations, where the descent starts.

Among the future plans there are comparative studies of spontaneous vs. induced fission for Cm isotopes. This spectrometer also serves as a prototype of the double-armed spectrometer with internal target "LEMOS" at VVR-M reactor in Gatchina, which is under construction in collaboration with Dr. G.Petrov's group .

1. A.A.Alexandrov,I.A.Alexandrova,A.V.Ermolenko et al, Nucl.Instrum.Meth., A303(1991) 323
2. Oed A., Geltenbort P., Gonnenwein F. et al, Nucl.Instrum.Meth., A205(1983) 421
3. In.: Registration and spectrometry of fission fragments /Gangrsky Yu.P., Markov B.N. Perelyugin V.P.,M.,1981
4. S.L.Podshibyakin,Yu.V.Pyatkov, S.I. Sitnikov et al, Pryb.Tekhn. Exper. 1(1992)66
5. Lang W.,Clerc H.-G.,Wohlfart H. et al, Nucl.Phys. A345(1980)34
6. A.I.Per'kov,Yu.V.Pyatkov and A.I.Slyusarenko, in. Experimentsl Methods of Nuclear Physics, Moscow 1985,p.18
7. H.W.Shmitt,W.E.Kiker,C.W.Williams, Phys.Rev. 137(4B)(1965) 837
8. P. Siegler, T. Schunk, M.Mutterer et al, Proc.Int.Workshop Dynamical aspects of nuclear fission, Smolenice 1991,p.60
9. A.A.Alexandrov,I.A.Alexandrova,S.L.Podshibyakin et al, Abstr.Int.Conf. "50-th anniversary of nucl.fission" Leningrad 1989 p.127
10. A.A.Alexandrov,I.A.Alexandrova,S.L.Podshibyakin et al, roc.Int.Workshop Dynamical aspects of nuclear fission, Smolenice 1991,p.60
11. H.-G.Clerc, W. Lang, M. Mutterer et al, Nucl.Phys. A452(1986)277
12. F.Gonnenwein, J. Kaufmann, W. Mollenkopf et al, Proc. Int. Workshop Dynamical aspects of nuclear fission, Smolenice 1991,p.60
13. H.H.Knitter, F.J. Hambsch, C. Budz-Jorgensen, Nucl.Phys. 536 N2 (1992) 222

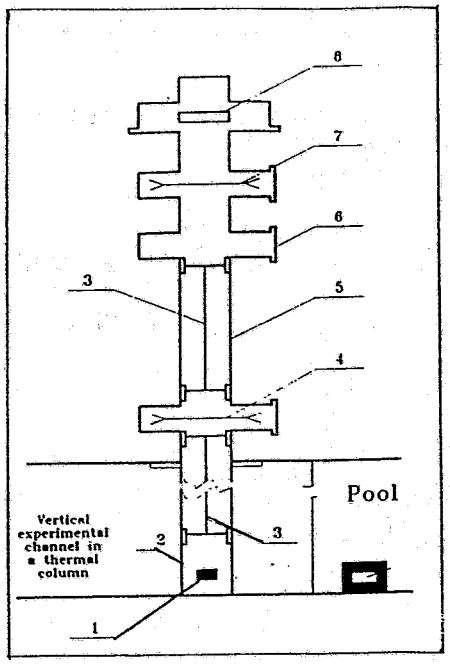

Fig.1 General scheme of the spectrometer. For details see text.

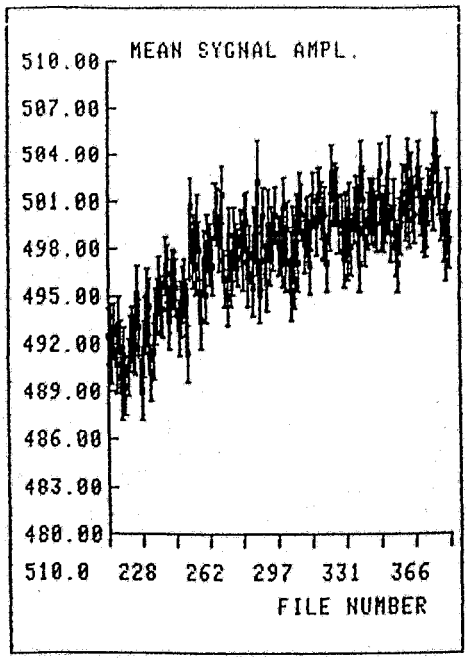

Fig.2 Mean amplitude of the ionization chamber's sygnal dependence vs file number. Statistics in each file - - 12000 counts. FF flux intensity - 20 s^{-1} .

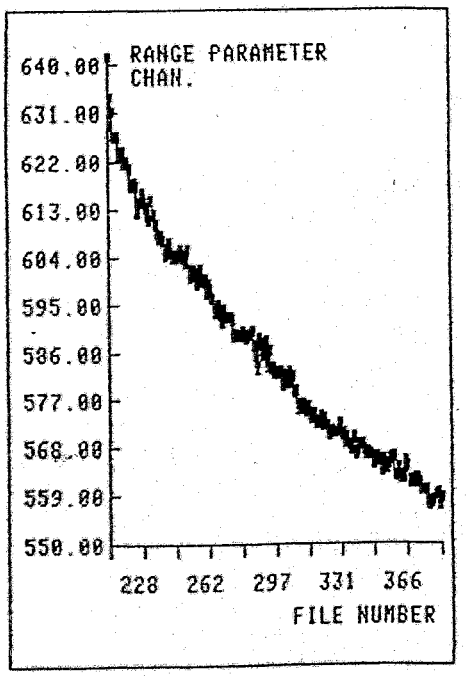

Fig.3 Mean range parameter dependence vs file number.

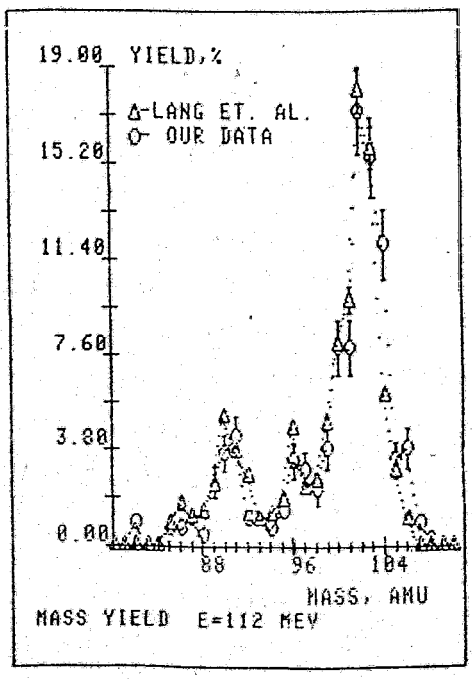

Fig.4 Mass yield distribution of $^{235}U(n_{th},f)$ FF at 112 MeV kinetic enegy.

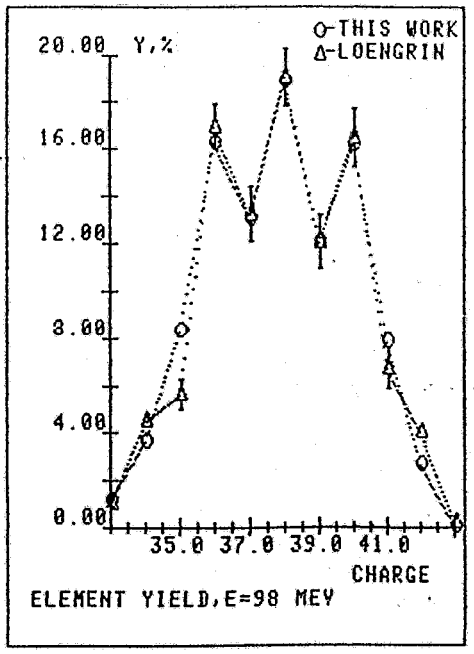

Fig.5 Element yield distribution for light FF at the kinetic energy E=98 MeV

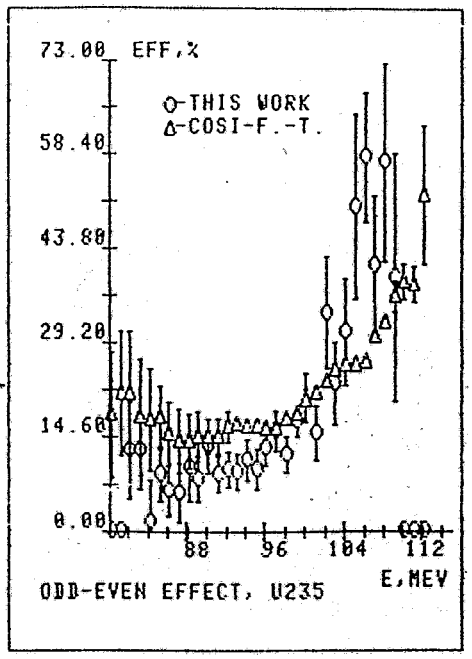

Fig.6 Proton odd-even effect as a function of the kinetic energy for the light FF for $^{235}U(n_{th},f)$ reaction.

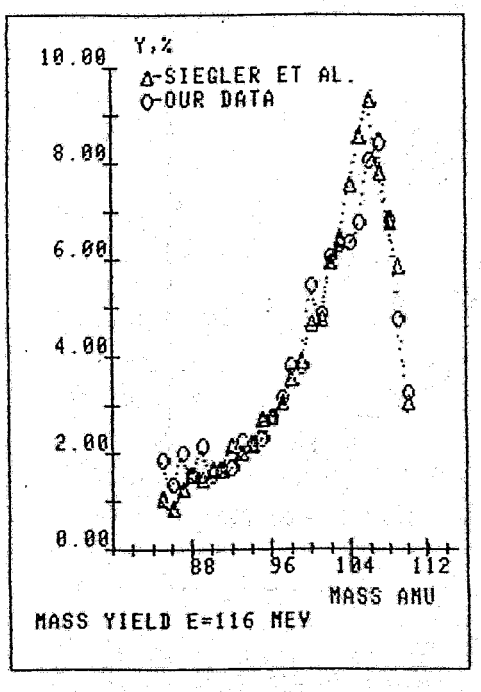

Fig.7 Mass yield distribution for $^{242m}Am(n_{th},f)$ - O and $^{241}Am(2n_{th},f)$ - Δ ref.[8] at the kinetic energy E=116 MeV

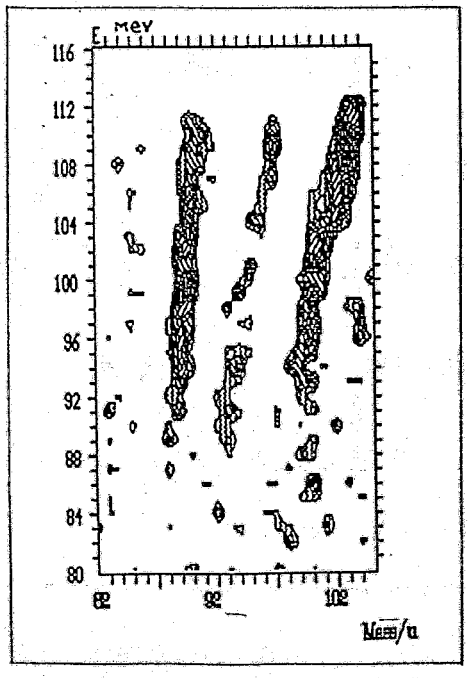

Fig.8 Fine struture in $^{235}U(n_{th},f)$ FF mass-energy spectra.

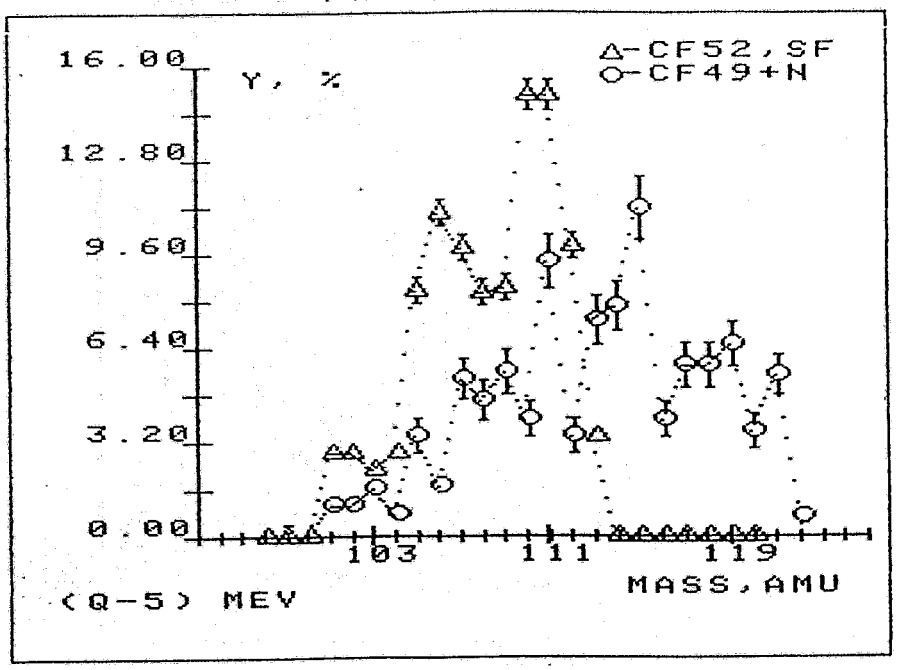

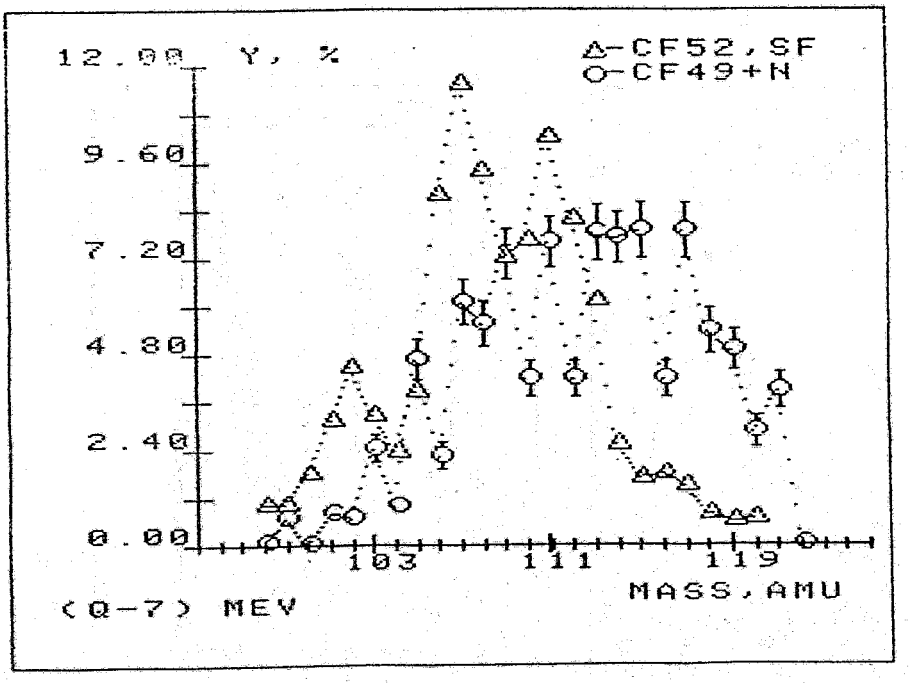

Fig.9 Mass yield distribution for $^{252}Cf(sf)$ and $^{249}Cf(n_{th},f)$ reactions for the total exitation energy (Q-5) MeV - (a), (Q-7) MeV - (b). △ - ref. [13], ○ - our data.
Q - is a reaction Q-value for each specific mass split.

AUTHOR INDEX

LIST OF PARTICIPANTS

Name	Address	Country
Aarle, J. van	Univ. Marburg	Germany
Birn, I.	TU Dresden	Germany
Düring, I.	TU Dresden	Germany
Fitzgerald, J.B.	MPI Heidelberg	Germany
Freiesleben, H.	Univ. Bochum	Germany
Geltenbort, P.	ILL Grenoble	France
Gönnenwein, F.	Univ. Tübingen	Germany
Graf, U.	Univ. Tübingen	Germany
Hambsch, F.-J.	CBNM Geel	Belgium
Hesse, M.	Univ. Tübingen	Germany
Jahnke, U.	HMI Berlin	Germany
Käubler, L.	FZ Rossendorf	Germany
Kaufmann, J.	Univ. Tübingen	Germany
Klein, A.	TU Dresden	Germany
Märten, H.	TU Dresden	Germany
Möller, A.	Univ. Tübingen	Germany
Naumann, L.	FZ Rossendorf	Germany
Persyn, K.	Univ. Gent	Belgium
Petrov, G.	PNPI Gatchina	Russia
Pilz, W.	FZ Rossendorf	Germany
Pyatkov, Yu.	MEPI Moscow	Russia
Richter, D.	FZ Rossendorf	Germany
Ruben, A.	TU Dresden	Germany
Schilling, K.D.	FZ Rossendorf	Germany
Schwierz, R.	TU Dresden	Germany
Seidel, W.	FZ Rossendorf	Germany
Siemon, K.	Univ. Marburg	Germany
Singer, P.	TH Darmstadt	Germany
Vitko, I.	TU Dresden	Germany
Volny, D.	Univ. Bratislava	Slovakia